eman ta zabal zazu

Universidad del País Vasco
Euskal Herriko Unibertsitatea

Chain dynamics in crosslinked filled and unfilled polymer blends of different miscibility

PhD Thesis Submitted by

Lucía Ortega Álvarez

to the

University of the Basque Country

Supervised by

Dr. Silvina Cerveny
Dr. Gustavo A. Schwartz

Donostia – San Sebastián, 2018

(c)2018 LUCIA ORTEGA ALVAREZ

Institutions

Soft Matter group
Materials Physics Center
Donostia/San Sebastián

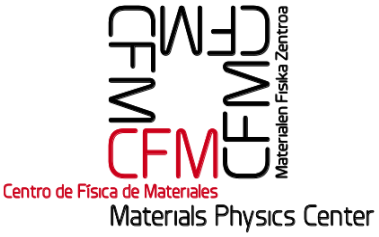

Donostia International Physics Center
Donostia/San Sebastián

Goodyear Innovation Center (GIC*L)
Colmar Berg/Luxembourg

En memoria da miña querida avoa Lala

Contents

Abstract

Rubber compounds normally used in the tire industry are multiphase composites obtained by mixing elastomeric matrices based on natural or synthetic rubbers, with fillers, stabilizers, vulcanization additives, and other special ingredients. The result is a heterogeneous system; therefore, very complex to be analyzed from a basic point of view, whose final properties depend on the interactions among those ingredients.

Rubber blends are of great importance for the tire industry, providing new features not seen in the neat materials. Almost all important rubber products in industry applications include blends in their compositions. The usual reason for blending rubbers is to combine two or more desirable features exhibited by vulcanizates of the individual polymers in a single material. Depending on the thermodynamics of the mixing process, rubber blends can be miscible or immiscible, both of great interest for the tire industry. The study of the dynamics of polymer blends is essential when designing new materials with desired properties, by tuning the type and concentration of the neat polymers comprising the blend.

In this PhD-work we present a study concerning the dynamics of crosslinked natural rubber (NR), butadiene rubber (BR), styrene butadiene rubber (SBR) with different microstructures, and chain-end functionalized styrene butadiene rubber (fSBR), as well as their blends. Unfilled and silica-filled composites were studied by means of broadband dielectric spectroscopy (BDS), differential scanning calorimetry (DSC), atomic force microscopy (AFM), and

complementary techniques such as energy dispersive X-ray spectroscopy (EDX) and transmission electron microscopy (TEM).

In Chapter 4, the dielectric response of vulcanized fSBR has been analyzed by means of BDS. In spite of the fact that this response was observed and analyzed before in literature, we find that besides the segmental relaxation, an additional low frequency contribution was observed. The origin of this process has been investigated and related to the presence of diphenyl guanidine (DPG), a secondary accelerator used in vulcanization.

In Chapter 5, we proposed an extension to the Adam-Gibbs (AG) model to describe the segmental dynamics of miscible polymer blends with strong interactions, at different temperatures and concentrations. Based on the dynamics of the neat compounds, this modified AG approach gives an accurate description of the temperature dependence of the relaxation times. The model has only two fitting parameters (A and B) which depend on the characteristics of both polymers.

Finally, in Chapter 6 we have analyzed immiscible blends of NR and fSBR by means of different techniques (BDS, DSC, TEM and EDX). We observed a phase morphology consisting on fSBR islands in an NR matrix due to its tendency to self-aggregation. We have found that the dynamics of NR is not significantly affected by the mixing, while for fSBR, changes in the glass transition temperature (T_g) as well as in the dielectric response have been observed.

AFM results reveal a radial variation in the mechanical modulus of the fSBR islands. This change in the mechanical properties is attributed to an inhomogeneous distribution of the additives inside the fSBR phase. These results are in agreement with EDX measurements, where a radial distribution of sulphur has been observed for the same regions. This could lead to an

heterogeneous crosslink density, which is most likely the origin of the variation observed in the mechanical properties.

The main objective of this PhD thesis is to enhance the knowledge about the dynamics of polymer blends, with applications in the tire industry. An advanced understanding of the polymer dynamics as well as the interactions between polymer and additives will improve the design of materials with desired properties.

Key-words: polymer blends, blend dynamics, miscible blends, immiscible blends, dielectric spectroscopy, differential scanning calorimetry, atomic force microscopy.

Resumen

El caucho es un polímero de alta elasticidad que experimenta deformaciones bajo esfuerzos relativamente débiles, recuperando su forma original una vez que la fuerza aplicada ha cesado. Los cauchos se utilizan en muchas aplicaciones industriales y, en particular, es la materia prima por excelencia en la industria del neumático. En este caso, los compuestos utilizados son sistemas complejos ya que, además de mezclas de las matrices elastoméricas (basadas en cauchos sintéticos o naturales), se incorporan otros ingredientes como cargas, estabilizantes, aditivos del sistema de vulcanización y otras substancias especiales. El resultado es un sistema altamente heterogéneo, cuyas propiedades finales son determinadas por las interacciones entre todos sus componentes.

En la industria del neumático, además, es muy común utilizar mezclas de cauchos (*blends*) que muestran propiedades singulares y que no pueden obtenerse a partir de los materiales puros. Mezclando dos cauchos se puede conseguir nuevos compuestos con propiedades intermedias a las de los polímeros puros, sin necesidad de llevar a cabo una nueva síntesis, reduciendo los costos y los tiempos de fabricación. El conocimiento de las propiedades dinámicas de los compuestos de caucho es esencial a la hora de diseñar materiales con propiedades deseadas. Mediante la variación de la concentración y los tipos de polímeros que componen una mezcla, podremos afinar sus propiedades finales.

En esta tesis se han analizado compuestos vulcanizados de caucho natural (NR), caucho de butadieno (BR), caucho de estireno-butadieno (SBR) con

diferentes microestructuras, y caucho de estireno-butadieno con funcionalización terminal de cadena (fSBR). Se han analizado compuestos puros sin carga (*unfilled*) y compuestos puros cargados con partículas de sílice (*filled*) así como también mezclas de cauchos con diferentes concentraciones. Las principales técnicas utilizadas fueron: espectroscopía dieléctrica (BDS), calorimetría diferencial de barrido (DSC) y microscopía de fuerza atómica (AFM). Adicionalmente su utilizaron técnicas complementarias como la espectroscopía de dispersión de rayos-X (EDX), y la microscopía electrónica de transmisión (TEM).

En el capítulo 4, se analiza la dinámica de compuestos de fSBR puros. Además de la relajación segmental, se ha observado un proceso lento. El origen de éste proceso ha sido investigado en esta tesis, y se ha relacionado con la presencia de los acelerantes utilizados en el proceso de vulcanización.

En el capítulo 5, se propone una extensión del modelo de Adam-Gibbs (AG) para describir las dinámicas segmentales de las mezclas con interacciones fuertes (tal como los entrecruzamientos del caucho vulcanizado), a diferentes temperaturas y concentraciones. Basándonos en las dinámicas de los polímeros puros, esta extensión del modelo de AG da una descripción precisa de la dependencia de la temperatura con los tiempos de relajación, teniendo solamente dos parámetros de ajuste (llamados A y B en esta tesis) que se pueden extraer a partir de los polímeros puros.

Finalmente, en el capítulo 6 se han caracterizado la dinámica de mezclas inmiscibles de NR y fSBR por medio de la espectrocopía dieléctrica. Los aspectos estructurales se han analizado por medio de AFM, TEM y EDX. Para estos *blends*, se ha observado una morfología consistente en islas de fSBR sobre una matriz de NR. Las propiedades térmicas y dinámicas de la

fase NR no se ven significativamente afectadas, mientras que en el caso de la fase fSBR se observan cambios en la T_g así como en su respuesta dieléctrica.

Los resultados estructurales obtenidos a partir de mediciones de AFM muestran una variación radial del módulo mecánico dentro de las islas de fSBR. Estas variaciones en las propiedades mecánicas han sido atribuidas a una distribución no homogénea de los aditivos dentro de las islas de fSBR. Éstos resultados están en concordancia con los resultados obtenidos por EDX, en los que se ha observado una distribución radial de azufre en dicha zona. Ésta podría ser la causa de una densidad de entrecruzamiento no homogénea, causante a su vez de las variaciones observadas en las propiedades mecánicas.

Palabras-clave: mezclas poliméricas, dinámicas de mezclas, mezclas miscibles, mezclas inmiscibles, espectroscopía dieléctrica, microscopía de fuerza atómica.

1

Introduction

In this chapter we introduce the most relevant concepts about polymers, rubbers, the vulcanization reaction as well as the additives industrially used to produce an efficient product after vulcanization. Then, we focus on the characteristics of the dynamics of miscible and immiscible polymer blends. Finally, the objectives of this thesis are described.

1.1 Polymers and rubbers

A polymer is a large macromolecule consisting essentially of repeating structural units called monomers[1]. When a polymer is synthesized by using only one type of monomer, it is called homo-polymer. When two or more different types of monomers are used, the polymer is called copolymer, and it can lead to different structures depending on the relative positions of the monomers. When two monomers are arranged in alternated positions (-A-B-A-B-A-B-A-B-) it is called alternating copolymer, whereas in a random copolymer the two monomers do not follow a particular order (-B-B-A-B-B-A-A-B-).

Pendant groups can be arranged along the backbone chain of the polymers in different ways. When the pendant groups are attached on the same side of the polymer chain are called *isotactic*, in alternating sides are called *syndiotactic*, and when there is no particular order are *atactic*.

Polymers can be natural (e.g. proteins, cellulose or silk) or produced by synthesis (e.g. polystyrene (PS), polyethylene (PE) or nylon). In some cases, naturally occurring polymers can also be produced synthetically[1]; for instance, poly(isoprene) (IR) is the synthetic form of the natural rubber (NR).

Rubbers are a type of polymer that presents a viscoelastic behaviour showing relatively low elastic properties. But this type of material, and only this type, shows a unique mechanical behaviour which is the ability to endure very high deformation yields (up to 1000%) under an imposed force, and deformation recoverability after force removal. In rubbers, the polymer chains must have a high degree of flexibility and deformability to undergo large deformations. Rubbers show a recoverability which is not complete. In order to obtain a total recoverability, chemical bonds are artificially formed between macromolecular chains. The formation event of inter-chain chemical bonds is called *crosslinking* and the resulting chemical bonds are known as crosslinks. The formation of crosslinks creates a three-dimensional network of macromolecular chains jointed together. Thus, rubbers have the ability of passing, under the effect of a crosslinking reaction (for instance, vulcanization), from a predominantly viscous behaviour (with low elasticity) to a mainly viscoelastic one[2].

1.2 Types of rubber

1.2.1 Natural rubber (NR)

Natural rubber is a biopolymer created by enzymatic processes in many plants, and industrially obtained[3] mainly from the tree called "*Hevea Brasiliensis*". Natural rubber consists of pure cis-1.4 isoprene units (it contains more than 99.9 % of cis-1.4 units). The linear isoprene chain is terminated in one end (the so called α–terminal) by a mono- or di-phosphate group, linked to phospholipids. The other end, referred to as the ω–terminal, has been postulated to be a modified dimethyl allyl unit linked to a functional group,

which can be associated with proteins to form cross–links through intermolecular hydrogen bonding (see Figure 1.1). This significant amount of proteins and lipids is the result of the biosynthesis mechanism of rubber formation[4]. The presence of proteins and phospholipids in NR induces a multi-scaled microstructure characterized by natural cross–linking among the terminal groups of linear polyisoprene chains[4]. Inorganic constituents like K, Mg, Cu, Fe, Na, Ca, $PO_4^{3-}$are also present.

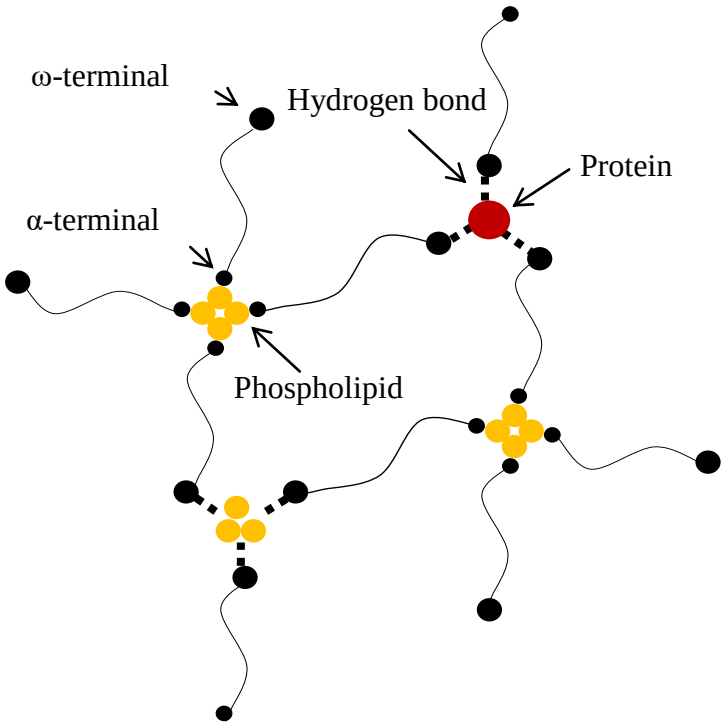

Figure 1.1 Representation of natural rubber occurring network.

The synthetic version of natural rubber is poly (isoprene) (IR), having the same formula as NR but without the presence of proteins and organic compounds. The properties of IR depend on the amount of cis-1,4-units, due to their influence on crystallization and regularity of the structure. An increase in

cis-1,4 content provokes an increase in the glass transition temperature, improving some properties such as the mechanical modulus. Tensile strength and tear resistance are slightly worse in synthetic IR than in NR, whose cis-1,4- content is almost 100 %[5]. The most significant advantages of synthetic IR compared to NR are their purity, good processability and homogeneity of polymer structure.

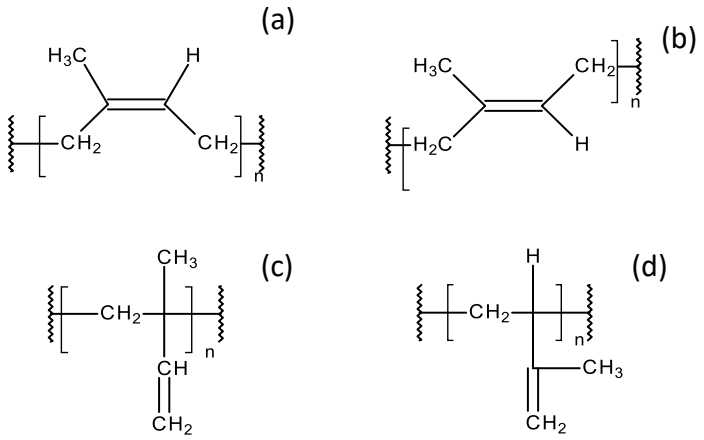

Figure 1.2 Isomeric structures of polyisoprene: cis-1,4-addition (a), trans-1,4-addition (b), 1,2-addition (c) and 3,4-addition (d)

1.2.2 Synthetic rubbers

The increased demand of rubbers in the 1890s, due to the expanded use of vehicles and particularly motor vehicle tires, became necessary the investigation of the synthetic rubber polymerization. The first synthetic rubber was poly(isoprene) (IR), polymerized in 1909 by Fritz Hofmann[6]. Synthetic rubbers are artificially made basically using petrochemical sources such as oils. The different types of rubbers have their own individual properties and advantages, and are determined by their structures.

Butadiene rubber (BR)

Butadiene rubber is the second most used rubber and it is produced by solution polymerization of 1,3-butadiene. It can be composed by three different structural units (see Figure 1.3) which can be obtained by varying the catalyst and the polymerization conditions.

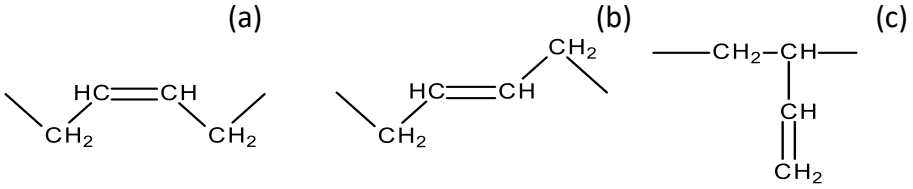

Figure 1.3 Butadiene structural units: cis-1,4 (a), trans-1,4 (b) and 1,2 vinyl (c)

The physical properties of the polymers are mainly determined by its microstructure. For instance, trans-1,4 BR does not show elastic properties, while high cis-1,4 BR has the best elastic properties but due to its linear conformation exhibits crystallization.

BR is a non-polar, highly unsaturated rubber[5], with properties such as high resistance against abrasion (which is increased with increasing cis units), high resilience and good elastic properties at low temperatures. These properties are maintained even when mixed with other rubbers. More than 90 % of produced BR is consumed in the production of tires, providing resilience and fatigue crack propagation resistance.

Styrene butadiene rubber (SBR)

Styrene-butadiene rubber is a copolymer of styrene and butadiene, and it can be synthesized by different routes[5] like emulsion or solution polymerization. It contains four different basic construction units; three of them arising from butadiene (see Figure 1.4).

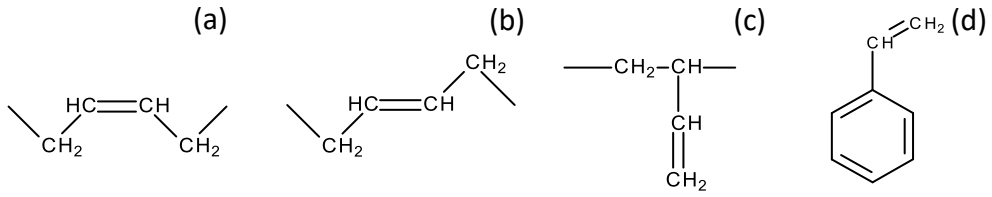

Figure 1.4 Structural units of SBR: butadiene structural units cis-1,4 (a), trans-1,4 (b), 1,2 (c) and styrene (d)

Mutual arrangement of styrene and butadiene units can give random, partially block or block character. Variations of the microstructure and contents of styrene and butadiene in the copolymer molecules allow the production of SBR rubbers with different properties: SBR with low styrene content is suitable for low-temperature applications while SBR with high content of styrene acts as self-reinforcing rubbers[5]. Variations on the amount of styrene and 1.2 structural units contribute to modify the T_g and, therefore, SBR can be tailored to the desired application.

1.3 Rubber vulcanization

Several rubber articles used in daily life, such as tires, cannot be made without vulcanization[7]. Vulcanization is a process in which individual polymer chains are converted into a three-dimensional network through chemical cross-linking. A crosslink is a chemical bridge between two chains as shown in Figure 1.5.

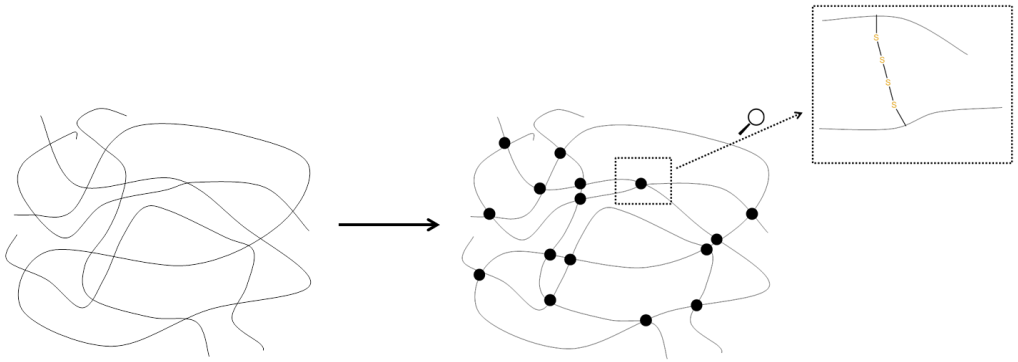

Figure 1.5 Representation of the structure of a cross-linked rubber by sulphur vulcanization reaction.

Vulcanized rubber products are characterized by high resilience following mechanical deformation: the original shape is restored almost immediately after the force is released. This elasticity is a consequence of the three-dimensional network structure formed during the vulcanization process. The restoring force after deformation is a function of the number of network-forming polymer chains per unit volume. Increasing the number of cross-links distributes tension over more polymer chains and thus increases the restoring force. Vulcanization causes highly significant changes at the molecular level becoming rubber essentially an elastic material which cannot be reshaped without being destroyed. Thus, it is essential that vulcanization only occurs after the rubber article is in its final geometric shape.

1.4 Vulcanization additives

Unsaturated rubbers such as SBR, BR, and NR can be cross-linked using sulphur as cross-link agent. Accelerated sulphur vulcanization is preferred due to both the better controllability of the vulcanization and the possibility to affect the nature of the cross-links by the type and the quantity of accelerators and the amount of sulphur[8].

In order to allow the vulcanization reaction to occur in an efficient way, the neat rubbers are mixed with a series of ingredients in a process called *compounding*. The ingredients used for compounding are classified into accelerators, activators, antioxidants, fillers and reinforcing agents, processing oils and vulcanizing agents. To give a complete list of compounding additives would be too long and it is out of the scope of this thesis; however, the additives used in this work are briefly described below.

1.4.1 Cross-link agents

Sulphur is the most well-known vulcanizing agent for unsaturated rubbers[9], remaining as the most successful and economical cross-linking agent, even nowadays. Using sulphur as vulcanization agent, rubber is converted into a non-tacky, tough and elastic product.

1.4.2 Antioxidants

Rubber is prone to degradation by oxidation[10] and, in order to prevent it, inhibitors are used during rubber compounding. Antioxidants[11] are highly effective ingredients and have a strong impact on the service life of the rubber product although being present at extremely low concentrations (0.5 –3.5 phr). Antioxidants do not completely eliminate oxidative degradation, but they substantially inhibit the rate of auto oxidation by interfering with the radical propagation reaction.

1.4.3 Processing oils

Plasticizers that improve flow properties and processability are frequently known as processing oils. Processing oils constitute by far the most important group of plasticizers in terms of quantity. Processing oils[9] are added to aid in the processing operations such as mixing, calendering and extruding. They can

be broadly classified into three basic groups: paraffinic, naphthenic and aromatics. They are used along with fillers to reduce the cost of the compound. Treated distillate aromatic extract oil (TDAE) is green rubber oil with characteristics such as high aromatic content, environmental protection, non-toxic, non-carcinogenic, which can be used as a substitute for existing aromatic oil.

1.4.4 Resins

Hydrocarbon resins[9] can be defined as low molecular weight polymers with high softening points, commonly used to improve processing by lowering the viscosity of the compound, influence surface tack, and to modify the viscoelastic properties of a compound[12]. Compatibility between the resin and the rubber is an important factor to achieve the desired properties.

1.4.5 Fillers

A large number of natural and synthetic rubbers need additional reinforcing fillers to achieve the desired properties in the final product. The most common reinforcing fillers are carbon blacks ("black" fillers) and precipitated amorphous silica ("white" fillers). Reinforcing "white" fillers are effective in rubber formulations to improve mechanical properties such as resilience, tear strength, abrasion resistance, hardness, stiffness and aging resistance[13, 14]. Compared to carbon black, silica has weaker filler-polymer interactions and stronger filler-filler interactions. The combination of silica with a coupling agent results in higher reinforcing effect compared to carbon black[14]. The world production of silica is 1.3 million tons of which one third is used in tire production[13].

Silica is commonly used in the treads of tires to reduce the fuel consumption of vehicles, thus contributing to a reduction in vehicle emissions of greenhouse gases[15]. This filler is produced from vitreous silicate by

dissolving it in water and transferred to a reactor in which, through acidification and under agitation, is precipitated. During this precipitation, there is an instantaneous formation of primary particles (from 2 to 40 nm) of a very short lifespan. These particles, however, immediately cluster to form non-dissociable aggregates (from 100 to 500 nm in size) based on covalent bonds. Due to the strength of covalent bonds, these aggregates cannot break under standard conditions; binding together to form agglomerates (1 to 40 μm). Because of these aggregates and agglomerates, precipitated amorphous silica meets the ISO definition of a nanostructured material, but it does not meet the definition of a nano-object.

1.4.6 Coupling agents

Mixing silica with polymers involves many difficulties due to their large polarity difference[9,16]. A bifunctional organosilane such as bis(triethoxysilylpropyl) tetrasulphide (TESPT) is commonly used as coupling agent to enhance the compatibility between the silica and the rubber, by chemically modifying silica surfaces and eventually creating a chemical link between the silica aggregates and the rubber chains as shown in Figure 1.7.

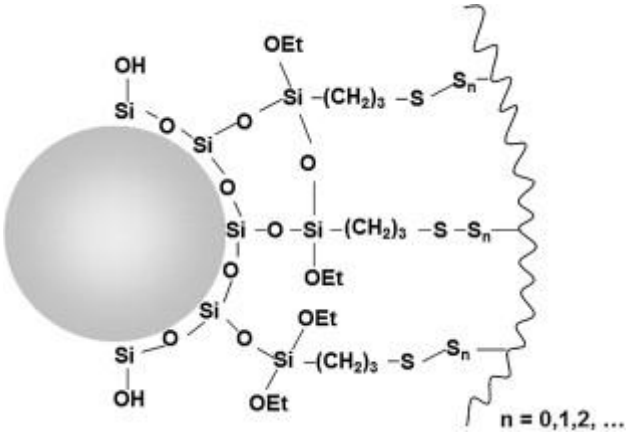

Figure 1.7 Representation of silica-TESPT-rubber coupling[16].

Coupling agents are generally added at an adequate processing step, so they can react with rubber in situ at the final step of heat-pressing[17].

1.4.7 Accelerators

Vulcanization of rubbers by sulphur alone is an extremely slow and inefficient process. The chemical reaction between the sulphur and the unsaturated rubber occurs mainly at the double bonds and, in absence of accelerators, each crosslink requires between 40 to 55 sulphur atoms[18]. The vulcanization process takes around 6 hours for completion, which is uneconomical by any production standards. The resulting materials, are extremely prone to suffer oxidative degradation and do not have adequate mechanical properties for practical rubber applications.

Initially, vulcanization was accomplished by heating elemental sulphur at a concentration of 8 parts per 100 parts of rubber (phr) for 6 h at 140 ºC. The addition of zinc oxide reduced the time to 3 h and with the use of accelerators, even in concentrations as low as 0.5 phr, the time is reduced to 1–3 min. As a result, rubber vulcanization by sulphur without accelerator is no longer of commercial significance.

An accelerator is defined as a chemical added into a rubber compound to increase the speed of vulcanization and to allow the vulcanization proceed at lower temperatures with greater efficiency. Accelerators also decrease the quantity of sulphur necessary for vulcanization and are classified as primary and/or secondary, based on the role they play in a given compound[8].

Generally, thiazoles and sulfenamide[8] are primary accelerators, due to their characteristics of good processing safety, a broad vulcanization plateau and optimum cross-link density as well as desired reversion delay. Basic accelerators such as guanidines, thiurams, and dithiocarbamates are used as secondary accelerators[8] to activate the primary ones, substantially increasing the speed of vulcanization.

1.4.8 Accelerator activators

The role of activators consist of helping accelerators in the vulcanization process[10]. The addition of zinc oxide to rubber compounds containing sulphur and accelerators considerably increases the cross-link density. Generally, the increase of zinc oxide dosages up to 5 phr leads to high tensile strength and stress values. Higher dosages have no further effect on these properties. The "rubber – sulphur – accelerator – zinc oxide" system is further activated by fatty acids, like stearic acid. Besides activation, fatty acids and their salts improve processability and filler distribution, which are important for vulcanized properties.

1.5 Rubber Blends

A polymer blend can be defined as a mixture of two or more polymers which generates a novel material with different properties. Since these properties can be tailored through selection of different components, ratios, and varying the processing method, polymer blends have interesting features from both scientific and technology points of view. Polymer-polymer miscibility plays an important role in determining the properties of the final system[19, 20]. Although some rubbers can be mixed to form an homogeneous blend, for instance SBR and BR, other mixtures such as SBR and NR are phase-separated at the microscopic scale[7]. The morphology of a rubber blend is a function of both the nature of the components[3] (their mutual compatibility and its rheological properties) as well as of the method employed to mix it.

Miscible rubber blends are not too common because of the high molecular weight of the elastomers. The most important relationship governing polymer blends[21] is:

$$\Delta G_m = \Delta H_m - T\Delta S_m \qquad (1.1)$$

where ΔG_m is the free energy of mixing, ΔH_m is the enthalpy of mixing, and ΔS_m is the entropy of mixing. To obtain a miscible blend, ΔG_m must be smaller than 0 and the next requirement must be also fulfilled:

$$\left(\frac{\partial^2 \Delta G_m}{\partial \phi_i^2}\right)_{T,P} > 0 \qquad (1.2)$$

Negative values of the left term in Equation 1.2, although the first condition is fulfilled ($\Delta G_m > 0$), can yield an area of the phase diagram where the mixture will separate into a phase rich in component 1 and a phase rich in component 2.

1.5.1 Dynamics of polymer blends

The molecular mobility of the polymers can be investigated by means of relaxation techniques[22] which use the response of the material to external applied fields. When the perturbation is weak, the evolution of the material properties is uniquely controlled by the thermodynamic spontaneous fluctuations of the system and therefore gives information about the molecular mobility of the material. Among the different relaxation techniques used for the investigation of the polymer dynamics, those detecting dielectric relaxations are of particular interest since most of the polymers have permanent molecular dipole moments associated to the monomeric units. In this case, the segmental dynamics of the polymer is detected through the spontaneous fluctuation of these dipole moments. In particular, using BDS techniques, weak relaxation processes can be detected, being possible the study of material with very small dipole moments. For more details of this technique the reader is referred to Chapter 2 (experimental techniques).

1.5.2 Miscible rubber blends

The dynamics of miscible rubber blends have largely been studied by using different techniques such as nuclear magnetic resonance (NMR)[23], neutron scattering (NS)[24], molecular dynamic simulations[25] and dielectric[26] and dynamic-mechanical[27] spectroscopies. These results have shown the presence of two separated time scales for the segmental dynamics[28].

In the last years, the segmental dynamics (also called α-relaxation and related with the calorimetric glass transition) of blends such as poly(vinyl ethylene)/poly(isoprene), poly(vinyl methyl ether)/polystyrene, poly(ethylene oxide)/poly(methyl methacrylate) or IR/butadiene rubber (BR) have been largely studied. The segmental dynamics of the two components in the blend is strongly modified depending on both the composition and the interactions between the components, resulting in properties not observed in the pure components[7]. Blending produces two main effects in the α-relaxation[29]: a) broadening of the relaxation, and b) dynamic heterogeneity[30], i.e., miscible polymer blends show two different relaxation times, each of them corresponding to the dynamics of each component modified by blending[29].

Different models have been proposed to account for the distinct component dynamics that emphasize different approaches[31]. Depending on the approaches taken into account, two main groups of models can be described[29]:

1. **Models based on thermally driven concentration fluctuations**: The role of concentration fluctuations was first introduced by Zetsche and Fischer[26] and later developed by Kumar and co-workers[32, 33]. These models are based on the idea that the local concentration fluctuations are quasi-stationary near the glass-transition of the blend, for instance, their lifetimes are much longer than the relaxation time of the segmental α-relaxation. As a consequence, the compound can be considered as an arrangement of independent domains, each of them with a given composition and a local glass transition temperature. The

relaxation function of a given blend component inside any of these regions is assumed to be equal to that corresponding to the pure component. Therefore, the distribution of these glass transition temperatures gives as a result a distribution of relaxation times. Despite the general agreement about the ability of concentration fluctuations to affect the distribution of relaxation times, several authors have argued about their role in determining the mean relaxation time[34, 35]. It is now generally accepted that concentration fluctuations cannot explain the presence of two relevant time scales and the effect of chain connectivity has to be taken into account[34].

2. **Models based on self-concentration**: Due to chain connectivity, the portion of matter relevant for segmental relaxation of one component is always richer in that component. This fact has been referred to as self-concentration effect, leading to an effective concentration higher than the blend average. Lodge and co-workers[34] proposed a temperature-independent length of the order of the Kuhn segment of the chain and, at least qualitatively, successfully predicted the component glass transition in several miscible blends. Leroy and coworkers[36, 37] modeled the segmental dynamics data of poly vinyl methyl ether/polystyrene (PVME)/(PS) and poly *o*-chlorostyrene/polystyrene (PoClS)/(PS) taking into account both the effect of concentration fluctuations and chain connectivity. They concluded that an essentially temperature independent length scale could be assumed. Hirose *et al.*[38] performed dielectric spectroscopy on polyisoprene/polyvinylethylene (IR)/(PVE) blends and, by measuring the terminal dynamics of IR and the segmental dynamics of both components, suggested that length scales of the order of the Kuhn length for IR are relevant for the segmental dynamics, whereas a larger length scale is needed for PVE.

In polymer mixtures with strong interactions such as hydrogen-bonded systems[39] or cross-linked rubber blends, the dynamic heterogeneity is normally broken and therefore single dynamics are observed[20, 30, 39, 40]. It has been reported in the bibliography some studies of the dynamics of miscible polymer blends exhibiting intermolecular hydrogen bonds, where both local and segmental relaxations are strongly influenced by the presence of these strong interactions. Zhang[39] and Runt studied the dynamics of miscible polymer blends of poly(vinyl methyl ether) and poly(2-vinylpyridine), finding a single segmental relaxation. This was attributed to the strong coupling due to the intermolecular hydrogen bonds.

The interactions between the components in cross-linked polymer blends strongly affect the dynamics and a new approach has to be applied in order understand it. By combination of the Adam-Gibbs (AG) theory with the self-concentration concept it is possible to account for the component segmental dynamics of non-interacting miscible polymer blends. In previous works[28, 40-43] different extensions of the Adam-Gibbs (AG) theory[44] have been proposed to account for the segmental dynamics of polymers, polymer blends and polymer/plasticizer mixtures under different conditions. This approach has also provided an excellent description of the temperature dependence for the component segmental relaxation time in concentrated polymer/solvent athermal mixtures at atmospheric pressure[43] and also for polymer/plasticizer binary mixtures at different temperatures and pressures[40]. Only for the latter case the interactions between components were taken into account. However, the strong interactions between components in vulcanized polymer blends (provided by the crosslinks) significantly affect the dynamics and therefore a new framework is necessary to describe it. We propose here a further extension of the AG theory to include the effects of these interactions (see Chapter 5).

1.5.3 Immiscible rubber blends

Due to the small entropy gain obtained when mixing high molecular weight polymers, the majority of these polymer blends are thermodynamically immiscible leading to a phase-segregated morphology[45]. These domains can range in size from a few tens of nanometers to microns with a broad size distribution[45].

The physical properties of immiscible blends depend on the characteristics of each pure component and also on other factors such as mixing procedures or even, in the case of rubbers, of the dispersion of curatives/additives in each phase[3]. The phases of an immiscible blend can be:

a) Co-continuous: normally when the two components have the same or similar viscosities (for instance BR and ethylene-propylene-diene terpolymer (EPDM)[46].

b) One of the components can be dispersed in a continuous matrix of the other component. In this case, normally the low viscosity component (continuous matrix) encapsulated the high viscosity component[15].

In particular, in the case of rubbers blends, vulcanization can affect the morphology because the creation of crosslinks connecting different phases. This could modify the interface between the two phases. In addition, distribution of fillers is also another factor. The affinity of the filler for one or other component may result in non-uniform distributions. Since the concentration of filler affects the melt viscosity, its inhomogeneous distribution can influence indirectly the phase morphology of the blend.

The unfilled and filled NR/SBR blends studied in this thesis belong to the category of immiscible or partially miscible blends. The presence of two distinct phases were detected using different experimental techniques (DSC,

SAXS, mechanical or dielectric properties, equilibrium swelling experiments, etc.) to evaluate its dynamics and microstructure[47-53].

1.6 General objectives of the present thesis

The main objective of this thesis is to analyse the dynamical behaviour of unfilled and filled rubber blends in a broad frequency and temperature range. To do this, different complementary techniques will be used, involving both, macroscopic (BDS and DSC) and microscopic characterization (AFM and EDX).

The study of the segmental dynamics by means of broadband dielectric spectroscopy, reveals (even in the neat compounds) the presence of a low frequency contribution in the dielectric spectra. We demonstrate in this thesis that the presence of this slow process, also seen in filled rubber compounds, and sometimes attributed to the interfacial immobilized polymer layer around the filler particles[54], is related to the presence of vulcanization additives, in particular to the presence of the accelerators.

In the case of miscible polymer blends, the purpose of this work is to propose a simple model to account for the temperature dependence of the segmental relaxation times of the blend´s components at different compositions. The aim is to extend the Adam-Gibbs model in order to include the effects of the strong interactions between both polymers due to the presence of the cross-links.

Finally, for immiscible SBR/NR blends, we propose to perform a complete thermal and dielectric characterization of the dynamics. However, to better understand the properties of this blend system, it is necessary to analyse the nano- scale microstructure as well as the interaction between the different

phases of the blend. Therefore, we also analyse the structure of the 50 NR 50FSBR blend using both atomic force and transmission electron microscopy.

1.7 References

1. Fried, J. R., *Polymer Science and Technology*. Prentice Hall: 2014.

2. Franta, I., *Elastomers and Rubber Compounding Materials*. Elsevier: 1989.

3. Bhowmick, A. K.; Stephens, H., *Handbook of Elastomers*. Marcel Dekker: 2000.

4. Carretero-Gonzalez, J.; Ezquerra, T. A.; Amnuaypornsri, S.; Toki, S.; Verdejo, R.; Sanz, A.; Sakdapipanich, J.; Hsiao, B. S.; Lopez-Manchado, M. A. Molecular dynamics of natural rubber as revealed by dielectric spectroscopy: The role of natural cross-linking. *Soft Matter* **2010,** 6 (15), 3636-3642.

5. Rubber chemistry. Virtual Education in Rubber Technology 2007.

6. Lanxess, N. D., *The Moving Powers of Rubber*. New York, 2009.

7. Erman, B.; Mark, J. E.; Roland, C. M., *The Science and Technology of Rubber*. Elsevier: 2013.

8. Vulcanization and accelerators. Nocil limited. Arvind Mafatlal Group: 2010.

9. Engels, H.-W.; Weidenhaupt, H.-J.; Pieroth, M.; Hofmann, W.; Menting, K. H.; Mergenhagen, T.; Schmoll, R.; Uhrland, S., *Ullmann's Encyclopedia of Industrial Chemistry*. Wiley-VCH: 2004.

10. Chandrasekaran, C., *Essential Rubber Formulary: Formulas for Practitioners*. Plastics design library: USA, 2007.

11. Antioxidants and Antidegradants. Nocil limited. Arvind Mafatlal group: 2010.

12. Shekleton, L. E.; Henning, S. K., Measuring the compatibility of petroleum-based hydrocarbon resins in elastomers. In *Fall 182nd Technical Meeting of the Rubber Division*, Rubber division: Cincinnati OH, 2012.

13. Reinforcing fillers in the rubber industry on tyres. European tyre and rubber manufacturers association: 2012.

14. Dierkes, W.; Blume, A., *Encyclopedia of Polymeric Nanomaterials*. Springer: 2014.

15. Visakh, P. M.; Thomas, S.; Chandra, A. K.; Mathew, A. P., *Advances in Elastomers I: Blends and Interpenetrating Networks*. Springer: 2013.

16. Sarkawi, S. S.; Dierkes, W. K.; Noordermeer, J. W. M. The influence of non-rubber constituents on performance of silica reinforced natural rubber compounds. *Eur. Polym. J.* **2013,** 49 (10), 3199-3209.

17. Ikeda, Y.; Kato, A.; Kohjiya, S.; Nakajima, Y., *Rubber Science: A Modern Approach*. Springer: 2017.

18. Datta, R. N., *Current Topics in Elastomer Research*. CRC Press: New York, 1954.

19. Masser, K. A.; Runt, J. Dynamics of Polymer Blends of a Strongly Interassociating Homopolymer with Poly(vinyl methyl ether) and Poly(2-vinylpyridine). *Macromolecules* **2010,** 43 (15), 6414-6421.

20. Zhang, S.; Painter, P. C.; Runt, J. Dynamics of Polymer Blends with Intermolecular Hydrogen Bonding: Broad-Band Dielectric Study of Blends of Poly(4-vinyl phenol) with Poly(vinyl acetate) and EVA. *Macromolecules* **2002,** 35, 8478-8487.

21. Robeson, L. M., *Polymer Blends*. Hanser: 2007.

22. Alegria, A.; Colmenero, J. Dielectric relaxation of polymers: segmental dynamics under structural constraints. *Soft Matter* **2016,** 12 (37), 7709-7725.

23. Chung, G. C.; Kornfield, J. A.; Smith, S. D. Component dynamics miscible polymer blends: A two-dimensional deuteron NMR investigation. *Macromolecules* **1994,** 27 (4), 964-973.

24. Cendoya, I.; Alegria, A.; Alberdi, J. M.; Colmenero, J.; Grimm, H.; Richter, D.; Frick, B. Effect of blending on the PVME dynamics. A dielectric, NMR, and QENS investigation. *Macromolecules* **1999,** 32 (12), 4065-4078.

25. Yang, H.; Li, Z. S.; Qian, H. J.; Yang, Y. B.; Zhang, X. B.; Sun, C. C. Molecular dynamics simulation studies of binary blend miscibility of poly(3-hydroxybutyrate) and poly(ethylene oxide). *Polymer* **2004,** 45 (2), 453-457.

26. Zetsche, A.; Fischer, E. W. Dielectric studies of the α-relaxation in miscible polymer blends and its relation to concentration fluctuations. *Acta Polym.* **1994,** 45 (3), 168-175.

27. Jain, A. K.; Nagpal, A. K.; Singhal, R.; Gupta, N. K. Effect of dynamic crosslinking on impact strength and other mechanical properties of polypropylene/ethylene-propylene-diene rubber blends. *J. Appl. Polym. Sci.* **2000,** 78 (12), 2089-2103.

28. D., C.; Schwartz, G. A.; Alegria, A.; Colmenero, J. Combining configurational entropy and self-concentration to describe the component dynamics in miscible polymer blends. *J. Chem. Phys.* **2005,** 123 (14), 9.

29. Colmenero, J.; Arbe, A. Segmental dynamics in miscible polymer blends: recent results and open questions. *Soft Matter* **2007,** 3 (12), 1474-1485.

30. Mpoukouvalas; Floudas, K.; Zhang, G.; Runt, S. H. Effect of temperature and pressure on the dynamic miscibility of hydrogen-bonded polymer blends. *Macromolecules* **2005,** 38 (2), 552-560.

31. Mpoukouvalas, K.; Floudas, G. Effect of pressure on the dynamic heterogeneity in miscible blends of poly(methyl methacrylate) with poly(ethylene oxide). *Macromolecules* **2008,** 41 (4), 1552-1559.

32. Kamath, S.; Colby, R. H.; Kumar, S. K.; Karatasos, K.; Floudas, G.; Fytas, G.; Roovers, J. E. L. Segmental dynamics of miscible polymer blends: Comparison of the predictions of a concentration fluctuation model to experiment. *J. Chem. Phys.* **1999,** 111 (13), 6121-6128.

33. Kumar, S. K.; Colby, R. H.; Anastasiadis, S. H.; Fytas, G. Concentration fluctuation induced dynamic heterogeneities in polymer blends. *J. Chem. Phys.* **1996,** 105 (9), 3777-3788.

34. Lodge, T. P.; McLeish, T. C. B. Self-concentrations and effective glass transition temperatures in polymer blends. *Macromolecules* **2000,** 33 (14), 5278-5284.

35. Lutz, T. R.; He, Y. Y.; Ediger, M. D.; Pitsikalis, M.; Hadjichristidis, N. Dilute polymer blends: Are the segmental dynamics of isolated polyisoprene chains slaved to the dynamics of the host polymer? *Macromolecules* **2004,** 37 (17), 6440-6448.

36. Leroy, E.; Alegria, A.; Colmenero, J. Quantitative study of chain connectivity inducing effective glass transition temperatures in miscible polymer blends. *Macromolecules* **2002,** 35 (14), 5587-5590.

37. Leroy, E.; Alegria, A.; Colmenero, J. Segmental dynamics in miscible polymer blends: Modeling the combined effects of chain connectivity and concentration fluctuations. *Macromolecules* **2003,** 36 (19), 7280-7288.

38. Hirose, Y.; Urakawa, O.; Adachi, K. Dielectric study on the heterogeneous dynamics of miscible polyisoprene/poly(vinyl ethylene) blends: Estimation of the relevant length scales for the segmental relaxation dynamics. *Macromolecules* **2003,** 36 (10), 3699-3708.

39. Zhang, S. H.; Painter, P. C.; Runt, J. Dynamics of polymer blends with intermolecular hydrogen bonding: Broad-band dielectric study of blends of poly(4-vinyl phenol) with poly(vinyl acetate) and EVA70. *Macromolecules* **2002,** 35 (22), 8478-8487.

40. Schwartz, G. A.; Paluch, M.; Alegria, A.; Colmenero, J. High pressure dynamics of polymer/plasticizer mixtures. *J. Chem. Phys.* **2009,** 131 (4), 9.

41. Schwartz, G. A.; Alegria, A.; Colmenero, J. Adam-Gibbs based model to describe the single component dynamics in miscible polymer blends under hydrostatic pressure. *J. Chem. Phys.* **2007,** 127 (15), 8.

42. Schwartz, G. A.; Tellechea, E.; Colmenero, J.; Alegria, A. Correlation between temperature-pressure dependence of the alpha-relaxation and configurational entropy for a glass-forming polymer. *J. Non-Cryst. Solids* **2005,** 351 (33-36), 2616-2621.

43. Schwartz, G. A.; Cangialosi, D.; Alegria, A.; Colmenero, J. Describing the component dynamics in miscible polymer blends: Towards a fully predictive model. *J. Chem. Phys.* **2006,** 124 (15), 5.

44. Adam, G.; Gibbs, J. H. On temperature dependence of cooperative relaxation properties in glass-forming liquids. *J. Chem. Phys.* **1965,** 43 (1), 139-142.

45. Roland, C. M., Immiscible rubber blends. In *Advanced Structured Materials*, Springer, Ed. 2013; Vol. 11, pp 167-181.

46. Avgeropoulos, G. N.; Weissert, F. C.; Biddison, P. H.; Böhm, G. G. A. Heterogeneous blends of polymers. Rheology and morphology. *Rubber Chem. Technol.* **1976,** 49 (1), 93-104.

47. Bijarimi, M.; Zulkafli, H.; Beg, M. D. H. Mechanical properties of industrial tyre rubber compounds. *Journal of Applied Sciences* **2010,** 10, 1345-1348.

48. Fernandez-Berridi, M. J.; Gonzalez, N.; Mugica, A.; Bernicot, C. Pyrolysis-FTIR and TGA techniques as tools in the characterization of blends of natural rubber and SBR. *Thermochim. Acta* **2006,** 444 (1), 65-70.

49. Ghilarducci, A.; Cerveny, S.; Salva, H.; Matteo, C. L.; Marzocca, A. J. Influence of the blend composition in the internal friction of NR/SBR compounds. *Kautschuk Gummi Kunststoffe* **2001,** 54 (7-8), 382-386.

50. Mansilla, M. A.; Silva, L.; Salgueiro, W.; Marzocca, A. J.; Somoza, A. A study about the structure of vulcanized natural rubber/styrene butadiene rubber blends and the glass transition behavior. *J. Appl. Polym. Sci.* **2012,** 125 (2), 992-999.

51. Salgueiro, W.; Somoza, A.; Marzocca, A. J.; Torriani, I.; Mansilla, M. A. A SAXS and Swelling Study of Cured Natural Rubber/Styrene-Butadiene Rubber Blends. *J. Polym. Sci. Pt. B-Polym. Phys.* **2009,** 47 (23), 2320-2327.

52. Salgueiro, W.; Somoza, A.; Silva, L.; Consolati, G.; Quasso, F.; Mansilla, M. A.; Marzocca, A. J. Temperature dependence on free volume in cured natural rubber and styrene-butadiene rubber blends. *Phys. Rev. E* **2011,** 83 (5).

53. Marzocca, A. J.; Salgueiro, W.; Somoza, A., *Advances in Elastomers II*. Springer: 2013.

54. Hernandez, M.; Carretero-Gonzalez, J.; Verdejo, R.; Ezquerra T.A.; Lopez-Manchado, M. A., Molecular dynamics of natural rubber/layered silicate nanocomposites as studied by dielectric ralaxation spectroscopy. *Macromolecules* **2010**, 43 (2), 643-651.

2

Experimental Techniques

In this thesis the characterization of rubbers compounds was accomplished by means of differential scanning calorimetry (DSC), broadband dielectric spectroscopy (BDS) and atomic force microscopy (AFM). This chapter discusses these techniques in detail, and explains the experimental setup used to perform the experiments.

2.1 Differential scanning calorimetry (DSC)

Differential scanning calorimetry (DSC) is a thermal analytical technique to study physical transformations of materials such as phase transitions. In a DSC experiment, a sample of known mass is heated, cooled or held at constant temperature, and the changes in its heat capacity are registered as changes in the heat flow. This allows the detection of endothermic or exothermic transitions such as melting, glass transition, phase changes, or curing. Figure 2.1 shows a schematic diagram of the different components of the DSC equipment.

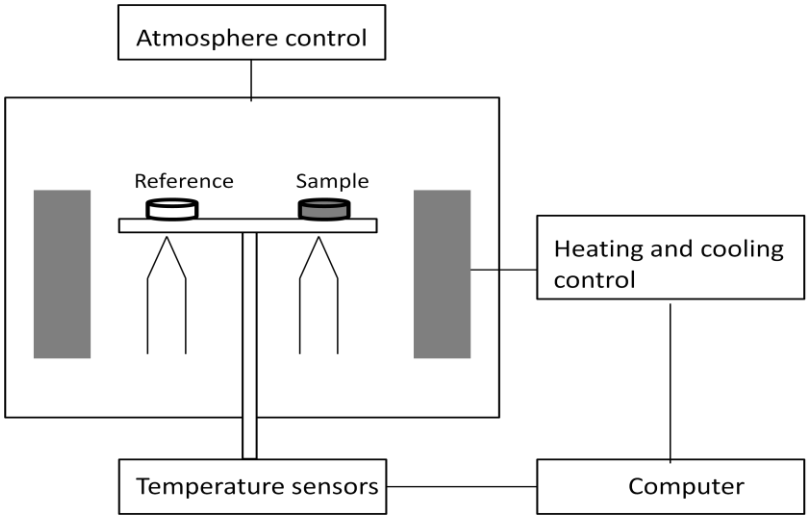

Figure 2.1 Schematic diagram of a differential scanning calorimeter.

The apparent heat capacity of the sample C_p is related to the differential heat flow (HF) by the heating rate *(dT/dt)*, assuming that the weight of the sample and reference pans is identical:

$$HF = C_p \frac{dT}{dt} \tag{2.1}$$

Figure 2.2 shows a representative curve of the most common types of thermal transitions observed in DSC defined below.

• *Glass transition temperature* (T_g) is defined as a reversible transition in amorphous materials (or regions within semi-crystalline materials) from a hard and relatively brittle "glassy" state into a viscous or rubbery state, as the temperature increases. T_g characterizes the range of temperatures over which this transition occurs.

• *Crystallization* is an exothermic transition associated to a partial alignment of molecular chains. The spatial conformation is reorganized forming ordered regions called *lamellae*. Crystallization processes affect optical, mechanical, thermal and chemical properties of the polymer.

• *Melting* is an endothermic transition (upon heating) from a crystalline solid state to a liquid state. The polymer loses its crystalline structure becoming a disordered liquid.

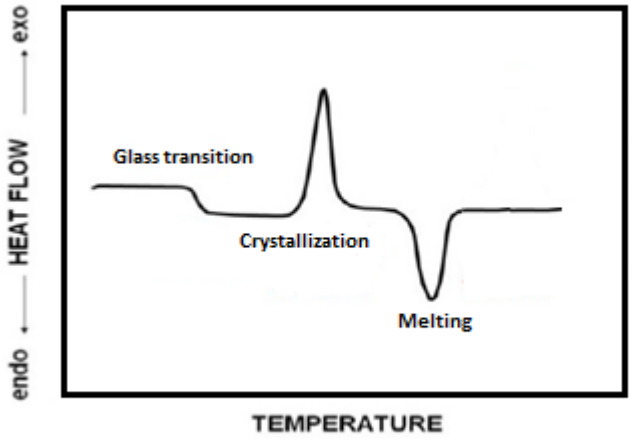

Figure 2.2 Representation of the heat flow as a function of temperature obtained from a DSC experiment showing a range of different transitions (glass transition, crystallization, melting) of a polymer.

2.2 Modulated temperature differential scanning calorimetry (MTDSC)

The operating principle of MTDSC[1, 2] differs from standard DSC in that it uses two simultaneous heating rates; a linear heating rate that provides information similar to standard DSC, and a sinusoidal or modulated heating rate that lets the simultaneous measurement of the sample's heat capacity (see Figure 2.3). This provides extra information about the thermal processes of the sample.

The sinusoidal temperature variation requires selecting a modulation period (seconds) and modulation temperature amplitude.

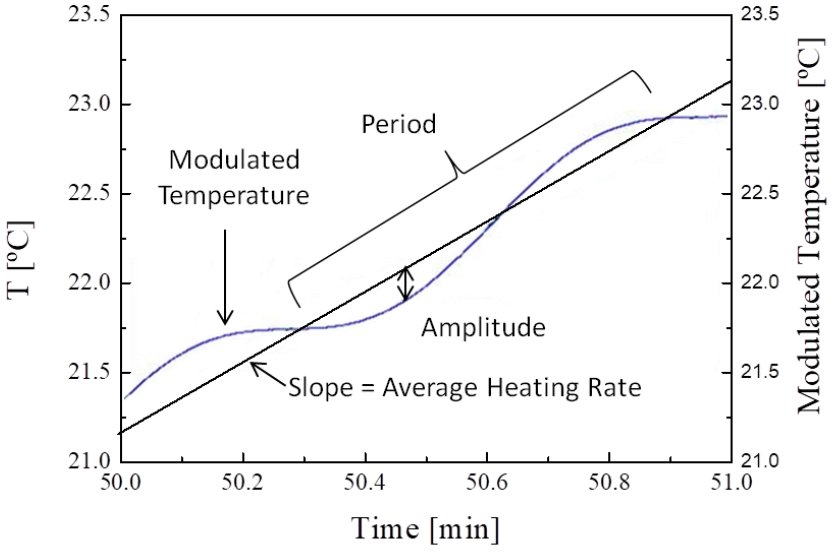

Figure 2.3 Temperature profile of a MTDSC experiment

In general, the use of MTDSC allows the separation of reversible and non-reversible components from the total heat flow[3]. The total heat flow is the sum of all the thermal events and it is similar to the heat flow seen in conventional DSC. The reversible heat flow includes thermal events that respond to changes in the ramp rate. A reversible event is, for instance, the glass transition temperature. On the contrary, those events that do not respond to changes in the ramp rate (e.g. crystallization) belong to the non-reversible heat flow. To perform this separation the heat flow signal is given by:

$$\frac{dH}{dt} = C_p \frac{dT}{dt} + f(T,t) \qquad (2.2)$$

Total = Reversible + Non-reversible

where dH/dT is the total heat flow due to the linear heating rate (equivalent to standard *DSC* at the same average heating rate). $C_p\, dT/dt$ give the reversible heat flow component, (where C_p is the heat capacity, and dT/dt corresponds to the measured heating rate, and finally the function $f\ (T,\ t)$ corresponds to the non-reversible component of the total heat flow.

2.2.1 DSC experimental setup

In the present thesis, the main objective of the DSC measurements is to determine the glass transition temperature (T_g), the increment in the heat capacity (ΔC_p) at T_g, and the width of the glass transition temperature (Δw).

Differential scanning calorimetry measurements performed in this thesis were carried out by using a DSC Q2000 from TA Instruments (see Figure 2.4) in standard and modulated modes. For standard DSC, cooling-heating cycles between -150 and 50 ºC with a heating/cooling rate of 10 K/min were carried out. For modulated DSC, the period was 100 s, the amplitude was 0.5 K and the underlying heating rate of 0.25 K/min was used. All DSC experiments were performed using nitrogen as transfer gas. The annealing time between cooling and heating runs was 5 minutes. In order to eliminate the thermo-mechanical history, the samples were annealed above T_g for 5 minutes. When samples have the ability to crystallize, a faster cooling ramp was used to avoid crystallization. The samples were prepared by encapsulating approximately 10 mg of each material in aluminum crucibles.

Figure 2.4 DSC Q2000 from TA Instruments used to measure the calorimetric response.

The glass transition temperature (T_g) was determined at the inflection point of the endotherm curve, heat capacity increment (ΔC_p) was estimated from the difference between the extrapolated heat capacity of the melt and the glass states both at T_g, and the width (Δw) of the glass transition was determined from the distance between the onset and end of the transition region (Figure 2.5).

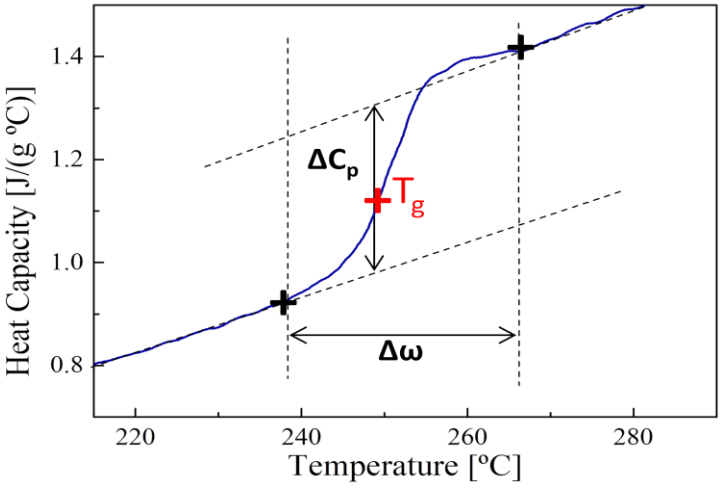

Figure 2.5 Example of the determination of T_g, ΔC_p and $\Delta\omega$ from DSC measurements.

2.3 Broadband dielectric spectroscopy (BDS)

2.3.1 Basis of dielectric relaxation and polarization mechanisms

Dielectric spectroscopy is a technique mainly used to study the relaxations caused by the rotational fluctuations of molecular dipoles. The study of the interaction of electromagnetic waves with matter in the frequency regime between 10^{-6} and 10^{12} Hz, is the core of BDS. The basis of dielectric relaxation spectroscopy as a tool to investigate molecular dynamics is the '*Fluctuation-Dissipation Theorem*', which states that the response of a system in thermodynamic equilibrium to a small applied disturbance (linear regime) is the same as its response to a spontaneous fluctuation[4, 5].

When materials containing permanent dipoles (with spontaneous fluctuation and randomly oriented due to thermal fluctuations) are placed in an alternating (sinusoidal) external electric field, the latter distorts the arrangement of molecular dipoles which tend to be preferentially oriented in the direction of the external field[4]. As shown in Figure 2.6, the dipolar orientation depends on the frequency of the applied field, and it is related to the dielectric permittivity (ε). This parameter characterizes the dielectric properties of materials containing polar molecules, and it can be defined as the measure (on neglecting atomic and electronic polarization) of the number of dipoles oriented by an external electric field with a constant magnitude[6]. Dielectric permittivity is usually written in the complex form[4]

$$\varepsilon^*(\omega) = \varepsilon'(\omega) - i\varepsilon''(\omega) \tag{2.3}$$

where ε^* is the complex dielectric permittivity, and ε' and ε'' the real and the imaginary parts, respectively. Regarding the frequency, the following equation is fulfilled; $\omega = 2\pi f$.

Relaxation processes are characterized by a peak in the imaginary part and a step-like decrease of the real part of the complex dielectric function with increasing frequency[4]. A schematic representation of the frequency dependence of $\varepsilon^*(\omega)$ is given in Figure 2.6. Both, the step in ε' and the loss peak in ε'' are centred at a characteristic frequency. At low frequencies, molecular dipoles can follow the electric field with a complete orientation giving rise to a plateau of the dielectric permittivity. This static value in the real part of the complex permittivity is called the static permittivity, ε_S, and is defined as $\varepsilon_s = \lim_{\omega \to 0} \varepsilon'(\omega)$ [4].

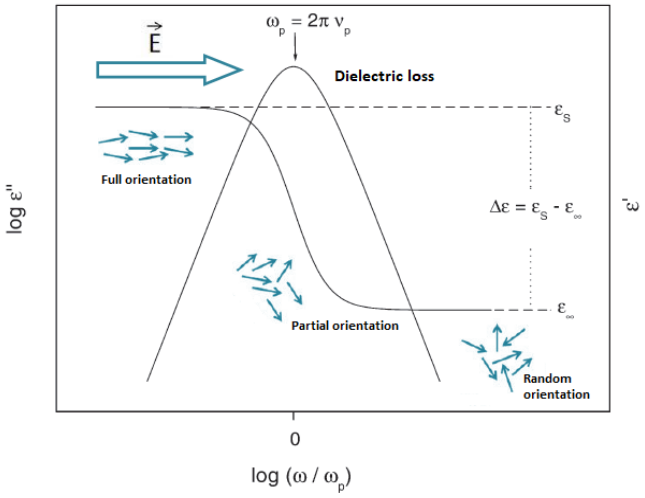

Figure 2.6 Scheme of the behaviour shown by dipoles when an external electric field is applied.

Thus, the dielectric orientational relaxation time (τ) can then be defined as the time required for dipoles to become field-oriented when applying an electric field[6]. For symmetric peaks, the relaxation time can be determined from the reciprocal of the loss peak frequency (when the dipolar relaxation reaches its maximum), ranging from several picoseconds, in low viscosity

liquids, to hours in glasses and even years (aging below the glass temperature)[7]. Equation (2.4) describes the relaxation time in function of the frequency

$$\tau = \frac{1}{2\pi\omega_{max}} \tag{2.4}$$

where ω_{max} corresponds with the frequency at the maximum loss.

The mayor drawback of this technique is that within this broad dynamic range, together with dipolar fluctuations, charge transport and interfacial polarization effects also take place[7]. All conductive systems contain dissolved free ions which, under the influence of an electric field, tend to move towards the electrode/sample interface. Interfacial polarization occurs when charge carriers are trapped at interfaces in heterogeneous systems, or when they are trapped at the electrode surface; namely, electrode polarization[7]. When arriving at the metallic electrodes, free ions are accumulated in thin layers immediately beneath the sample surface, leading to the development of ionic layers in such regions[8]. Unwanted effects, such ionic conductivity and electrode polarization, lead to difficulties in the interpretation of the dielectric spectra. Electrode polarization depends on the sample temperature, the structure of the electrodes, their composition and even the roughness of the electrode surface[9].

2.3.2 Dielectric experiments. Debye equation and other empirical models

In a typical dielectric experiment, the sample is placed between two gold plated electrodes creating a parallel plate capacitor with the sample as insulator (Figure 2.7).

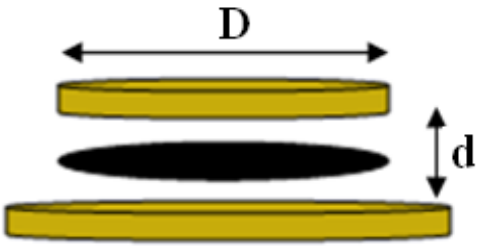

Figure 2.7 In BDS experiments; the sample is placed between two plane-parallel gold coated electrodes, where *D* represents the diameter of the upper electrode, and *d* the distance between both electrodes.

The electrical capacitance (*C*) of the material, when held between two plane-parallel electrodes of area (*A*) separated by a distance (*d*), is defined by

$$C = \varepsilon \cdot C_0 = \varepsilon \cdot \varepsilon_0 \frac{A}{d} = \varepsilon \cdot \varepsilon_0 \frac{\pi D^2}{4d} \tag{2.5}$$

where *C* is the capacity, C_o the capacitance of the same arrangement without the sample, ε the dielectric permittivity of the sample, ε_o the permittivity in the vacuum (8.854 pF m^{-1}), *A* the area of the electrodes, *d* the distance between them and *D* the diameter of the upper electrode.

In a dielectric measurement, the capacitor is subjected to a sinusoidal electric field (V = 1 Volt and a frequency $f = \omega/2\pi$), which causes a sinusoidal current of the same frequency and a phase shift between the current and the

voltage described by the phase angle ∅. Thus, by considering a sinusoidal excitation, Equation 5 can be rewritten in the complex form as

$$C^*(\omega) = \varepsilon^*(\omega) \cdot \varepsilon_0 \frac{A}{d} = \varepsilon^*(\omega) \cdot \varepsilon_0 \frac{\pi D^2}{4d} \tag{2.6}$$

The complex permittivity can be described as

$$\varepsilon^*(\omega) = \varepsilon'(\omega) - i\varepsilon''(\omega) = C^*(\omega) \cdot \frac{d}{\varepsilon_0 A} \tag{2.7}$$

Moreover, Debye[10] showed that for non-interacting molecules with a single relaxation time, the permittivity can be written as

$$\varepsilon^*(\omega) = \varepsilon'(\omega) - i\varepsilon''(\omega) = \varepsilon_\infty + \frac{\varepsilon_S - \varepsilon_\infty}{1 + i\omega\tau} = \varepsilon_\infty + \frac{\Delta\varepsilon}{1 + i\omega\tau} \tag{2.8}$$

where $i = (-1)^{1/2}$, $\Delta\varepsilon = \varepsilon_S - \varepsilon_\infty$ is the dielectric strength, ε_S and ε_∞ refer to the low frequency permittivity and the high frequency permittivity respectively and τ is the Debye relaxation time. Equation (8) is the so-called Debye equation[10], applicable only for the case of ideal systems, i.e., systems with a single time constant (τ), and composed of non-interacting dipoles. According to the previous equation, the real part corresponding to the permittivity factor, ε', is given by

$$\varepsilon'(\omega) = \varepsilon_\infty + \frac{\varepsilon_S - \varepsilon_\infty}{1 + \omega^2\tau^2} \tag{2.9}$$

whereas the imaginary component, ε'', known as the dielectric loss factor is given by

$$\varepsilon''(\omega) = \frac{(\varepsilon_s - \varepsilon_\infty)\omega\tau}{1+\omega^2\tau^2} \quad (2.10)$$

ε' is proportional to the energy stored reversibly in the system per period, and ε'' is proportional to the energy dissipated per period, that is, it accounts for the "delay" of the response to the excitation being proportional to the dissipated energy[4]. The Debye relaxation function shows a symmetric loss peak with a narrow width, being the full width at half maximum (FWHM) 1.14 decades in frequency for the dielectric loss[4] (see Figure 2.8).

The Debye equation represents the simplest problem of polarization, as it only considers a single relaxation time. However, this simple behaviour is not usually found, and only in rare cases a Debye-like relaxation behaviour is observed. Therefore, this model fails for describing the relaxation behaviour of many materials, which usually shows a loss peak significantly broader than that predicted by the Debye function. Moreover, in these cases, the dynamics is somewhat 'spread', making their shape asymmetric, and it is characterized by a distribution of several relaxation times rather than by a single time. This is the so called non-Debye or non-ideal relaxation behavior[4].

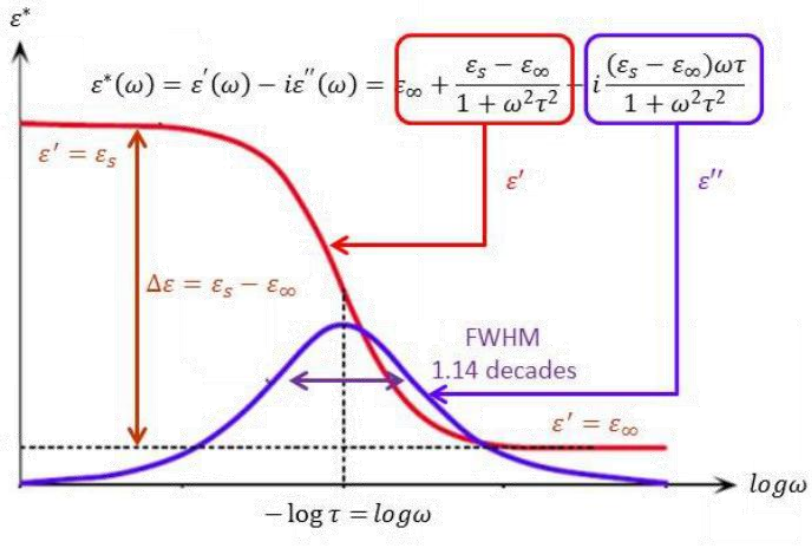

Figure 2.8 Frequency variation of the real and imaginary parts of the dielectric permittivity.

There are different empirical equations to account for the broadening and the asymmetry of the relaxation processes by generalizing the Debye function[4]. Among these empirical model functions the most important are the Cole - Cole (CC)[11,12, 13], and the Havriliak - Negammi (HN)[14, 15] equations in the frequency domain.

Cole-Cole equation

This empirical equation was given by K. S. Cole and R. H. Cole in 1941 to describe $\varepsilon^*(\omega)$. The Cole - Cole equation models a symmetrically-broadened loss curve (ε''), and it is described by:

$$\varepsilon^*(\omega) = \varepsilon_\infty + \frac{\Delta\varepsilon}{[1+(i\omega\tau_{cc})^\alpha]} = \varepsilon_\infty + \frac{\varepsilon_s - \varepsilon_\infty}{[1+(i\omega\tau_{cc})^\alpha]}$$

$$\varepsilon'(\omega) = \varepsilon_\infty + (\varepsilon_S - \varepsilon_\infty)\frac{1+(\omega\tau_{cc})^\alpha sin\frac{1}{2}(1-\alpha)\pi}{1+(\omega\tau_{cc})^\alpha sin\frac{1}{2}(1-\alpha)\pi+(\omega\tau_{cc})^{2\alpha}} \quad (2.11)$$

$$\varepsilon''(\omega) = (\varepsilon_S - \varepsilon_\infty)\frac{(\omega\tau_{cc})^\alpha cos\frac{1}{2}(1-\alpha)\pi}{1+2(\omega\tau_{cc})^\alpha sin\frac{1}{2}(1-\alpha)\pi+(\omega\tau_{cc})^{2\alpha}}$$

where $\Delta\varepsilon = \varepsilon_0 - \varepsilon_\infty$ is the relaxation strength and α parameter quantifies the symmetrical broadening of the relaxation time distribution around the so-called Cole-Cole relaxation time (τ_{CC}), which gives the position of maximal loss by $\omega = 2\pi f = 1/\tau_{CC}$. α parameter varies in the range (0,1]. This expression reduces to the Debye equation for α = 1.

The Havriliak-Negami equation

For representing broadened and asymmetrically shaped dispersion and loss curves, the Havriliak - Negami (HN) equation is considered. It is the most versatile fitting function:

$$\varepsilon*(\omega) = \varepsilon_\infty + \frac{\Delta\varepsilon}{[1+(i\omega\tau_{HN})^\alpha]^\beta}$$

$$\varepsilon'(\omega) = \varepsilon_\infty + (\varepsilon_S - \varepsilon_\infty)\frac{cos\beta\varphi}{\left[1+2(\omega\tau_{HN})^\alpha sin\frac{1}{2}(1-\alpha)\pi+(\omega\tau_{HN})^{2\alpha}\right]^{\frac{\beta}{2}}} \quad (2.12)$$

$$\varepsilon''(\omega) = (\varepsilon_S - \varepsilon_\infty)\frac{sin\beta\varphi}{\left[1+2(\omega\tau_{HN})^\alpha sin\frac{1}{2}(1-\alpha)\pi+(\omega\tau_{HN})^{2\alpha}\right]^{\frac{\beta}{2}}}$$

where φ is given by:

$$\varphi = \frac{arctg\left[(\omega\tau_{HN})^\alpha cos\frac{1}{2}\pi(1-\alpha)\right]}{1+(\omega\tau_{HN})^\alpha sin\frac{1}{2}\pi(1-\alpha)} \quad (2.13)$$

α and β parameters represent the shape of the dielectric spectra. For $\beta = 1$ this equation is reduced to a Cole - Cole equation and the Debye equation is recovered when $\alpha = \beta = 1$.

2.3.3 Dielectric relaxations and their temperature dependence

Many experiments in different systems show that two types of relaxation processes occur, distinguished by their temperature dependence of the relaxation time. These are the so-called α-and β-relaxations. The α-relaxation is a cooperative process related to the structural relaxation of the material. β-relaxations are secondary relaxations, attributed to localized rotational fluctuations of the dipole vector, i.e., local conformational rearrangements[4]. α- and β-relaxation processes describe motions subjected to interactions of both intra and intermolecular nature[4]. By increasing the temperature, these relaxation processes move to higher frequencies (or shorter times) (see Figure 2.9). Depending on the temperature dependence of the relaxation times, these processes can be described by the Arrhenius equation or the Vogel - Fulcher - Tammann equation.

The Arrhenius equation

It was originally introduced to describe the variation of the rate constant (k) of a chemical reaction with temperature, based on the idea that particles are pushed by thermal fluctuations to make transitions between two energetic levels where an energy barrier E_a must be overcome. It also represents a widely used way for describing the linear inverse temperature dependence of relaxation times:

$$k = Ae^{-E_a/RT} \rightarrow \tau = \tau_0 exp\left(\frac{E_a}{kT}\right) \tag{2.14}$$

where E_a is the activation energy related to rotational barriers, k is the Boltzmann's constant and τ_0 is related to the vibrational molecular motion. In systems which exhibit local molecular mobility below T_g, the inverse temperature dependence of the relaxation times corresponding to β-relaxation processes is linear (Figure 2.9), and therefore, described by the Arrhenius law.

Vogel-Fulcher-Tammann equation (also called super Arrhenius)

The nonlinearity dependence of the relaxation times with inverse temperature can be described via the empirical Vogel - Fulcher - Tamman (VFT) equation:

$$k = Ae^{-DT_0/(T-T_0)} \rightarrow \tau = \tau_o exp\left(\frac{DT_o}{T-T_o}\right) \tag{2.15}$$

where D is the fragility parameter and T_0 denotes the Vogel temperature, sometimes also called ideal glass transition temperature, which is usually found to be approximately 40 K below T_g.

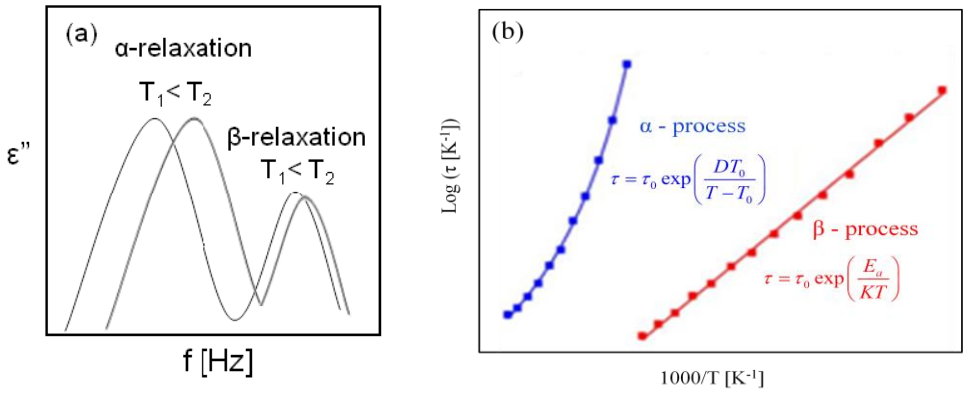

Figure 2.9 a) Relaxations move to higher frequencies when increasing temperature. (b) Relaxation times against the inverse of the temperature. Comparison of the temperature dependence for α- (VFT temperature dependence) and β-processes (Arrhenius temperature dependence).

2.3.4 BDS experimental setup

BDS measurements were carried out on a high-resolution dielectric analyser from Novocontrol (Figure 2.10) in the frequency range from 10^{-2} to 10^{6} Hz. Isothermal frequency scans were performed every five degrees below T_g, and every third degrees above T_g. The sample temperature was controlled by means of a Quattro temperature controller using nitrogen gas flow providing temperature stability better than ± 0.1 K. Figure 2.11 shows a diagram of the equipment and the constituent parts.

Figure 2.10 Novocontrol alpha analyzer and nitrogen Dewar.

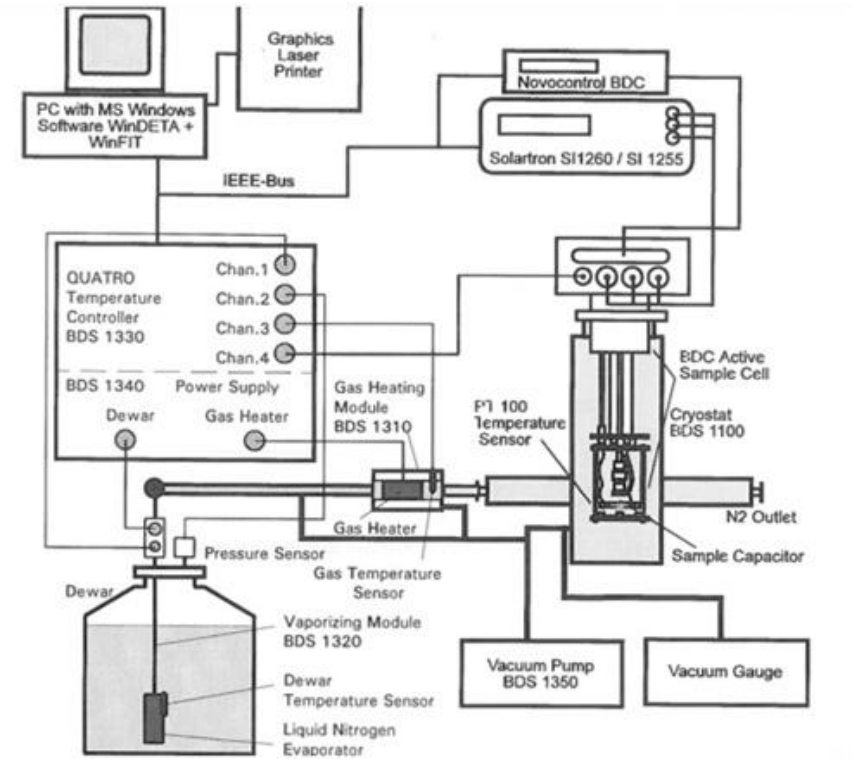

Figure 2.11 Diagram of a Novocontrol dielectric analyser and temperature controller.

The dielectric analyser relates the measured impedance (Z^*) with the complex permittivity by means of:

$$Z^*(\omega) = \frac{1}{i\omega\varepsilon^*(\omega)c_0} \tag{2.16}$$

where C_0 is the vacuum capacitance of the arrangement, and ε^* the permittivity of free space.

2.3.5 Fitting dielectric results

Fittings of the experimental data were performed using the Winfit software (version 3.4). The obtained dielectric permittivity results were analysed by fitting the real and the imaginary parts of the complex permittivity (see Figure 2.12).

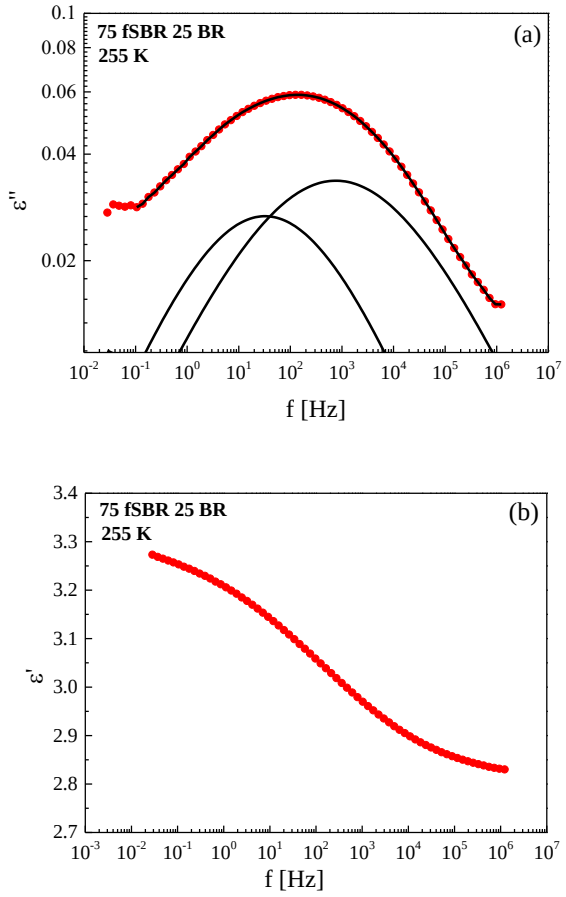

Figure 2.12 Example of the fittings of the imaginary (a) and real (b) parts of the dielectric permittivity for the 75 SBR 25 BR sample at T = 255 K.

2.4 Atomic force microscopy (AFM)

Atomic force microscopy is a widely used technique for the structural characterization of materials at the nano-scale. In general, it works by measuring the vertical motion of a probe with a sharp tip. AFM can be broadly divided into three parts:

- Probe: sharp tip at the end of a flexible cantilever
- Detector and feedback electronics
- Piezoelectric transducers

A schematic picture of an AFM is shown in Figure 2.13.

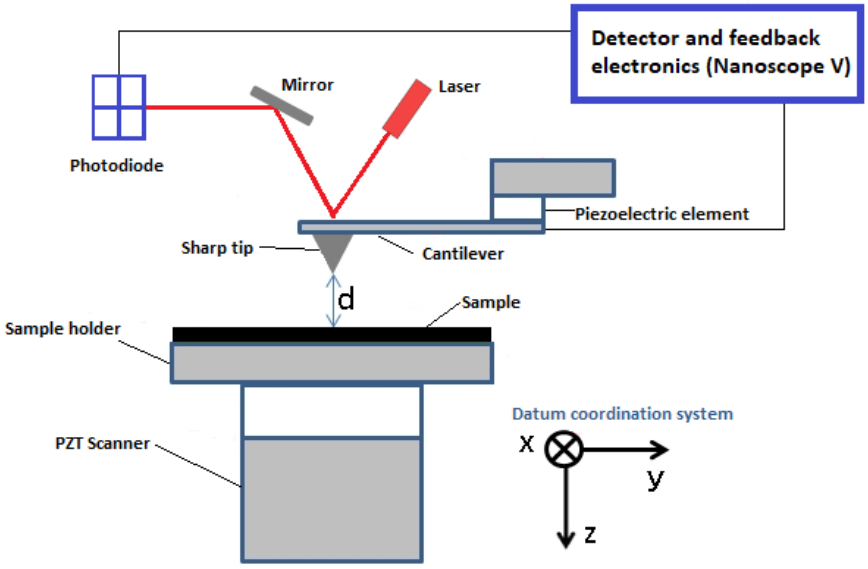

Figure 2.13. Schematic representation of an AFM.

The principle of AFM operation is to sense the tip-sample forces. This is achieved by using a mechanical probe made of a cantilever having a sharp tip at the end. When the tip is close to the sample surface, forces between the tip

and the sample lead to a deflection of the cantilever according to Hooke's law. Typically, the deflection of the cantilever is measured using a laser spot reflected from its top surface into a four-segment photodiode. When the probe interacts with the sample surface, the path of the reflected laser beam changes which in turn brings about changes in the four-segment photodetector. The force, thus, can be monitored by measuring the change in the light detected by the four-segment photodetector[16].

2.4.1 Imaging modes

Traditionally, AFM has been used to image the topography of the sample's surface. Imaging can be performed by operating the AFM in different modes, depending on the application. In general, imaging modes are divided into: 1) static (*contact*), 2) dynamic (*non-contact*) or 3) intermittent contact (*tapping*) modes. Here, we will focus on the last two modes.

Dynamic mode (non-contact mode)

In this mode, the cantilever is externally excited, using an additional piezoelectric crystal close to its fundamental resonance frequency. When the oscillating cantilever scans the sample surface, its oscillation amplitude, phase and resonance frequency are modified due to tip-sample interactions.

Intermittent contact (tapping mode)

In the tapping mode[17], the cantilever scans the surface while vibrating at a certain frequency (close to its resonance frequency generally in the range of 15 and 300 KHz). The system feedback controls the vibration of the tip at a certain amplitude set-point, imposing that the amplitude of the periodic

movement must be kept constant as topographic features are found and therefore producing a vertical deflection on the cantilever beam.

2.4.2 Mechanical property measurements

AFM measures the tip-sample interaction at each (*x,y*) data points of the sample surface. Topography of the sample is acquired from tip-sample interactions using a feedback loop. Likewise, the tip-sample interaction can also be used to derive the information about mechanical, chemical, electromagnetic, and thermal properties of the sample surface. In tapping mode, AFM can provide information about the mechanical properties of the surface of the sample by means of the phase imaging while, at the same time, information of the topography is also acquired[18-19].

In addition, it is also possible to measure the mechanical response at a given point of the sample's surface. In these cases, the data from an experiment is often displayed as a simple x-y plot[18] being "*x*" the tip-sample distance and "*y*" the force between the tip and the sample. The deflection of the cantilever, gives a direct measure of the interaction force. These "force-distance" plots are often called "force curves" (see Figure 2.14).

In order to obtain the mechanical modulus, the force curves were fitted using the Derjaguin–Muller–Toporov (DMT) model[19]:

$$F - F_{adh} = \frac{4}{3} E^* \sqrt{R(d - d_0)^3} \tag{2.17}$$

where F is the force on the cantilever relative to the adhesion force F_{adh}, R is the tip end radius, and $(d - d_0)$ is the deformation of the sample, i.e. penetration of the tip in the sample. The result of this fit is the reduced modulus E^*. Then, the Young's Modulus (E) of the sample can be calculated with the following equation:

$$E^* = \left[\frac{1-\nu_s^2}{E} + \frac{1-\nu_{tip}^2}{E_{tip}}\right]^{-1} \quad (2.18)$$

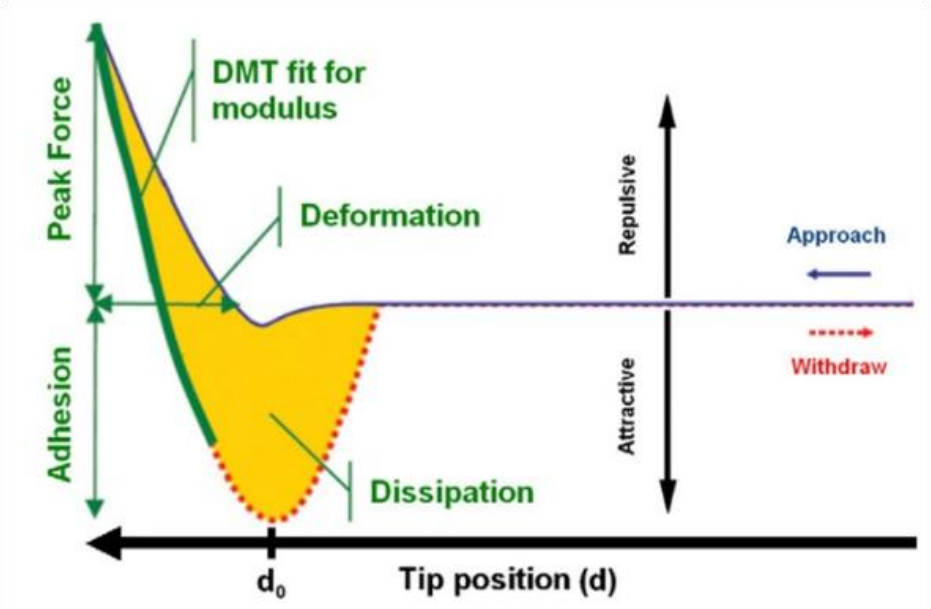

Figure 2.14. Schematic peak-force tapping Force-Separation curve[20]. The blue line shows the tip approach (up to the point in which the detected force equals the peak-force), while the red line stands for the tip withdrawal. In this working mode, the maximum force on the sample (i.e.: peak force) is constant throughout each approach-withdrawal cycle.

where ν_s is the Poisson's ratio of the sample, and ν_{tip} and E_{tip} are the Poisson's ratio and the mechanical modulus of the tip, respectively.

Dissipation

Energy dissipation[21] is given by the force times the velocity integrated over one period of the vibration (yellow area in Figure 2.14);

$$W = \int \vec{F} \bullet d\vec{Z} = \int_0^T \vec{F} \bullet \vec{v} dt \tag{2.19}$$

where W represents energy dissipated per cycle of interaction. F is the interaction force vector and dZ is the displacement vector. Because the velocity reverses its direction in each half cycle, the integration is zero if the loading and unloading curves coincide. For pure elastic deformation there is no hysteresis between the repulsive parts of the loading-unloading curve, corresponding to very low dissipation. In this case the work of adhesion becomes the dominant contributor to energy dissipation.

2.4.3 AFM experimental setup

The AFM measurements were done by using a Bruker Multimode 8 AFM from Bruker with a NanoScope V Controller. The scanner was a 7655JVHC from Veeco Instruments Inc (Bruker). Samples for AFM were cut using a cryo-microtome at low temperatures with a thickness of ~10 μm. Figure 2.15 shows a schematic picture, as well as the different components of the equipment used in this thesis.

A nano-mechanical mapping of the surface was performed operating in Peak-Force Tapping Mode. RTESP-A 150 probes (Bruker) were calibrated with Sapphire (for the spring constant and photodiode sensitivity) and PS samples (for the tip radius). To avoid tip damage, the peak force set point was kept at about 3 (± 0.5) nN for all the experiments.

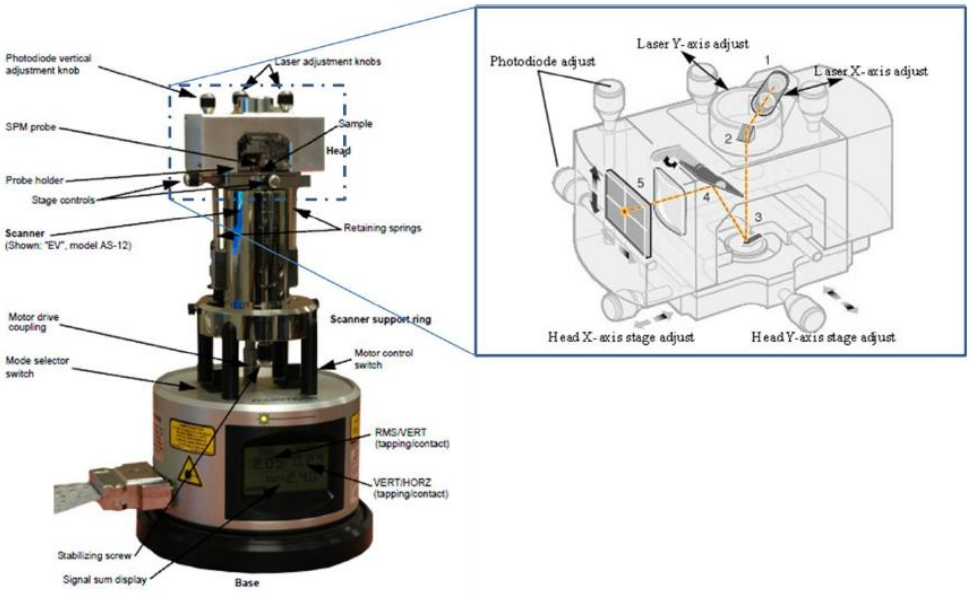

Figure 2.15. Multimode 8 AFM from Bruker

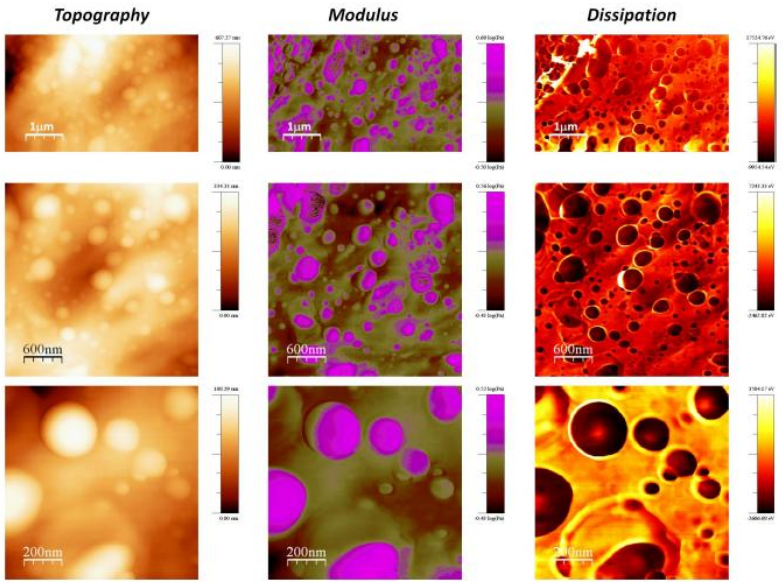

Figure 2.16. Topography, DMT modulus and dissipation images for 50 fSBR/50 NR blend.

In addition to the topographical images, PeakForce QNM provides maps of several mechanical properties, such as adhesion, dissipation, elastic modulus (DMT-modulus), and deformation. Figure 2.16 shows an example of the images obtained for the 50 fSBR 50 NR immiscible blend. As can be seen, SBR islands are embedded in a NR matrix.

2.5 Crosslink density determination

Equilibrium swelling is a simple and common experiment to determine the crosslink density of networks. By using this method, the crosslink density of fSBR compounds containing different amount of accelerators (Chapter 6) has been calculated.

Samples were immersed in toluene at 25 ºC for a period of 72 h, renewing the solvent every 24 h. Later, the samples were dried using tissue paper to remove the excess of toluene weighed immediately. Finally, the samples were dried in a vacuum oven for 24 h at 60º C until constant weight.

The density of the samples was determined with the aid of a liquid whose density (ρ_l) is known (ethanol). The solid was weighed in air and then in ethanol. The density (ρ) was calculated from the two weighing by using Equation (2.20):

$$\rho = \frac{P_a \rho_a - P_l \rho_a}{P_a - \rho_l} \tag{2.20}$$

where P_a and P_l are the weights of the sample in air and ethanol respectively, ρ_l is the density of ethanol (0.806 cm^3/g), and ρ_a is the density of the air (0.002 cm^3/g for relative air humidity of 75% and 25 ºC).

The determination of P_a has been performed by using an analytical balance Sartorius Instrument CPA224s with a resolution of ± 0.1 mg, and a density kit (see Figure 2.17). The density of the compounds was calculated after and before swelling in toluene in order to establish the contribution of all the soluble compounds present in the sample.

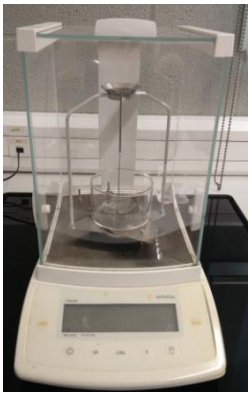

Figure 2.17 Analytical balance and density kit used for the density calculation.

Once the density of the compounds is known, crosslink density can be calculated by[22]:

$$\mu = \frac{\rho}{2 \cdot M_c} \tag{2.21}$$

where M_c is the average mass of network chains between crosslinks[23].

A more complete description of the method for the determination of the crosslink density can be seen in the appendix section.

2.6 References

1. Thomas, L. C., Modulated DSC. An Overview and Summary of Advantages and Disadvantages Relative to Traditional DSC TA instruments: 2005.

2. Newman, A., Using thermal techniques for amorphous materials. In *Pharmaceutical powder X-ray diffraction symposium*, 2012.

3. Thomas, L. C. Modulated DSC. An Overview and Summary of Advantages and Disadvantages Relative to Traditional DSC *TA instruments* **2005,** Paper 1.

4. F.Kremer; Schönhals, A., *Broadband Dielectric Spectroscopy*. 2003.

5. Kubo, R., *The fluctuation-dissipation theorem*. Reports on Progress in Physics: 1966; Vol. 29.

6. Gregory, R. B., *Protein-solvent interactions*. Marcel Dekker, Inc.: 1995.

7. Floudas, G., *Polymer Science: A Comprehensive Reference*. Elsevier: 2012; Vol. 2.

8. Emmert, S.; Wolf, M.; Gulich, R.; Krohns, S.; Kastner, S.; Lunkenheimer, P.; Loidl, A. Electrode polarization effects in broadband dielectric spectroscopy. *European Physical Journal B* **2011,** 83 (2), 157-165.

9. Ben Ishai, P.; Talary, M. S.; Caduff, A.; Levy, E.; Feldman, Y. Electrode polarization in dielectric measurements: a review. *Measurement Science and Technology* **2013,** 24 (10).

10. Debye, P., *Polar molecules*. J. Soc. Chem. Ind.: 1929; Vol. 48.

11. Cole, K. S.; Cole, R. H. Dispersion and absorption in dielectrics I. Alternating current characteristics. *J. Chem. Phys.* **1941,** 9 (4), 341-351.

12. Davidson, D. W.; Cole, R. H. Dielectric relaxation in glycerine *Journal of Chemical Physics* **1950,** 18 (10), 1417-1417 DOI: 10.1063/1.1747496.

13. Davidson, D. W.; Cole, R. H. Dielectric relaxation in glycerol, propylene glycol and normal propanol. *Journal of Chemical Physics* **1951,** 19 (12), 1484-1490 DOI: 10.1063/1.1748105.

14. Havriliak, S.; Negami, S. A complex plane analysis of α-dispersions in some polymer systems. *Journal of Polymer Science Part C-Polymer Symposium* **1966,** 14 (1), 99-117.

15. Havriliak, S.; Negami, S. A complex plane representation of dielectric and mechanical relaxation processes in some polymers. *Polymer* **1967,** 8 (4), 161-210.

16. Eaton, P.; West, P., *Atomic Force Microscopy*. Oxford: 2010.

17. Kaemmer, S. B., Introduction to Bruker's scanasyst and peakforce tapping AFM technology. Bruker: 2011.

18. A practical guide to AFM force spectroscopy and data analysis JPK instruments: 2005.

19. García, R., *Amplitude Modulation Atomic Force Microscopy*. Wiley-VCH: 2010.

20. Maybrun, M., PeakForce QNM e-Training. Veeco: 2010.

21. Pittenger, B.; Erina, N.; Su, C. Quantitative mechanical property mapping at the nanoscale with peakforce QNM. **2012**.

22. Gronski, W.; Hoffmann, U.; Simon, G.; Wutzler, A.; Straube, E. Structure and density of crosslinks in natural-rubber vulcanizates. A combined analysis by NMR spectroscopy, mechanical measurements, and rubber-elastic theory. *Rubber Chem. Technol.* **1992,** 65 (1), 63-77.

23. Valentin, J. L.; Carretero-Gonzalez, J.; Mora-Barrantes, I.; Chasse, W.; Saalwachter, K. Uncertainties in the determination of cross-link density by equilibrium swelling experiments in natural rubber. *Macromolecules* **2008,** 41 (13), 4717-4729.

3

Materials

This chapter includes a general introduction of the materials studied in this thesis. Neat polymers, additives and fillers are introduced and afterwards, the formulation used to vulcanize the compounds is also given. Finally, the composition of the samples used in each chapter is also reported. Full formulations of the compounds are given in the appendix.

3.1 Materials

3.1.1 Polymers

The following polymers, with interest to the tire industry, have been used in this thesis:

- Natural rubber (NR)
- High cis polybutadiene rubber (BR)
- Three different styrene butadiene rubbers:

    1) Amine functionalized styrene butadiene rubber (SBR) with trade name: Trinseo SLR4601.

2) Chain end functionalized SBR (fSBR) functionalized with an alkoxysilane group and at least one of a primary amine group and thiol group. Trade name: Trinseo SLR4602.
3) Styrene butadiene rubber with a different microstructure compared to SBR (SBR2). This polymer is functionalized with an alkoxysilane group and at least one of a primary amine group and thiol group. Trade name: Trinseo SLR3402.

Figure 3.1 shows the molecular structure of the elastomers listed above. The microstructures as well as the molecular weight (Mw) are given in Table 3.1.

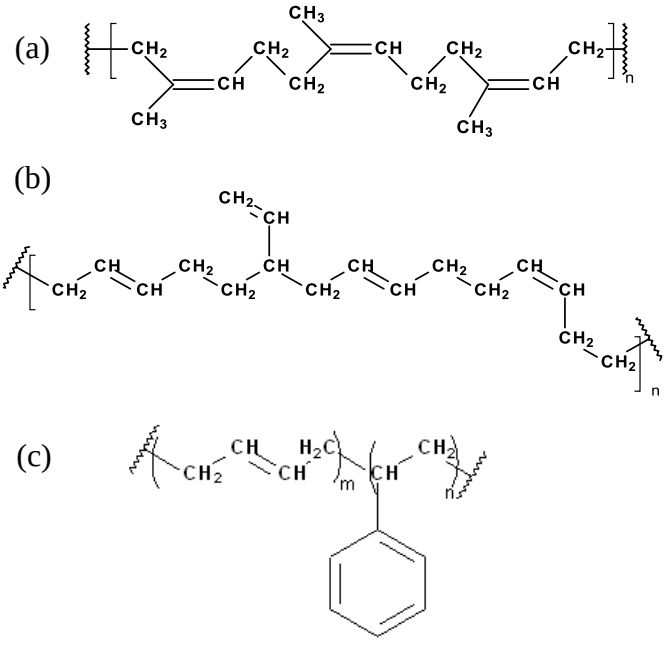

Figure 3.1 General structures of the polymers studied in this thesis. Natural rubber (NR) (a), butadiene rubber (BR) (b) and styrene butadiene rubber (SBR) (c).

Table 3.1 Microstructure of the materials studied in this thesis

	Styrene	**Cis**	**Trans**	**Vinyl**	**M_w**
SBR	21	11	18	50	288000
f SBR	21	11	18	50	288000
SBR 2	15	27.5	27.5	30	300000
BR	-	96	2	2	480000

Besides the study of neat compounds, miscible (SBR/BR, fSBR/BR, SBR2/BR) and immiscible (fSBR/NR) blends of these polymers have also been studied:

3.1.2 Filler

The filler used in this thesis, was precipitated amorphous silica (Hi-Sil 315 G-D from PPG) with a BET N_2 specific surface area of 125 m^2/g. Filler particles are typically added to rubber blends to improve the mechanical properties of the compounds. Since silica contains a large number of hydrophilic silanol (Si-OH) groups on the surface that are not compatible with hydrophobic hydrocarbon rubbers, coupling agents have to be included in the formulation to modify the surface of the silica and to improve the compatibility between the filler and the polymers[1].

The coupling agent was bis[3-(triethoxysilyl)propyl] tetrasulfide (TESPT). Figure 3.2 shows a possible structure of the resulting product after the reaction between the silica, TESPT, and the polymer.

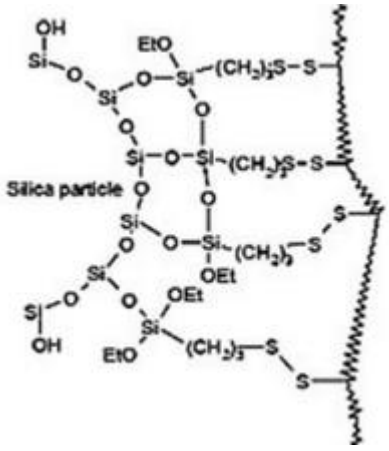

Figure 3.2 Schematic representation of rubber-to-filler-bonds.

3.1.3 Curing additives - Accelerators

Sulphur vulcanized rubber compounds are obtained by mixing a neat polymer or crude mixture with a series of additives before being subjected to high temperature and pressure. The type of the neat polymer as well as the additives is closely related to the properties and applications to be achieved. Rubber vulcanization using sulphur alone is a slow and inefficient process. The use of accelerators makes the vulcanization process faster and more efficient[2]. Functionally, accelerators are classified as primary and secondary, based on the role they play in the vulcanization reaction. Primary accelerators provide considerable scorch delay, medium/fast cure, and good mechanical properties, whereas secondary accelerators provide very fast cure, and are generally used in combination with primary accelerators to obtain even faster cures[3].

The formulation of the materials studied in this thesis includes both primary and secondary accelerators. The secondary accelerator is 1,3-Diphenylguanidine (DPG), and the primary accelerator is N-Cyclohexylbenzothiazole-2-sulphenamide (CBS). Figure 3.3 shows the chemical structure of these additives.

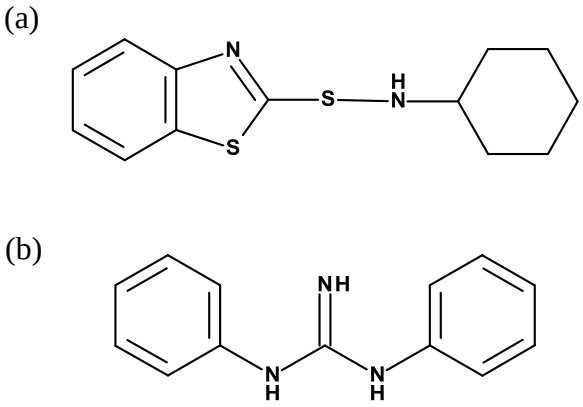

Figure 3.3 Chemical structure of N-Cyclohexylbenzothiazole-2-sulphenamide (CBS) (a) and 1,3-Diphenylguanidine (DPG) (b)

3.2 Formulation of the compounds

All the compounds used in this thesis were provided and prepared at Goodyear Tire and Rubber Company (Goodyear Innovation Centre, Luxembourg). The samples were prepared following a simplified procedure as used in tire industry. All the ingredients except sulphur and accelerators were added in a first stage to an internal mixer, where the batch reaches 150 °C. In a second stage, sulphur and accelerators were added and mixing continued until the batch reached 110 °C.

The formulation of the vulcanization recipe used for the preparation of the compounds is summarized in Table 3.2 (unfilled samples) and Table 3.3 (filled samples).

Table 3.2 Formulation [phr] of the cure system for the unfilled compounds.

Unfilled samples	
Rubber	100
Wax	2
Antioxidant	4
Processing Oil	3
Stearic Acid	3
ZnO	2.5
Sulphur	1.4
Accelerator (DPG)	0 - 1.6
Accelerator (CBS)	0 - 1.6
Sulphur-Donor	2

Table 3.3 Formulation [phr] of the cure system for the filled compounds.

Filled samples	
Rubber	100
Wax	2
Antioxidant	4
Processing Oil	40
Stearic Acid	3
Coupling Agent (TESPT)	7.5
Silica	120
ZnO	2.5
Sulphur	1.4
Accelerator (DPG)	1.6
Accelerator (CBS)	3.5
Sulphur-Donor	2

Cured square sheets of 100 x 100 x 0.7 mm dimensions were obtained in a curing press held at 170 °C for ten minutes. The compounds were stored in a freezer at -15 ºC in order to avoid aging.

3.2.1 Additives and neat functionalized SBR (Chapter 4)

The compounds studied in chapter 4 are made of chain end functionalized (fSBR). Two different sets of samples have been analysed. On the one hand, six samples with the same formulation, but each of them, excluding one additive class. On the other hand, seven samples with variations in the amount of accelerators ((0 to 1.2) for DPG, and (0.4 and 1) for CBS) were prepared. The composition of all the samples studied in this chapter is shown in Tables 3.4 and 3.5.

Table 3.4 Formulation [phr] of the samples studied in Chapter 4, where for each sample one ingredient was systematically removed leaving the rest of the formulation used for vulcanization unchanged.

Sample	Full	No oil/wax	No Antiox.	No Sulphur donor	No accelerators	No stearic acid
fSBR	100					
Wax	2		2	2	2	2
Antioxidant	4	3.25		4	4	4
Processing Oil	3		3	3	3	3
Stearic Acid	3	3	3	3	3	
ZnO	2.5	2.5	2.5	2.5	2.5	2.5
Accelerator (DPG)	1.6	1.6	1.6	1.6		1.6
Accelerator (CBS)	1.2	1.2	1.2	1.2		1.2
Sulphur	1.4	1.4	1.4	1.4	1.4	1.4
Sulphur-Donor	2	2	2		2	2

Table 3.5 Composition [phr] of the samples studied in Chapter 4, where the amount of one accelerator has kept constant and the other one has been varied.

Sample	f-SBR	DPG	CBS
1.2 DPG	100	1.2	1.6
0.9 DPG		0.9	
0.6 DPG		0.6	
0.3 DPG		0.3	
0 DPG		0	
1 CBS		1.2	1
0.4 CBS			0.4

3.2.2 Miscible blends (Chapter 5)

Blending is a favourable method to obtain new materials with desirable properties (normally between those of the neat components) using already known polymers. Filled and unfilled miscible blends of high cis butadiene rubber (BR), styrene butadiene rubber (SBR2), and chain-end functionalized styrene butadiene rubber (fSBR) were studied in Chapter 5. For the unfilled SBR2/BR samples, the secondary accelerator (DPG) was not used in order to avoid the low frequency contribution analysed in Chapter 4. Tables 3.6 to 3.8 give the composition of all the samples studied in this chapter.

Table 3.6 Composition [phr] of the unfilled and filled fSBR/BR samples studied in chapter 5.

Samples	fSBR	BR
100fSBR	100	-
75fSBR 25BR	75	25
60SBR 40BR	60	40
50fSBR 50BR	50	50
40fSBR 60BR	40	60
25fSBR 75BR	25	75
100BR	-	100

Table 3.7 Composition [phr] of the unfilled and filled SBR/BR samples studied in Chapter 5.

Samples	SBR	BR
100SBR	100	-
75SBR 25BR	75	25
60SBR 40BR	60	40
50SBR 50BR	50	50
40SBR 60BR	40	60
25SBR 75BR	25	75
100BR	-	100

Table 3.8 Composition [phr] of the unfilled and filled SBR2/BR samples studied in Chapter 5.

Samples	SBR2	BR
100SBR2	100	-
75SBR2 25BR	75	25
50SBR2 50BR	50	50
25SBR2 75BR	25	75
100BR	-	100

3.2.3 Immiscible blends (Chapter 6)

In the majority of cases, polymer blends are immiscible therefore resulting in segregation of phases. The study of the phase morphology gives the possibility of obtaining new materials with different properties. Unfilled immiscible blends of chain-end functionalized styrene butadiene rubber (fSBR) and natural rubber (NR) have been studied in Chapter 6.

Table 3.9 Composition [phr] of the unfilled fSBR/NR samples studied in Chapter 6.

Samples	fSBR	NR
100fSBR	100	-
75fSBR 25NR	75	25
50fSBR 50NR	50	50
25fSBR 75NR	25	75
100NR	-	100

3.3 Sample preparation procedures for BDS measurements

Samples required for BDS experiments were punched out from the rubber sheets using a die of 30 mm. For the filled samples, gold was sputtered on their surface (Figure 3.4) to improve the electric contact between the sample and the electrodes, using an Edwards Scancoat six sputter coater for five minutes at 1.3 kV, 35 mA, $8 \cdot 10^{-2}$ mbar.

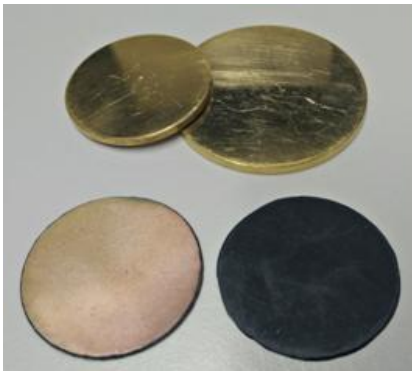

Figure 3.4 Filled sample with gold sputter coating and unfilled sample, respectively.

To remove the humidity adsorbed at the surface of the silica particles, the samples were dried under nitrogen atmosphere during 4 hours at T = 100 ºC and 2 more hours at T = 60 ºC. In addition before the measurements, both unfilled and filled samples were cleaned with acetone in order to remove impurities from the surface.

3.4 References

1. Salimi, D.; Khorasani, S. N.; Rezaei, M.; Jahanbani, S., Optimization of physico-mechanical properties of silica-filled NR/SBR compounds. *Advances in Polymer Technology* **2009,** *28* (4), 224-232.

2. Vulcanization and accelerators. Nocil limited. Arvind Mafatlal Group: 2010.

3. Datta, R. N., *Current Topics in Elastomer Research*. CRC Press: New York, 1954.

4

Influence of vulcanization additives on the dielectric response of chain-end functionalized styrene butadiene rubber

Rubber compounds used in the tire industry[1] are vulcanized in order to enhance different properties (e.g. mechanical, thermal, etc) in the final products[2]. Un-vulcanized rubbers are not strong materials due to their stickiness and plasticity, nevertheless after vulcanization, the chemical structure changes due to the formation of crosslinks and the polymer becomes stiffer[2-3]. Due to the "new" molecular network (i.e. the sulfur network) rubber compounds can retract to their original shape even after the application of a large deformation[4-5]. In other words, the vulcanization process (i.e. the creation of crosslinks) decreases the plasticity and increases the elasticity of the rubber, due to deep changes in the polymers structure at the molecular level[6,4].

Rubbers are combined with different additives and subjected to pressure and high temperatures to produce crosslinks[7]. In fact, the vulcanization of rubbers using only sulfur is an extremely slow and inefficient process which is uneconomical by any production standards[2]. Therefore, other additives have to be included in the formulation to accelerate this process and, in addition, to improve the final properties of the products. In Chapter 1 of this thesis, we have

explained in detail the additives used for vulcanization. Here, we list the additives[8-9] normally used in compounding[10-11]:

- Sulfur: One of the most common vulcanization agents.
- Sulfur donor: It is used mainly in combination with accelerators for the production of heat-resistant articles.
- Accelerator: It is used to increase the speed of vulcanization even at low temperatures.
- Zinc Oxide: It is an effective activator of accelerated sulfur cross-linking
- Resins: Commonly used to achieve high hardness combined with good processing ability.
- Processing oils: Used as extenders to improve the processability.
- Wax: In relatively low dosages, these products act mainly as lubricants.
- Antioxidants: Used to protect the polymers from degradation.

The presence of these additives in rubber compounds has to be taken into account when analyzing its response to the different stimuli applied with the different experimental techniques. In particular, here we focus on the dynamics as seen by broadband dielectric spectroscopy (see Chapter 2). BDS is based on the interaction of an external electric field with the electric dipole moment of the molecules of the sample[12]. Therefore, the molecules which possess a dipole moment could contribute to the dielectric spectrum modifying the response. For instance, N-Cyclohexyl-2-benzothiazole sulfenamide (CBS)[13] (the primary accelerator used in this thesis) has a strong dipole moment (2.9 D) and this fact should be taken into account when analyzing the dynamics of vulcanized polymers using dielectric spectroscopy.

Therefore, in this chapter we focus on the effect of the vulcanization additives, particularly the accelerators[14-15], on the dielectric response of chain end functionalized (fSBR) compounds. First, we introduce the general features of the dielectric spectra of different vulcanized fSBR focusing on the behavior of the α-relaxation. We observe that the main peak, typically related only with the α-relaxation, is in fact composed of two different contributions.

The aim of this chapter is to investigate the origin of this additional dielectric process. In order to define the possible sources of these two processes, we have analyzed the dynamics of fSBR compounds with different vulcanization additives, by means of DSC and BDS.

4.1 The α-relaxation of neat and vulcanized SBR as seen by dielectric spectroscopy – the role of vulcanizing additives

As previously described (see Chapter 2), the dielectric response of neat polymers is frequently characterized by the presence of a secondary relaxation (or β-relaxation) related to localized motions (for instance side groups reorientations) and a segmental relaxation (or α-relaxation) related to the cooperative motion of the polymer chains. The α-relaxation is associated with the glass transition temperature measured by DSC. An example of the imaginary part of the dielectric permittivity (ε'') of neat SBR and vulcanized fSBR as a function of the frequency for different temperatures is shown in Figure 4.1 (a and b respectively).

For both materials, in the frequency window of 10^{-2} to 10^{6} Hz, the spectra display a noticeable peak due to the segmental relaxation and, at lower temperatures the β-relaxations can be detected. The segmental relaxation shifts to higher frequencies with increasing temperature. However, we can notice that for neat SBR the main process is a single peak whereas for vulcanized SBR the main peak seems to be composed by two different processes (see the spectrum at T = 271 K in Figure 4.1 (b)).

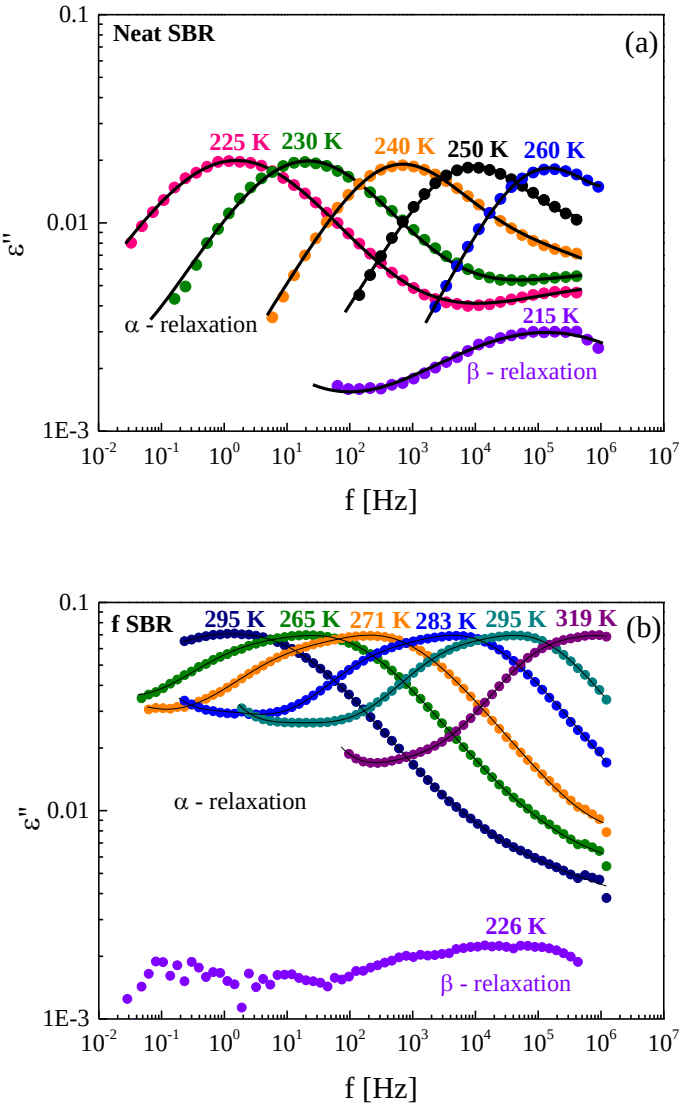

Figure 4.1 Imaginary part of the dielectric permittivity (ε'') as a function of the frequency for different temperatures of neat SBR (a) and vulcanized fSBR (b). Solid lines represent the fit of the experimental data (see text).

Moreover, in Figure 4.2 we show the imaginary part of the dielectric permittivity for three samples: two different types of vulcanized SBR (functionalized and non-functionalized) as well as the response of the neat SBR (no additives). Again the α-relaxation of neat SBR shows a single broad peak (see Figure 4.2c). However, in the case of vulcanized SBR and fSBR, we can observe two separated contributions in the dielectric response (labeled as slower and faster processes respectively).

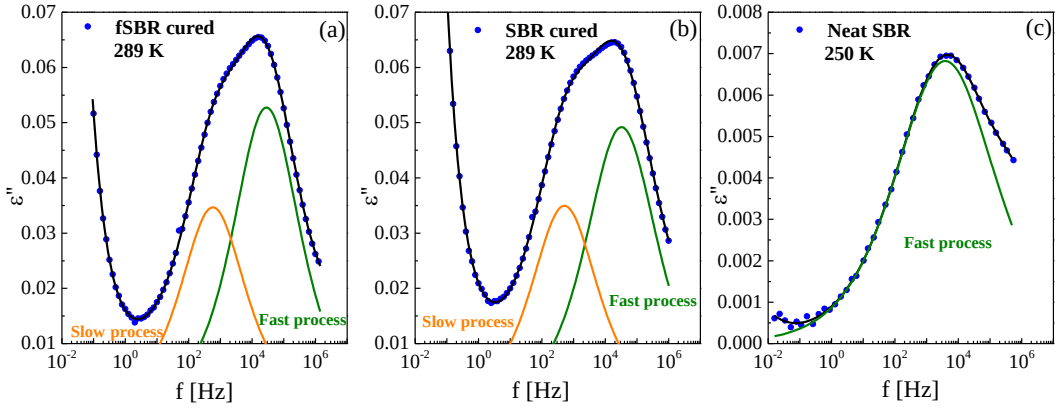

Figure 4.2 Imaginary part of the dielectric permittivity (ε") as a function of the frequency for vulcanized fSBR (a) and SBR (b) compounds and neat SBR (without additives) (c). Solid lines represent the fit of the experimental data.

The data in Figure 4.2 have been fitted at the different temperatures using a single CC function for neat SBR[16] and two CC functions for both vulcanized SBR and fSBR to determine the shape parameters and the relaxation times (see full lines in Figure 4.2).

The temperature dependence of the relaxation time is shown in Figure 4.3. As shown, the evolution of the relaxation time as a function of the temperature is well described using a VFT law:

$$\tau_\alpha = \tau_0 \, exp\left(\frac{DT_0}{T\text{-}T_0}\right) \tag{4.1}$$

where T_0 is the temperature at which τ would diverge and D a coefficient related to the fragility.

The extrapolation of the VFT equation to a relaxation time of 100 s allows obtaining a dielectric estimation of the glass transition temperature, $T_{g,100s}$ which is similar to that obtained by DSC. Therefore, the fastest process observed in the vulcanized SBR and fSBR in Figure 4.2 can be identified as the α-relaxation. Note that in the case of neat SBR (uncured), the additional process used to fit the dielectric response of SBR and fSBR (slow process) is absent[16].

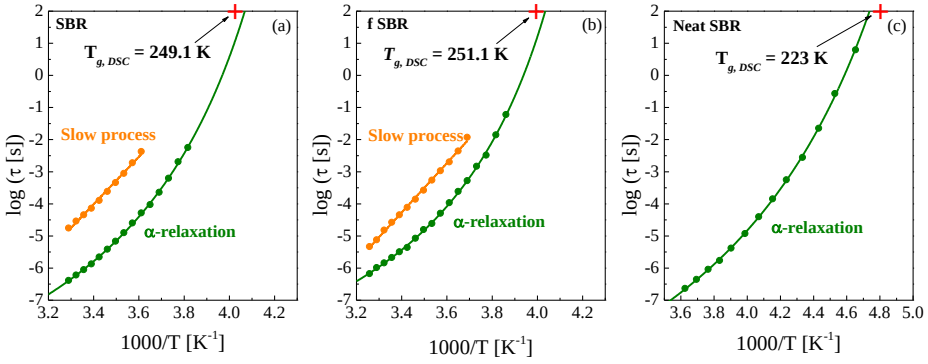

Figure 4.3 Temperature dependence of the relaxation time for the α-relaxation and slow process for SBR (a), fSBR (b) and neat SBR (c). Solid lines represent the fitting using the VFT equation. The red cross at 100 s indicates the T_g measured by DSC.

Since the low frequency contribution is not observed in the neat uncured SBR, it can be assumed that the appearance of this process is related to the presence of some vulcanization additives or due to some new product generated during the vulcanization. In the following section, we analyze the origin of this slow process.

4.2 Influence of remaining products of vulcanization on the dielectric response of fSBR

To investigate the nature of the slow dielectric process observed in the previous section, vulcanized fSBR (containing all the additives) was allowed to stand in pyridine during 12 hours at room temperature. After swelling, the sample was left to air dry for 5 days, and then for 24 hours at 343 K under vacuum to evaporate the solvent. Pyridine is an effective solvent for fats, waxes, and numerous other organic compounds and therefore we expect to remove both impurities and other remaining products of vulcanization. In this section, we analyze how the dielectric response of fSBR is modified after swelling in pyridine.

Figure 4.4 shows the imaginary part of the dielectric permittivity before (a) and after (b) cleaning using pyridine. It is clear that the dielectric response suffers profound changes as seen in Figure 4.4c where a comparison of both signals is displayed.

For vulcanized fSBR it is possible to observe the α-relaxation as well as the low frequency contribution. After cleaning, this last contribution is no longer observed. In addition, the intensity of the dielectric signal is drastically reduced. This fact can be explained if we consider that pyridine is a powerful solvent, which sweeps molecules which are not linked to the polymer chain. These compounds do not contribute anymore to the dielectric response and therefore the intensity of the signal decreases.

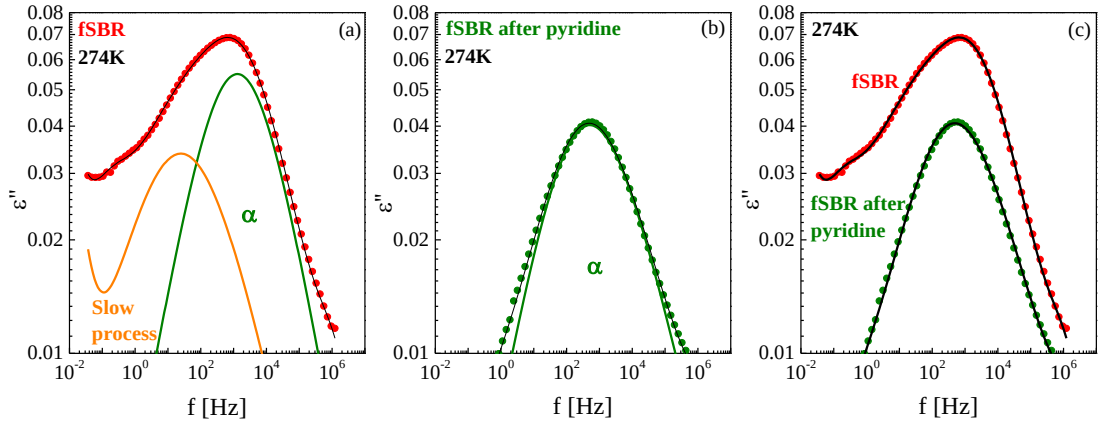

Figure 4.4 Imaginary part of the dielectric permittivity (ε'') as a function of the frequency for fSBR (a) and fSBR after the cleaning with pyridine (b) pyridine. Figure (c) shows a comparison of the signal before and after the cleaning. Solid lines represent the fit to the experimental data. In (a) the fitting of the dielectric response before the experiment is showed.

We can therefore conclude that the origin of the low frequency contribution can be attributed to a process arising from some component that is not covalently bonded to the polymer chain. In fact, during the vulcanization several reactions among the additives, the rubber and the sulfur, occur and even some new complexes are created. At the end of the vulcanization the sulfur bridges link two rubber chains, but other products remain in the compound without being chemically attached to the rubber chain, and not contributing to the final properties of the product.

4.3 Analyzing the effect of the additives in the dielectric response of fSBR

There is a lack of information in the scientific literature about the impact of each vulcanization ingredient on the final dielectric response of the rubber

compounds. Therefore, in order to analyze the effect of the different additives on the dielectric spectrum, we have prepared six different samples by removing one additive type of each sample and leaving the rest of the formulation used for vulcanization unchanged (see a complete description of the formulation in Chapter 3). The samples analyzed are:

a) SBR including all the additives normally used for vulcanization (labeled as "full").
b) SBR in which both accelerators (CBS and DPG) were removed from the formulation (labeled as "NO accelerators").
c) SBR in which all the processing oil was removed from the formulation (labeled as "NO Oil")
d) SBR in which stearic acid was removed from the formulation (labeled as "NO Stearic acid").
e) SBR in which antioxidants were removed from the formulation (labeled as "NO antioxidants").
f) SBR in which sulfur donor was removed from the formulation (labeled as "NO Sulfur donor")

Figure 4.5 shows the dielectric permittivity as a function of the frequency at T = 298 K for all these samples. It is clear that, the slow component is still visible in Figure 4.5 (a, and c to f) but for the sample without accelerators (Figure 4.5 b), the intensity of the slow process has significantly decreased. Therefore, it is expected that accelerators play a major role regarding the presence of this slow process. Therefore, in the next section we analyze the effect of the accelerators on the dielectric response of fSBR.

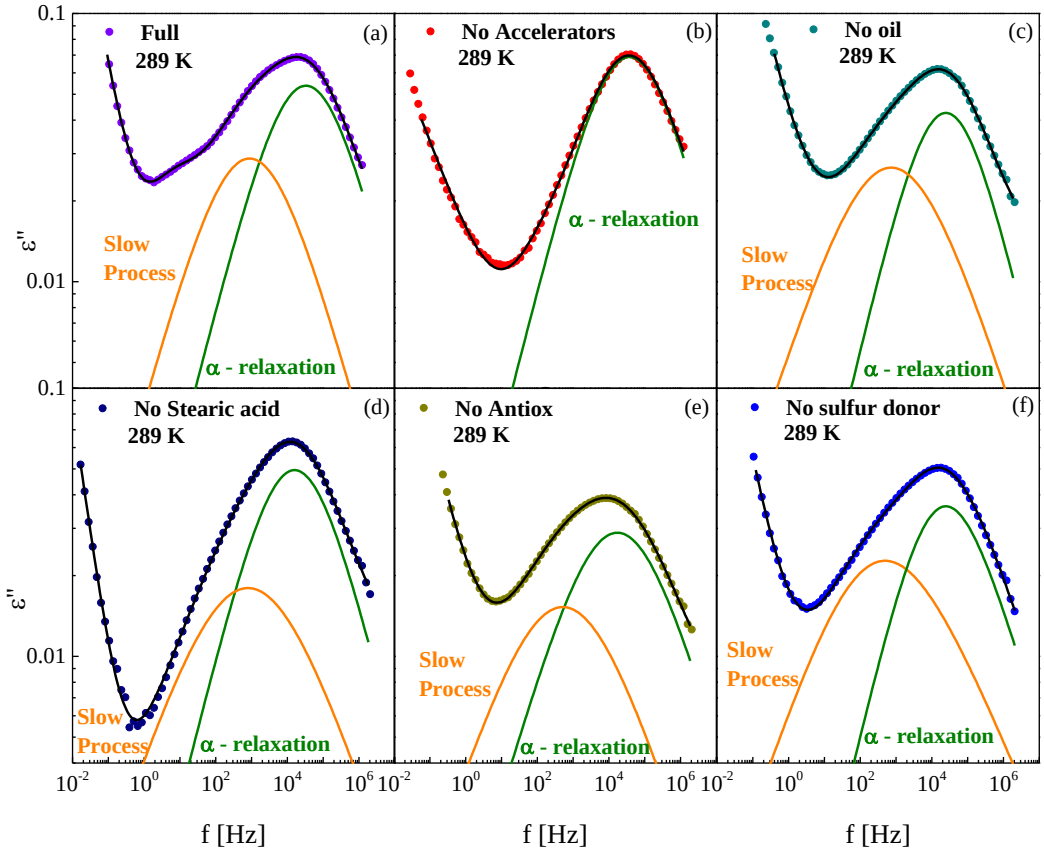

Figure 4.5 Imaginary part of the dielectric permittivity (ε'') as a function of the frequency for fSBR: full formulation (a), without accelerators (b), without oil (c), without stearic acid (d), without antioxidants (e), and without sulfur donor (f), at T = 289 K. Solid lines represent the fit to the experimental data. In all the cases two dielectric processes are observed but in the sample without accelerators a single relaxation is observed.

4.4 The effect of the accelerators on the dielectric response of SBR

The formulation of the samples includes two different accelerators (N-Cyclohexyl-2-benzothiazole sulfonamide (CBS), and diphenyl guanidine (DPG)). To analyze the influence of both accelerators on the dielectric response, we have prepared compounds with different DPG contents (0 to 1.2 phr, at fixed CBS content (1.6 phr)). In addition, we also prepared compounds with different CBS contents (0.4 to 1.6 phr, at fixed DPG content (1.2 phr)). For more details regarding these samples see Chapter 3.

The aim of these experiments is to determine whether the type of the accelerator affects the slow process and in such a case, how the addition of this accelerator modifies this slow process.

4.4.1 Differential scanning calorimetry (DSC)

The glass transition temperature (T_g) was determined by DSC for all the compounds whose formulation is shown in Table 4.1. Besides CBS and DPG, these compounds contain the rest of the regular additives to produce vulcanization (see Chapter 3). It is important to note that the T_g value of all the samples is approximately ~250 K, independently of the type and amount of accelerators used in the different formulations. We therefore do not expect strong changes in the α-relaxation corresponding to all these compounds. Note that the compound with 1.2 phr of DPG and 0.4 phr of CBS has the lowest T_g value compared with the rest of the compounds.

Table 4.1 Glass transition temperature (T_g) for compounds with different amount of accelerators indicated.

Sample	DPG [phr]	CBS [phr]	T_g [K]
0 DPG 1,6CBS	0.0	1.6	250.5 ± 0.2
0,3DPG 1,6CBS	0.3	1.6	250.9 ± 0.2
0,6DPG 1,6CBS	0.6	1.6	250.4 ± 0.2
0,9DPG 1,6CBS	0.9	1.6	250.6 ± 0.2
1,2DPG 1,6CBS	1.2	1.6	250.8 ± 0.3
1,2DPG 1CBS	1.2	1.0	250.6 ± 0.2
1,2DPG 0,4CBS	1.2	0.4	249.5 ± 0.2

4.4.2 Determination of the crosslink density

The relative amounts of accelerators and sulphur used in the curing process of rubbers, determines the quantity and type of crosslinks formed[17,2]. Due to the fact that the glass transition temperature remains almost constant for all the compounds, we want to know whether the crosslink density is affected. To analyse the effect of the accelerators on the crosslink density, we have performed swelling experiments for all the compounds.

One of the most extended approaches to measure the crosslink density is equilibrium swelling measurements. This technique allows the determination of the average molecular weight between crosslinks (M_c), which can also be expressed as crosslink density ($\mu = 1/2M_c$). The general procedure followed to perform the experiments is detailed in the chapter 2. The results of the crosslink density for the compounds are shown in Table 4.2 and Figure 4.6 respectively.

Table 4.2 Crosslink density for all the compounds in Table 4.1

DPG [phr]	**CBS [phr]**	**μ (·10^{-5}) [mol/cm^3]**
0.0	1.6	3.5 ± 0.1
0.3	1.6	4.0 ± 0.1
0.6	1.6	3.8 ± 0.1
0.9	1.6	4.0 ± 0.1
1.2	1.6	3.9 ± 0.1
1.2	1.0	3.3 ± 0.1
1.2	0.4	2.3 ± 0.1

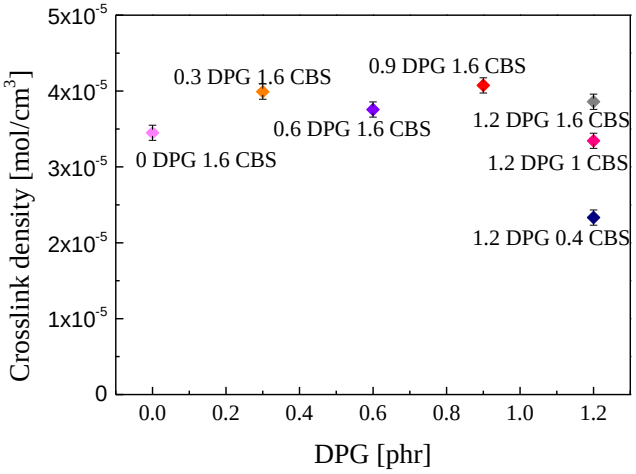

Figure 4.6 Crosslink density as a function of the DPG content for compounds in Table 4.1.

The crosslink density is similar for most of the compounds in Figure 4.6 but some small variation is observed for the sample with 1.2 DPG and 0.4 CBS which also has the lowest T_g value. Apart of this sample, the crosslink density has the same order of magnitude for the rest of the compounds. This indicates that the variations in the accelerators content have not a strong impact on the

number or structure of the sulphur bridges during vulcanization. Changes in the crosslink density directly affect the temperature dependence of the relaxation times[18]. As shown in our case, α-relaxation does not show significant changes in agreement with the almost constant crosslink density values.

4.4.3 Broadband dielectric spectroscopy (BDS)

Figure 4.7 shows the imaginary part of the dielectric permittivity of fSBR using a constant amount of CBS (a) and DPG (b) in the formulation, respectively. As a general remark, by increasing the DPG content, the low frequency contribution of the dielectric signal strongly increases. However, this behavior is not observed when increasing the CBS content at fixed DPG content. In this case, the variation of the permittivity is less significant for all the CBS contents (Figure 4.7 (b)).

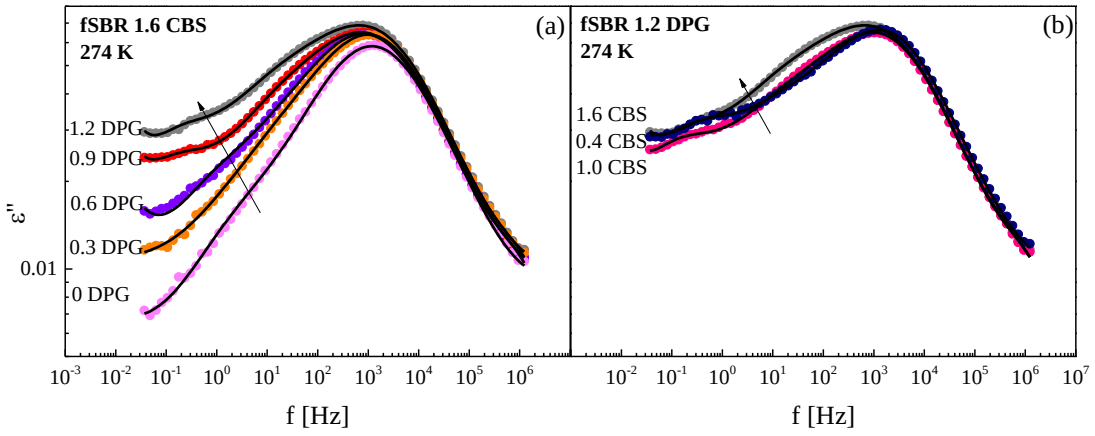

Figure 4.7 Imaginary part of the dielectric permittivity for samples with variations in the accelerator contents indicated in Table 4.1. In (a) the content of CBS is fixed at 1.6 CBS and DPG varies from 0 to 1.2 phr whereas in (b) the DPG content is fixed at 1.2 DPG and the CBS content varies from 1.0 to 1.6 phr.

As discussed in the previous sections, we do not expect significant variations of the α-relaxation of these compounds using the different formulations. Therefore, to fit the signal in Figure 4.7 we have used two CC functions (one to consider the slow process and the other for the α-relaxation). Firstly, the fitting parameters for the sample with 0-DPG were left free to identify the parameters corresponding to α-relaxation (τ, α, and $\Delta\varepsilon$). We have fixed the relaxation time and shape parameters for the rest of the samples. The values were $\Delta\varepsilon \simeq 0.25$ and $0.47 < \alpha < 0.58$ (see Figures A.1 and A.2 in the Appendix).

Figure 4.8 (a and b) shows the performed fittings for the samples with 1.2 phr of DPG and 1.6 phr of CBS, and 0 phr of DPG and 1.6 phr of CBS, respectively. In both cases two processes were necessary to fit the data; however, the dielectric strength of the sample containing full DPG (a) is much higher than in the case of the sample without DPG (b) in the composition and therefore we can relate the slow process with the presence of DPG.

Moreover, Figure 4.9(a) shows the evolution of the low frequency contribution as a function of the DPG content. The intensity of the slow process systematically increases with the DPG amount (see Figure 4.9(b)).

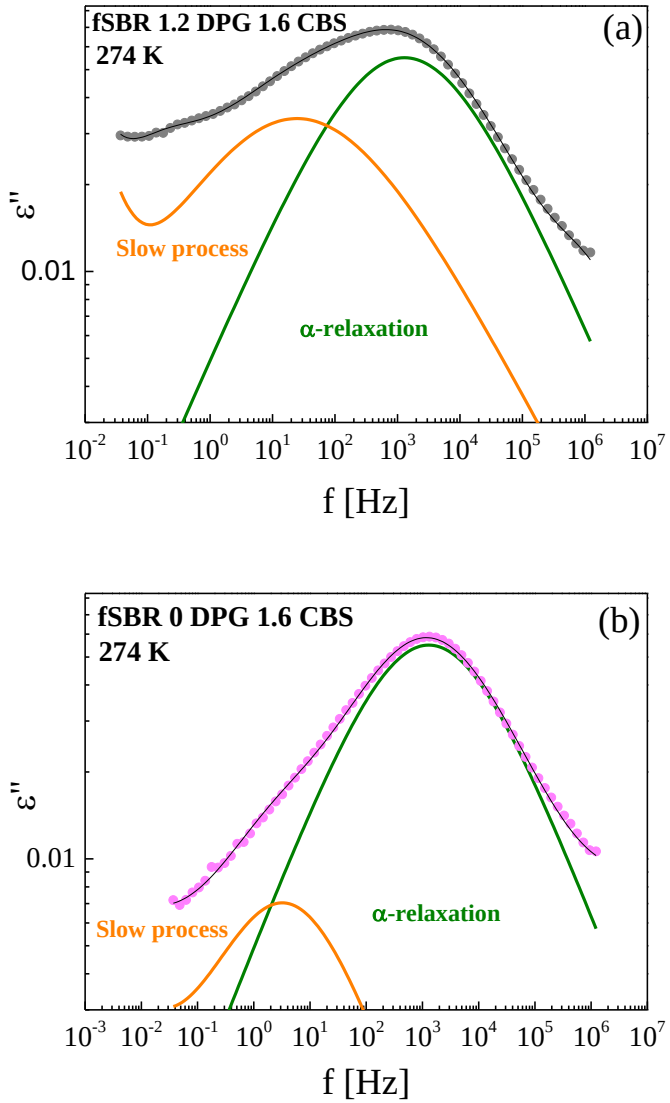

Figure 4.8 Imaginary part of the dielectric permittivity (*ε''*) as a function of the frequency at T = 274 K for samples with full accelerator content (a) and without DPG (b). The solid line through the data points is a least square fit to a superposition of two Cole-Cole functions.

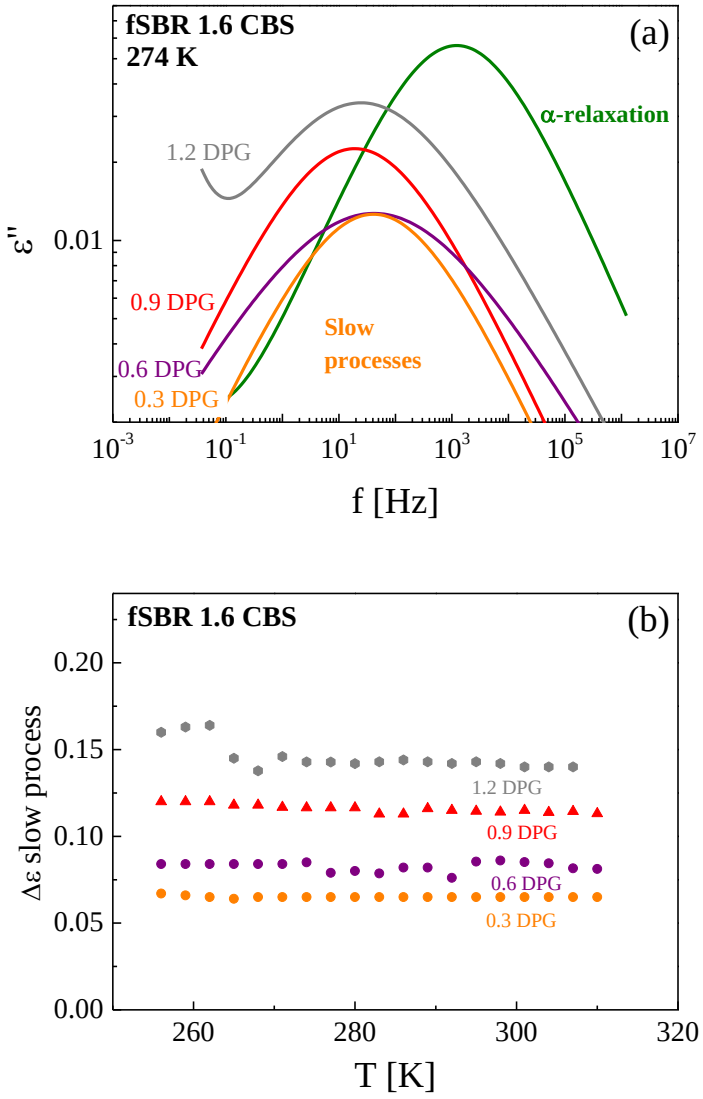

Figure 4.9 (a) Imaginary part of the dielectric permittivity (ε") of the slow process used to fit the data in Figure 4.7. (b) Temperature dependence of the dielectric strength for the slow process for the compounds with variations in the amount of DPG.

Figure 4.10 shows the temperature dependence of the relaxation time of samples with constant amount of CBS (a) and constant amount of DPG (b) in the formulation. As can be appreciated, the relaxation times of the segmental relaxation are not affected by the presence of the accelerators. Therefore, we can conclude that CBS has a little influence in the presence of this slow peak, while it shows a strong dependence with DPG content. In all cases the α-relaxation remains unaffected by the variations on DPG/CBS contents.

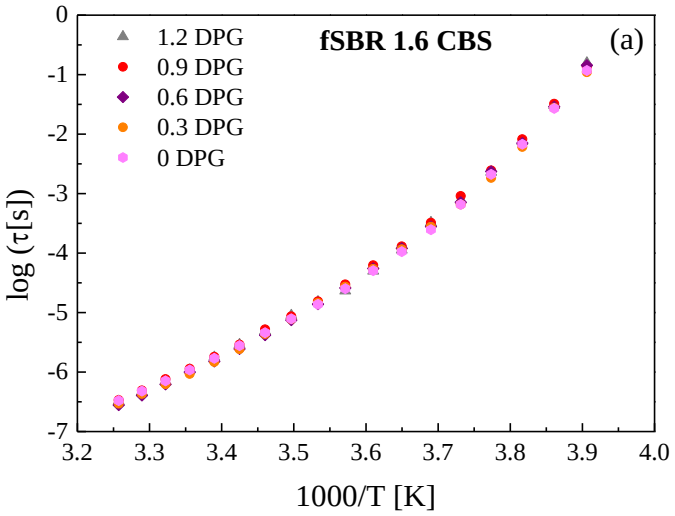

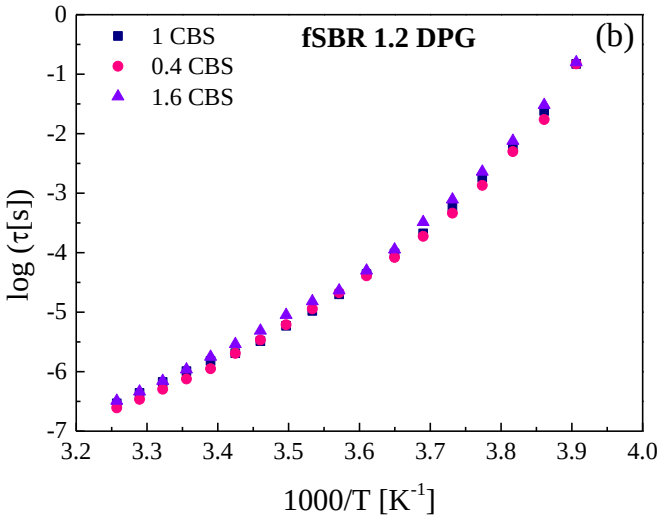

Figure 4.10 Temperature dependence of the relaxation time obtained from the fitting of the samples with a change in the accelerants compositions for constant CBS (a) and constant DPG (b) contents.

4.5 Tracing the origin of the low frequency contribution

Understanding the origin of this slow process is of the utmost relevance to properly analyze the dielectric response of both filled and unfilled rubber compounds. The presence of an additional dielectric contribution, slower and close to the segmental relaxation, has been previously reported in the literature[19-20]. However, despite the intense research in this area, contradictory interpretations can be found concerning to the origin of this process. Some researchers suggested that this extra dielectric contribution is related to the immobilized layer around the filler particles[21-27] or even around zinc oxide[28] (for unfilled compounds). On the other hand, in a recent work this process has been attributed to a Maxwell Wagner Sillars polarization arising from the presence of trapped charges at the boundaries of the filler particles[29]. However, we have shown in this chapter that this additional dielectric contribution can appear, in

the case of the samples here analyzed, even in the absence of zinc oxide or filler particles. Thus, we have clearly demonstrated that the presence of this extra contribution observed at low frequencies is due to the presence of some additives, particularly the accelerators, and not due to immobilized polymer around filler particles or zinc oxide. These findings will help to achieve a better understanding of the dielectric spectra of both filled and unfilled rubber compounds.

4.6 Conclusions

The α-relaxation of neat uncured SBR (without additives) shows a single dielectric peak whereas for vulcanized SBR the dielectric spectra around the α-relaxation splits into two different contributions (the α-relaxation and an additional process at lower frequencies). Since this low frequency contribution is not observed in the neat uncured SBR, it can be assumed that the origin of this process is related to the presence of some vulcanization additives or due to some new product generated during the vulcanization. Moreover, swelling experiments using pyridine as a solvent showed that the origin of the low frequency contribution can be attributed to a process arising from a component that is not covalently bonded to the polymer chain and not restricting the segmental dynamics.

We have measured compounds prepared by excluding on each of them only one of these vulcanization additives, and we found that accelerators play a major role regarding the presence of this slow process. We have also seen that by increasing the content of the secondary accelerator (DPG), the low frequency contribution of the dielectric signal strongly increases. However, this behavior is not observed when increasing the content of the primary accelerator (CBS). Independently of the type and amount of accelerators used in the different formulations, the T_g value, as well as the crosslink density, and the segmental relaxation, vary only slightly.

4.7 References

1. De, S. K.; White, J. R., *Rubber Technologist's Handbook*. iSmithers Rapra Publishing: 2001.

2. Datta, R. N., *Current Topics in Elastomer Research*. CRC Press: New York, 1954.

3. Erman, B.; Mark, J. E.; Roland, C. M., *The Science and Technology of Rubber*. Elsevier: 2013.

4. Dillon, J. H.; Johnston, N., The plastic properties of several types of unvulcanized rubber stocks at high rates of shear. *Journal of Applied Physics* **1933,** *4* (1), 225-235.

5. Dierkes, W.; Blume, A., *Encyclopedia of Polymeric Nanomaterials*. Springer: 2014.

6. Houwink, R.; Decker, H. K. d., *Elasticity, Plasticity and Structure of Matter*. 3 ed.; Cambridge University Press: 1971.

7. Mark, J. E.; Erman, B.; Eirich, F. R., *Science and Technology of Rubber*. Academic Press: 1994.

8. Engels, H.-W.; Weidenhaupt, H.-J.; Pieroth, M.; Hofmann, W.; Menting, K. H.; Mergenhagen, T.; Schmoll, R.; Uhrland, S., *Ullmann's Encyclopedia of Industrial Chemistry*. Wiley-VCH: 2004.

9. Marzocca, A. J.; Salgueiro, W.; Somoza, A., *Advances in Elastomers II*. Springer: 2013.

10. Barlow, F. W., *Rubber Compounding: Principles, Materials, and Techniques*. Marcel Dekker: 1993.

11. Ikeda, Y.; Kato, A.; Kohjiya, S.; Nakajima, Y., *Rubber Science: A Modern Approach*. Springer: 2017.

12. Kremer, F.; Schönhals, A., *Broadband Dielectric Spectroscopy*. Springer: Germany, 2003.

13. Vulcanization and accelerators. Nocil limited. Arvind Mafatlal Group: 2010.

14. Avramova, N., *Polymer Additives: the Miscibility of Blends*. Springer: Dordrecht, 1998; Vol. 1, p 513-518.

15. Kowalski, E. L.; de Oliveira, S. M.; de Souza, G. P.; Tomioka, J.; Silva, J. M. M.; Ruvolo, A.; Robert, R., *Dielectric Spectroscopy on Natural Rubber Flatted Sample with Different Temperature and Time of Vulcanization*. IEEE: New York, 2003; p 522-523.

16. Cerveny, S.; Bergman, R.; Schwartz, G. A.; Jacobsson, P., Dielectric alpha- and beta-relaxations in uncured styrene butadiene rubber. *Macromolecules* **2002,** *35* (11), 4337-4342.

17. Marzocca, A. J.; Goyanes, S., An analysis of the influence of the accelerator/sulfur ratio in the cure reaction and the uniaxial stress-strain behavior of SBR. *J. Appl. Polym. Sci.* **2004,** *91* (4), 2601-2609.

18. V. Yu Kramarenko, T. A. E., I. Šics, F. J. Baltá-Calleja, and V. P. Privalko Influence of cross-linking on the segmental dynamics in model polymer networks. *The Journal of Chemical Physics* **2000,** *113* (447).

19. Mujtaba, A.; Keller, M.; Ilisch, S.; Radusch, H. J.; Beiner, M.; Thurn-Albrecht, T.; Saalwachter, K., Detection of surface-immobilized components and their role in viscoelastic reinforcement of rubber-silica nanocomposites. *ACS Macro Lett.* **2014,** *3* (5), 481-485.

20. Hernandez, M.; Carretero-Gonzalez, J.; Verdejo, R.; Ezquerra, T. A.; Lopez-Manchado, M. A., Molecular dynamics of natural rubber/layered silicate nanocomposites as studied by dielectric relaxation spectroscopy. *Macromolecules* **2010,** *43* (2), 643-651.

21. Jha, V. Carbon Black Filler Reinforcement of Elastomers. University of London, 2008.

22. Twiss, D. F.; Gottlob, K., Technologie der Kautschukwaren. *Journal of the Society of Chemical Industry* **1925,** *44* (23), 587-588.

23. Dessewffy, O., Dependence of bound rubber on concentration of filler and on temperature. *Rubber Chem. Technol.* **1962,** *35* (599).

24. Kaufman, S.; Slichter, W. P.; Davis, D. D., Nuclear magnetic resonance study of rubber–carbon black interactions. *Journal of Polymer Science* **1971,** *9* (829).

25. O'Brien, J.; Cashell, E.; Wardell, G. E.; McBrierty, V. J., An NMR investigation of the interaction between carbon black and cis-polybutadiene. *Macromolecules* **1976,** *9*.

26. Dannenberg, E. M., Bound rubber and carbon-black reinforcement. *Rubber Chem. Technol.* **1986,** *59* (3), 512-524.

27. Wolff, S., Chemical aspects of rubber reinforcement by fillers. *Rubber Chem. Technol.* **1996,** *69* (325).

28. Marianella Hernández; Tiberio A. Ezquerra; Raquel Verdejo; Miguel A. López-Manchado, Role of vulcanizing additives on the segmental dynamics of natural rubber. *Macromolecules* **2011,** *45* (2), 1070-1075.

29. Otegi, J.; Cerveny, S.; Schwartz, G. A. *Bulk and surface chain dynamics under external constraints thermal characterization dielectric spectroscopy* Goodyear Innovation Center Luxembourg, 2012.

5

Adam-Gibbs approach to study the dynamics of cross-linked miscible rubber blends

In the search for new polymeric materials, the blending of polymers is a promising method for obtaining desirable features using already known polymers, with the potential to tailor their properties[1]. Such systems can provide a relatively simple solution to complex economic and technological problems, therefore, the study of polymer blends are of great scientific and industrial interest.[2] Since the properties of polymer blends are directly related to chain motions, the study of polymer dynamics can be a useful tool to enhance the understanding of the relaxation processes in rubber blend systems, opening the way for the prediction of the dynamics of polymer blends based on the dynamics of their neat components.

Athermal polymer blends display heterogeneous dynamics showing the presence of two relevant time scales[3-8]. Nevertheless, for vulcanized rubber blends, this trend changes showing one single dynamics[9-13], due to the strong interactions caused by the crosslinks. Several models have been proposed[6, 11, 14, 15] to describe the component segmental dynamics in miscible polymer blends. Some of these models are based on the influence of concentration fluctuations on the component dynamics. However, it is not enough to consider only the concentration fluctuations to quantitatively account for the

presence of the two different dynamics. The effect of chain connectivity has to be considered in order to have an accurate description of the dynamics.
The aim of this chapter is to explore the ability of an Adam Gibbs (AG) extended model to describe the crosslinked polymer blend segmental dynamics as measured by dielectric spectroscopy, at different polymer microstructure, temperatures, and blend compositions. The AG approach has been modified to take into account the effect of strong interactions between components due to the presence of the crosslinks.

5.1 Basis of the Adam Gibbs theory

The Adam Gibbs theory relates the increase of structural relaxation time (τ) to the reduction of configurational entropy (S_c)[16] by

$$\tau(T) = \tau_o exp\left(\frac{C_o}{TS_c}\right) \tag{5.1}$$

where τ_o is the relaxation time at very high temperature and C_o is a constant which depends on the polymer type. The configurational entropy is not experimentally accessible, and therefore it is usually estimated[14, 15] from the excess entropy ($S_c \propto S_{ex} = S_{melt} - S_{crystal}$). Thus, S_c can be written as

$$S_c(T) = gS_{ex}(T) = g\int_{T_k}^{T} \frac{\Delta C_p(T')}{T'} dT' \tag{5.2}$$

where $\Delta C_p(T)$ is the excess heat capacity and T_k is the Kauzmann temperature. As shown in Figure 5.1, a linear dependence of the type $\Delta C_p(T)$ = a + b T can be assumed for the temperature dependence of the excess heat capacity. Then, integrating Equation 5.2 and inserting the result in the Equation 5.1 the following temperature dependence for the segmental relaxation time is obtained:

$$\tau(T) = \tau_o exp\left[\frac{C}{T\left(a\, ln\left(\frac{T}{T_k}\right) + b(T - T_k)\right)}\right] \tag{5.3}$$

using $C = C_o/g$ as a constant related to the polymer type. Equation 5.3 gives a description of the segmental relaxation time for neat polymers with only three fitting parameters (τ_o, C and T_k) once a and b are determined from calorimetric experiments.

In the case of polymer blends, an appropriate way to express the excess entropy in the mixture needs to be established. Contrary to athermal mixtures where two different dynamics are observed[3-6], crosslinked polymer blends possess a single dynamics. This behaviour is commonly observed for interacting polymer blends[8-11] where both components are dielectrically active[8-11]. Thus, we can assume that for crosslinked polymer blends the interaction between the two components is strong enough to couple both dynamics. This means that the excess entropy of a blend composed of polymers A and B can be expressed as a linear combination of the corresponding quantity for each component weighted by the relative concentration plus an additional non-linear term to account for the interactions:

$$S_{ex}^{Blend} = \phi^A S_{ex}^A + (1 - \phi^A) S_{ex}^B + \phi^A (1 - \phi^A)\chi \tag{5.4}$$

where ϕ^A is the concentration of component A, $\boldsymbol{S_{ex}^{A,B}}$ is the excess entropy of each component and χ is a factor to account for the effects of the interaction between both components. The interaction factor can display non-trivial dependences with composition and temperature and is empirically defined,

following the definition of the Flory interaction parameter[17], as the sum of two terms:

$$\chi(T) = A + B/T \tag{5.5}$$

where A is referred to as the "entropic part" and B/T is called the "enthalpic part". If just one common dynamics exists in the blend, according to the AG theory (Equation 5.1), we can write the relaxation time as:

$$\tau^{Blend}(T) = \tau_o^{Blend} exp\left(\frac{C^{Blend}}{TS_{ex}^{Blend}}\right) \tag{5.6}$$

As a first order approximation, we can assume that τ_o and *C* are not strongly affected by the interactions between the two components and therefore we can express them as a linear combination of the corresponding values for the neat polymers. Thus, we have that:

$$\tau_o^{Blend} = \phi^A \tau_o^A + (1 - \phi^A)\tau_o^B \tag{5.7a}$$

$$C^{Blend} = \phi^A C^A + (1 - \phi^A)C^B \tag{5.7b}$$

$$S_{ex}^{Blend} = \phi^A S_{ex}^A + (1 - \phi^A)S_{ex}^B + \phi^A(1 - \phi^A)\chi \tag{5.7c}$$

In order to apply this approach to describe the segmental dynamics of crosslinked polymer blends, the dynamics and thermodynamics of the neat components need to be fully determined. Once this is done, the dynamics of the blend can be described at any temperature and composition by means of two fitting parameters (A and B) to account for the interactions.

5.2 Materials

In this chapter, we have investigated the dynamics of miscible blends of high cis butadiene rubber (BR), styrene butadiene rubber (SBR), styrene butadiene rubber with different microstructure (SBR2), and chain-end functionalized styrene butadiene rubber (fSBR). For the filled samples, 120 phr (parts per hundred rubber in weight) of precipitated amorphous silica was used. Full formulations of the compounds are given in Chapter 3.

5.3 Results and discussion

The segmental dynamics of the neat components of the blends were analyzed in terms of the Adam-Gibbs theory to obtain quantitative information about the component dynamics. Thus, once the calorimetric and dielectric responses from the neat components are studied, the extended AG model can be used to describe the dynamics of filled and unfilled crosslinked polymer blends, as we show below.

5.3.1 Neat polymers

5.3.1.1 Thermodynamic parameters

Figure 5.1 shows the reversible heat capacity (C_p) as a function of the temperature for the neat unfilled SBR compound. The lines represent the extrapolated C_p above and below the glass transition temperature. Similar curves were obtained for fSBR, SBR(2) and BR (filled and unfilled). The temperature dependence of the excess heat capacity can be described[15, 18] by means of a linear equation of the form $\Delta C_p(T) = a + b\,T$.

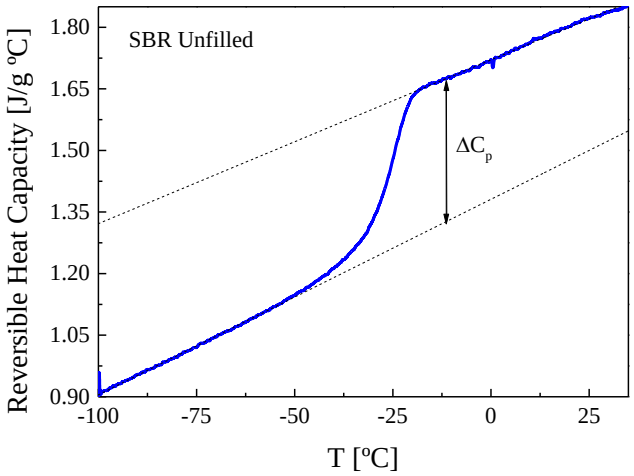

Figure 5.1 Reversible heat capacity as a function of temperature for unfilled SBR.

Table 5.1 shows the corresponding values of *a* and *b,* for both filled and unfilled neat SBR, fSBR, SBR(2) and BR.

Table 5.1 Thermodynamic parameters obtained from DSC measurements. Errors are ± 1 of the least significant digit.

Polymer	**a [J/K mol]**	**b [J/K^2 mol]**
Unfilled samples		
SBR	42.6	-0.061
fSBR	52.5	-0.091
SBR(2)	59.5	-0.155
BR	-6.1	0.135
Filled samples		
SBR	96.1	-0.12
fSBR	86.7	-0.057
SBR(2)	69.3	-0.169
BR	29.8	0.006

5.3.1.2 Dynamics parameters from BDS measurements

In order to study the segmental dynamics of the neat compounds, dielectric measurements were performed. Figure 5.2 shows the dielectric loss as a function of the frequency at different temperatures for unfilled SBR(2). A main peak is observed together with an additional contribution at lower frequencies due to the conductivity. Solid lines in Figure 5.2 represent the best fit of the experimental data by means of a Cole-Cole function to account for the segmental relaxation[19]. In addition, at higher temperatures a conductivity term ($\sigma/j\omega\varepsilon_0$) was added. To have a more trustable and accurate fit, both the imaginary and the real parts of the complex dielectric permittivity have been simultaneously fitted. In the following, we focus on the segmental relaxation time.

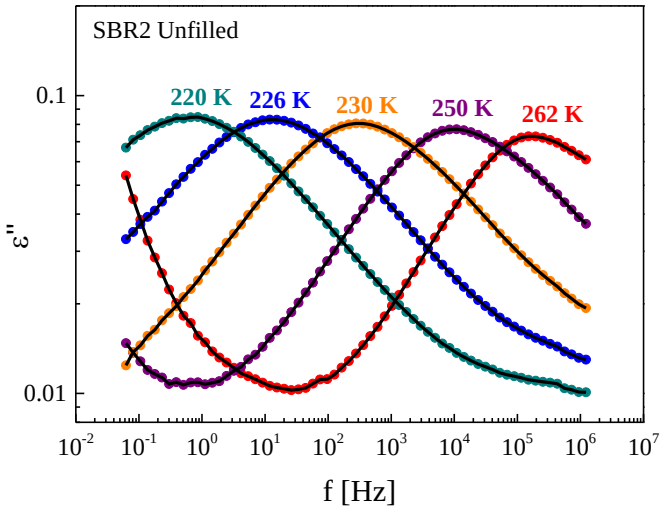

Figure 5.2 Dielectric loss as a function of the frequency at different temperatures for neat unfilled SBR(2) compound.

The temperature dependence of the maximum relaxation times obtained from the fittings was plotted in Figure 5.3 and Figure 5.4, and once the calorimetric response of the neat components is known, Equation 5.3 can be used to fit the corresponding temperature dependence of the segmental relaxation times. Orange and blue lines in Figure 5.3 show the accurate agreement between the experimental data and the AG model for neat unfilled and filled SBR and BR, respectively. Due to the partial crystallization of neat BR, the relaxation time is not experimentally accessible for some temperatures as shown in the plots below (orange lines). The fitting parameters for all the neat compounds are listed in Table 5.2.

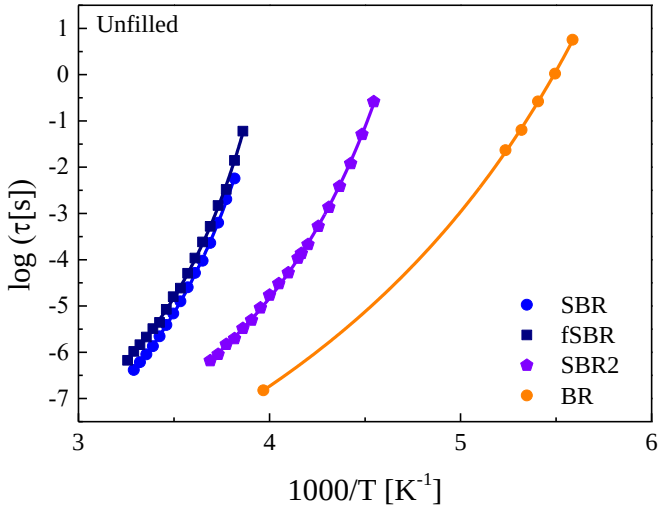

Figure 5.3 Relaxation map for unfilled neat SBR, fSBR, SBR2 and BR. Solid lines represent the best fit by means of the AG approach.

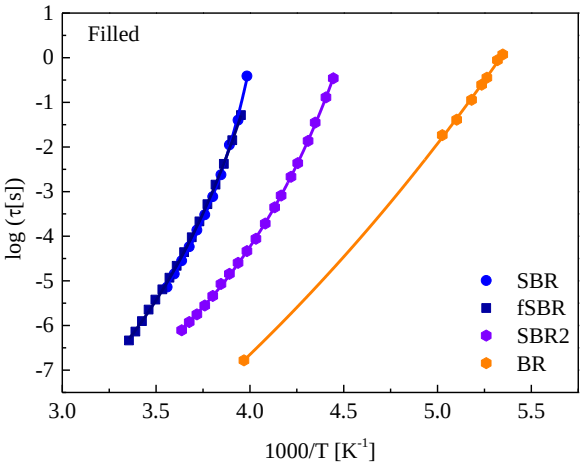

Figure 5.4 Relaxation map for filled neat SBR, fSBR, SBR2 and BR. Solid lines represent the best fit by means of the AG approach.

Table 5.2 Segmental dynamics parameters for the neat compounds.

Polymer	**T_g [K]**	**log(τ_o [s])**	**C [kJ/mol]**	**T_k [K]**
Unfilled samples				
SBR	249.1 ± 0.2	-11.3 ± 0.2	35.1 ± 1.1	209 ± 2.3
fSBR	251.1 ± 0.1	-10.5 ± 0.2	32.0 ± 1.0	215 ± 1.8
SBR(2)	217.6 ± 0.1	-11.3 ± 0.2	35.6 ± 0.9	175 ± 1.5
BR	172.1 ± 0.1	-10.3 ± 0.2	27.7 ± 0.7	113 ± 3.7
Filled samples				
SBR	242.5 ± 0.2	-9.6 ± 0.4	47.2 ± 2.6	220 ± 2.3
fSBR	243.6 ± 0.1	-12.0 ± 0.2	122.8 ± 2.7	194 ± 1.8
SBR(2)	218.5 ± 0.1	-11.9 ± 0.3	53.3 ± 1.9	175 ± 1.9
BR	175.2 ± 0.1	-13.7 ± 0.4	112.9 ± 5.9	100 ± 5.7

5.3.2 Describing the dynamics of the blends

Once a full characterization of the neat components has been performed, we can explore the ability of the proposed extended AG model to describe the dynamics of filled and unfilled crosslinked polymer blends.

5.3.2.1 The importance of taking into account the interactions

If we make the basic assumption that the interaction between the two components in the blend is negligible, the excess entropy for the blend can be written as:

$$S_{ex}^{Blend} = \phi_A S_{ex}^{A} + (1 - \phi_A) S_{ex}^{B} \tag{5.8}$$

Figure 5.5 shows the relaxation map for unfilled fSBR/BR at different blend compositions. From these results, it is evident that this approach, which does not take into account the interactions between the two components in the blend, does not give a good description of the polymer dynamics. At low temperatures, the dynamics of the blend (symbols) is faster than that predicted by the AG approach (solid lines). According to Equation 5.6, lower values of the excess entropy give higher relaxation times. This means that the real excess entropy should be higher than that resulting from the linear combination of the excess entropy of the components. Thus, the interaction term χ (at least at low temperatures) is expected to be positive and therefore to increase the total excess entropy in the blend. In fact, an increase in the excess entropy would be expected due to the presence of the crosslinks, which "freeze" part of the polymer leading to a poor packing of the polymer chains. This would result in an increasing excess entropy of the polymer blend with respect to the non-interacting case, giving lower relaxation times. In addition, Figure 5.5 shows that the difference between the relaxation times predicted by

the non-interacting AG approach and the experimental ones increases upon decreasing temperature.

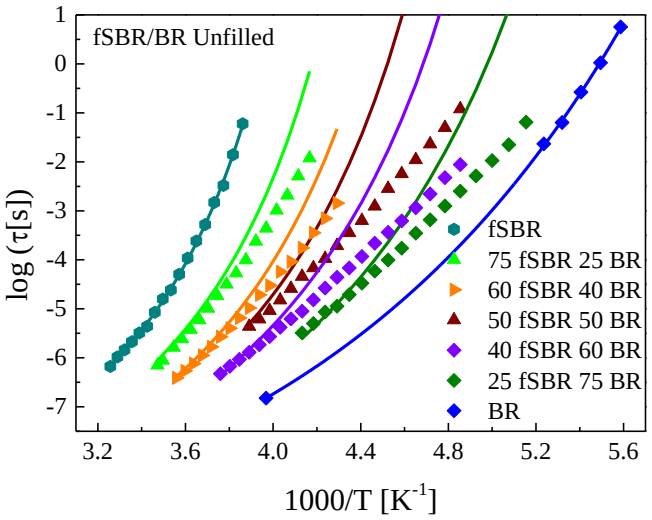

Figure 5.5 Relaxation map for unfilled fSBR/BR at different blend compositions. Solid lines represent the AG approach without taking into account the interactions (see text).

Based on the results showed in Figure 5.5, the need of an additional term to account for the effect of the interactions becomes evident. Thus, as explained in this chapter, an additional interaction term has to be included in the proposed AG equation, in order to obtain an accurate description of the segmental dynamics.

5.3.2.2 Fittings and interaction parameters

Figure 5.6 shows the dielectric loss (ε´´) as a function of the frequency at different temperatures for 75fSBR/25BR filled blend. The main feature in these spectra is the presence of a single segmental relaxation. Similar behaviour is observed for the rest of the blends. It is important to mention here

that both components are dielectrically active having comparable dielectric strengths. Therefore, the presence of a single peak indicates that both components are relaxing with the same (or very similar) relaxation times. This behaviour is typical of interacting polymer blends and random copolymers[20]. For non-interacting miscible blends, with large enough dynamical contrast (i.e. a large difference of T_g), two different dynamics are usually observed showing the so-called dynamical heterogeneity[3, 4, 6, 10].

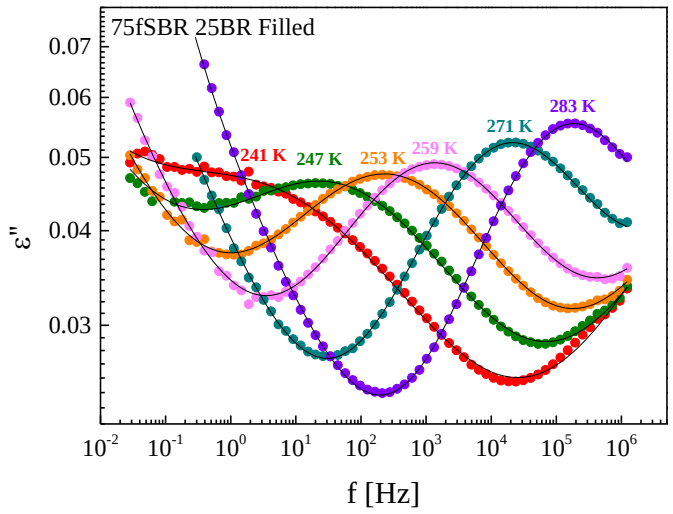

Figure 5.6 Dielectric loss (ε") as a function of frequency at different temperatures for 75/25 fSBR/BR filled sample.

The dielectric signal was fitted following the same criteria as for the neat compounds, and the temperature dependence of the relaxation times obtained from the fittings was plotted for all the blend compositions. Equation 5.6 gives the temperature dependence of the segmental relaxation time for each blend whereas the corresponding parameters are given by Equations 5.7a-5.7c with $\chi(T) = A + B/T$. Since the dynamics of the neat polymers as well as the

concentration of each component are known, only two free parameters (***A*** and ***B***) are necessary to fit the dynamics of each blend. The parameters A and B depend on the inter-chain monomer-monomer interaction[21] and since the composition changes in the different blends, it can be expected that the local environment that each monomer "sees" slightly changes as well. For this reason, we left A and B to vary as free parameters. Figures 5.7 to 5.9 show the fit results performed for the experimental relaxation times of unfilled and filled SBR/BR, fSBR/BR and SBR2/BR blends. As shown in these figures, we obtained an accurate fitting of the experimental data in all cases. The corresponding parameters A and B are listed in Table 5.3.

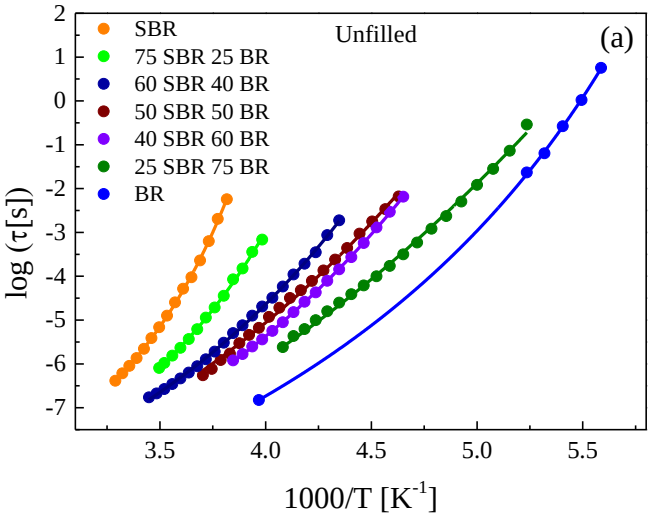

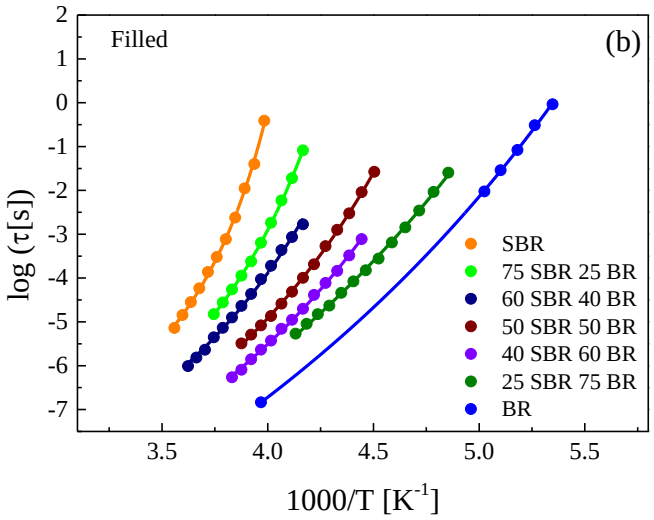

Figure 5.7 Relaxation map for unfilled (a) and filled (b) SBR/BR at different blend compositions. Solid lines represent the best fit by means of the AG approach (see text).

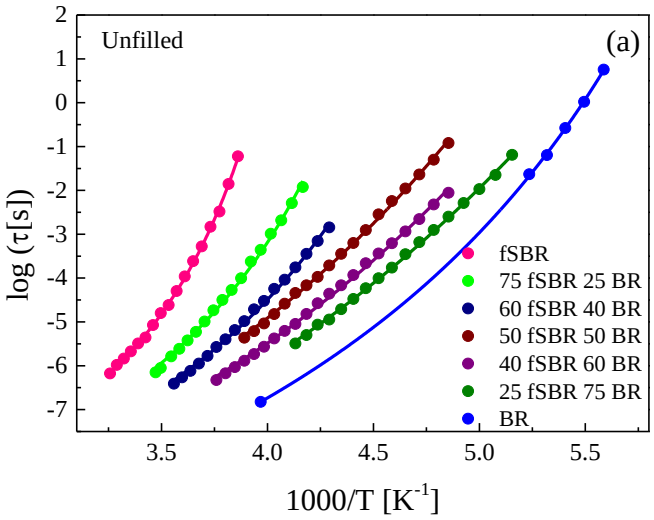

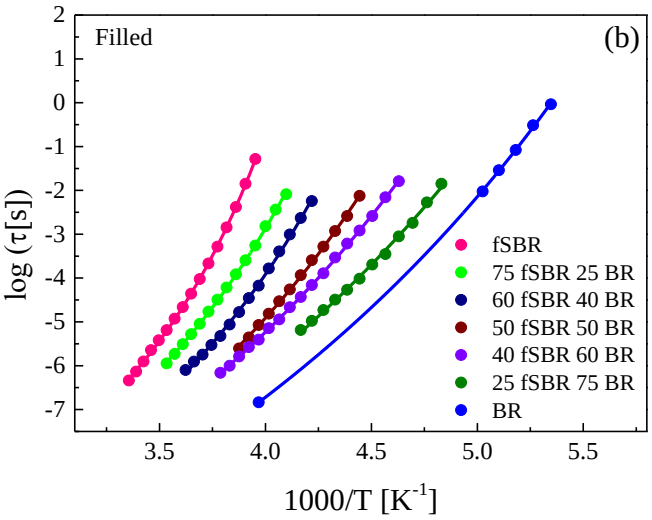

Figure 5.8 Relaxation maps for unfilled (a) and filled (b) fSBR/BR at different blend compositions. Solid lines represent the best fit by means of the AG approach (see text).

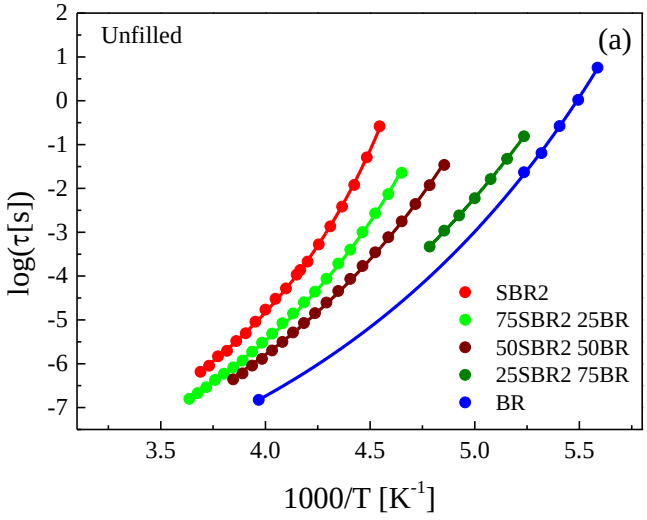

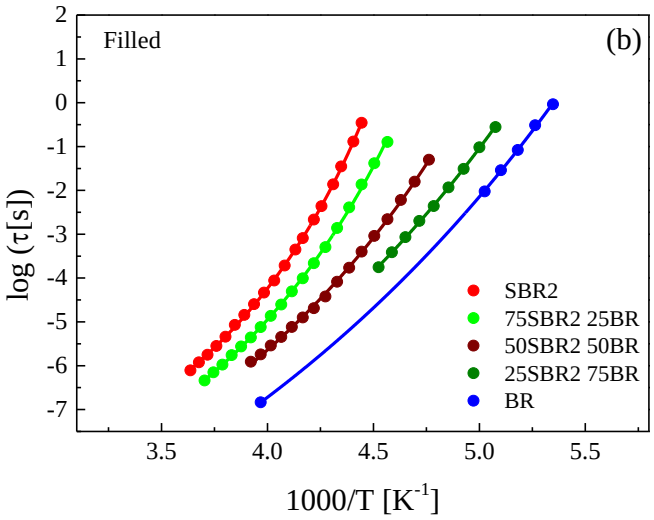

Figure 5.9 Relaxation maps for unfilled (a) and filled (b) SBR(2)/BR at different blend compositions. Solid lines represent the best fit by means of the AG approach (see text).

Table 5.3 Fitting parameters A and B for unfilled and filled SBR/BR, fSBR/BR and SBR(2)/BR at different blend compositions. Parameter A is given in [J/Kmol] and B in [J/mol].

Unfilled samples					
SBR/BR	**25 /75**	**40/60**	**50/50**	**60/40**	**75/25**
A	-46.4 ± 1.4	-33.6 ± 0.5	-42.1 ± 1.24	-36.4 ± 1.0	-27 ± 1.6
B	10915 ± 288	8159 ± 96	10638 ± 282	9503 ± 162	6538 ± 416
fSBR/BR	**25 /75**	**40/60**	**50/50**	**60/40**	**75/25**
A	-46.0 ± 1.0	-43.0 ± 1.0	-47.5 ± 1.0	-28.0 ± 1.7	-31.3 ± 2.3
B	11159 ± 192	11049 ± 235	12156 ± 181	7519 ± 410	8415 ± 591
SBR2/BR	**25 /75**	**40/60**	**50/50**	**60/40**	**75/25**
A	-18.8 ± 1.9	-	-3.6 ± 0.8	-	10.3 ± 1.5
B	3993 ± 512	-	929 ± 87	-	-2687 ± 235

Filled samples					
SBR/BR	**25 /75**	**40/60**	**50/50**	**60/40**	**75/25**
A	-29.3 ± 1.2	-8.6 ± 2.2	-14.9 ± 1.4	-22.5 ± 4.6	-10.5 ± 1.9
B	8592 ± 435	4834 ± 532	5936 ± 329	6534 ± 1162	3605 ± 469
fSBR/BR	**25 /75**	**40/60**	**50/50**	**60/40**	**75/25**
A	-34.0 ± 3.5	-42.1 ± 1.0	-23.1 ± 2.64	-13.8 ± 3.1	-47.1 ± 2.6
B	9915 ± 769	12221 ± 233	8078 ± 605	4446 ± 782	12712 ± 671
SBR2/BR	**25 /75**	**40/60**	**50/50**	**60/40**	**75/25**
A	-23.4 ± 2.3	-	-18.6 ± 1.7	-	-11.1 ± 1.2
B	5266 ± 398	-	4031 ± 307	-	2653 ± 312

Figure 5.10 shows the interaction parameter ($\chi(T) = A + B / T$) as a function of the inverse temperature for different blends and compositions. As explained before, at low temperatures the interaction factor is positive and therefore increases the entropy of the blend compared to athermal mixtures. By comparing filled and unfilled SBR/BR (Figure 5.10 (a) and (b)) we can observe higher values of the interaction and a higher composition dependence for filled compounds. In the case of unfilled compounds with SBR and fSBR (Figure 5.10(b) and (c)), similar values of the interaction parameter as well as a comparable composition dependence are observed. However, when comparing SBR (or fSBR) with SBR(2) much lower values of the interaction parameter are observed for the latter (see Figure 5.10 (d)).

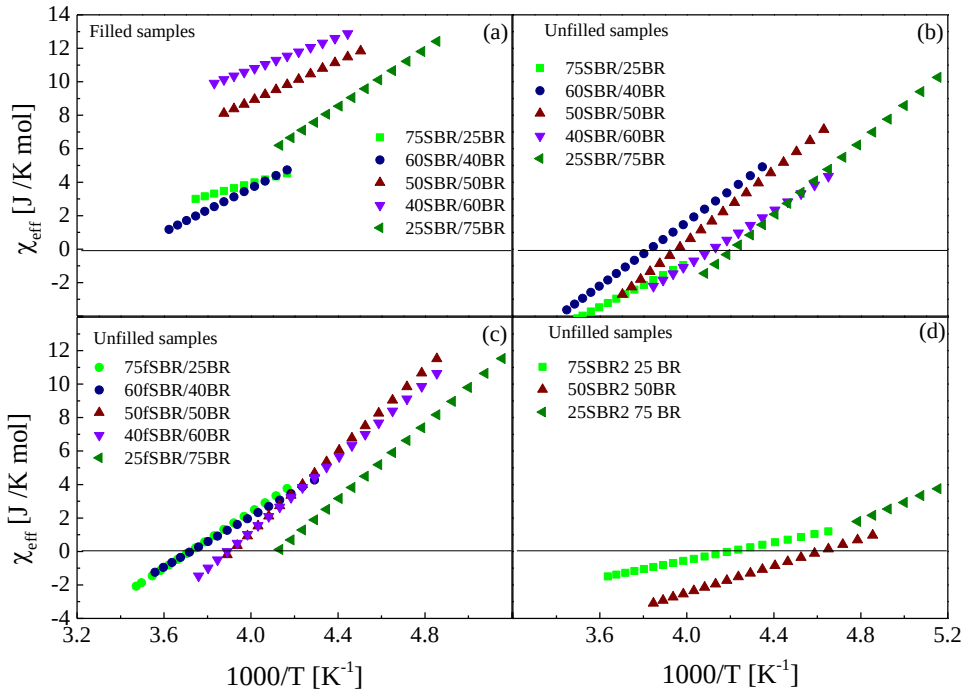

Figure 5.10 Interaction parameter as a function of inverse temperature for several compositions for filled SBR/BR (a), unfilled SBR/BR (b), unfilled fSBR/BR (c) and unfilled SBR(2)/BR (d) blends.

This is directly related to the microstructure of SBR2, which has less styrene and vynil groups. Other studies[21] show that the interaction between BR and SBR is dominated by the interaction with the styrene groups. Thus, by lowering the amount of styrene one should expect a lower interaction between both components. In addition, it is most likely that the reduction of "bulky" groups (styrene and vinyl) does not greatly affect the packing between both

polymers and, therefore, the entropy is not much affected compared to the athermal case.

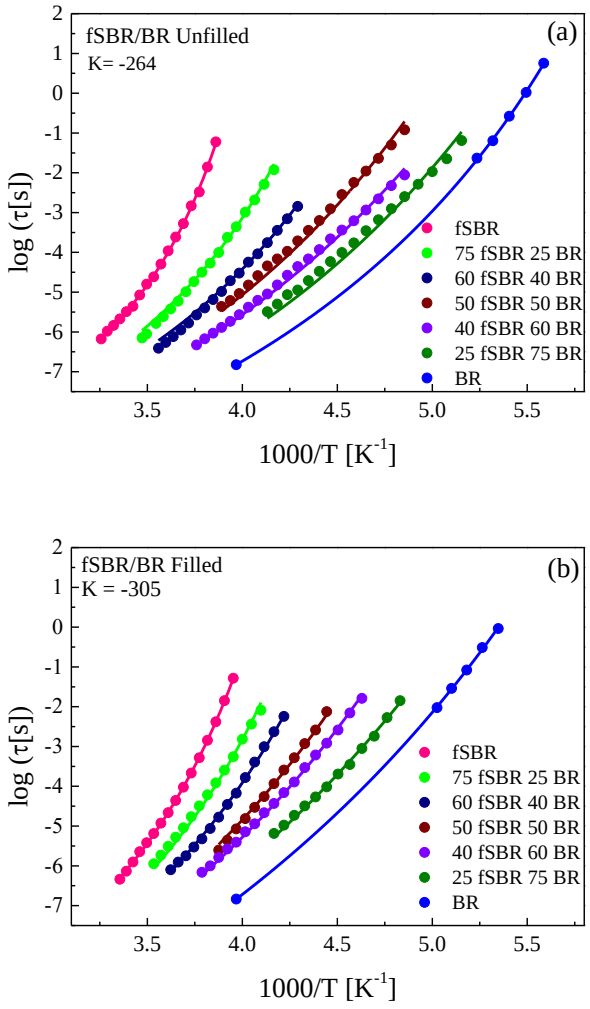

Figure 5.11 Relaxation time as a function of inverse temperature for unfilled (a) and filled (b) fSBR/BR blends with different compositions. Symbols represent experimental data whereas lines represent the best fit by means of the AG model with a fixed value for ***k***.

It is also worth to mention that parameters A and B are coupled in the sense that the ratio B/A is approximately constant for each blend. This would allow reducing even more the number of free parameters by writing the interaction parameter as $\chi(T) = A\,(1 + k / T)$ being ***k*** a constant parameters independent of the composition. Figure 5.11 shows an example of the fitting obtained for fSBR/BR blends by keeping ***k*** constant and leaving A free.

Moreover, it has been shown in a previous work[21] that the interaction parameter χ can be experimentally obtained by means of small-angle neutron scattering (SANS) or numerically predicted using the theory of random copolymer mixtures[22, 23]. In this case, the proposed extension of the AG model would become completely predictive. Thus, once the interaction parameter is known from independent experiments (or calculations), one could estimate the dynamics of a blend based on the characteristics and the dynamics of the neat components.

5.4 Conclusions

In this chapter we have analyzed an extension of the Adam-Gibbs model to account for the dynamics of crosslinked polymer blends with different microstructures at several temperatures and compositions. By adding a single term that accounts for the polymer/polymer interaction in the expression for the excess entropy we obtain an accurate description of the temperature dependence of the experimental relaxation time for the blends analysed in this work. The model has only two fitting parameters (***A*** and ***B***) that are characteristic to each polymer. However, based on previous works[21], these parameters are expected to be obtained from independent experiments or even from theoretical calculations, making this model completely predictive.

5.5 References

1. Avramova, N., *Polymer Additives: the Miscibility of Blends*. Springer: Dordrecht, 1998; Vol. 1, p 513-518.

2. Capaccio, G.; Gardner, A. J.; Hope, P. S.; Wilkinson, K. The industrial interest in blends. *Makromolekulare Chemie-Macromolecular Symposia* **1990,** 38, 267-273.

3. Haley, J. C.; Lodge, T. P.; He, Y. Y.; Ediger, M. D.; von Meerwall, E. D.; Mijovic, J. Composition and temperature dependence of terminal and segmental dynamics in polyisoprene/poly(vinylethylene) blends. *Macromolecules* **2003,** 36 (16), 6142-6151.

4. Roland, C. M.; Casalini, R. The role of density and temperature in the dynamics of polymer blends. *Macromolecules* **2005,** 38 (21), 8729-8733.

5. Mpoukouvalas, K.; Floudas, G. Effect of pressure on the dynamic heterogeneity in miscible blends of poly(methyl methacrylate) with poly(ethylene oxide). *Macromolecules* **2008,** 41 (4), 1552-1559.

6. Schwartz, G. A.; Alegria, A.; Colmenero, J. Adam-Gibbs based model to describe the single component dynamics in miscible polymer blends under hydrostatic pressure. *J. Chem. Phys.* **2007,** 127 (15), 8.

7. Alegria, A.; Colmenero, J. Dielectric relaxation of polymers: segmental dynamics under structural constraints. *Soft Matter* **2016,** 12 (37), 7709-7725.

8. Zhang, S.; Painter, P. C.; Runt, J. Dynamics of Polymer Blends with Intermolecular Hydrogen Bonding: Broad-Band Dielectric Study of Blends of Poly(4-vinyl phenol) with Poly(vinyl acetate) and EVA. *Macromolecules* **2002,** 35, 8478-8487.

9. Zhang, S. H.; Casalini, R.; Runt, J.; Roland, C. M. Pressure effects on the segmental dynamics of hydrogen-bonded polymer blends. *Macromolecules* **2003,** 36 (26), 9917-9923.

10. Mpoukouvalas; Floudas, K.; Zhang, G.; Runt, S. H. Effect of temperature and pressure on the dynamic miscibility of hydrogen-bonded polymer blends. *Macromolecules* **2005,** 38 (2), 552-560.

11. Schwartz, G. A.; Paluch, M.; Alegria, A.; Colmenero, J. High pressure dynamics of polymer/plasticizer mixtures. *J. Chem. Phys.* **2009,** 131 (4), 9.

12. Masser, K. A.; Runt, J. Dynamics of Polymer Blends of a Strongly Interassociating Homopolymer with Poly(vinyl methyl ether) and Poly(2-vinylpyridine). *Macromolecules* **2010,** 43 (15), 6414-6421.

13. Liu, C. Y.; Liu, Z. Y.; Yin, X. T.; Wu, G. Z. Tuning the dynamic fragility of acrylic polymers by small molecules: the interplay of hydrogen bonding strength. *Macromolecules* **2015,** 48 (12), 4196-4206.

14. Schwartz, G. A.; Tellechea, E.; Colmenero, J.; Alegria, A. Correlation between temperature-pressure dependence of the alpha-relaxation and configurational entropy for a glass-forming polymer. *J. Non-Cryst. Solids* **2005,** 351 (33-36), 2616-2621.

15. Schwartz, G. A.; Cangialosi, D.; Alegria, A.; Colmenero, J. Describing the component dynamics in miscible polymer blends: Towards a fully predictive model. *J. Chem. Phys.* **2006,** 124 (15), 5.

16. Adam, G.; Gibbs, J. H. On temperature dependence of cooperative relaxation properties in glass-forming liquids. *J. Chem. Phys.* **1965,** 43 (1), 139-142.

17. Rubinstein, M.; Colby, R. H., *Polymer Physics*. Oxford, 2008.

18. D., C.; Schwartz, G. A.; Alegria, A.; Colmenero, J. Combining configurational entropy and self-concentration to describe the component dynamics in miscible polymer blends. *J. Chem. Phys.* **2005,** 123 (14), 9.

19. Cole, K. S.; Cole, R. H. Dispersion and absorption in dielectrics I. Alternating current characteristics. *J. Chem. Phys.* **1941,** 9 (4), 341-351.

20. Cerveny, S.; Bergman, R.; Schwartz, G. A.; Jacobsson, P. Dielectric alpha- and beta-relaxations in uncured styrene butadiene rubber. *Macromolecules* **2002,** 35 (11), 4337-4342.

21. Sakurai, S.; Izumitani, T.; Hasegawa, H.; Hashimoto, T.; Han, C. C. Small-angle neutron scattering and light scattering study on the miscibility of poly(styrene-ran-butadiene)/polybutadiene blends. *Macromolecules* **1991,** 24 (17), 4844-4851.

22. Tenbrinke, G.; Karasz, F. E.; Macknight, W. J. Phase behavior in copolymer blends: Poly(2,6-dimethyl-1,4-phenylene oxide) and halogen-substituted styrene copolymers. *Macromolecules* **1983,** 16 (12), 1827-1832.

23. Paul, D. R.; Barlow, J. W. A binary interaction model for miscibility of copolymers in blends. *Polymer* **1984,** 25 (4), 487-494.

6

fSBR/NR immiscible blends

Blending of rubber polymers is an effective and economic approach to achieve a desired combination of properties compared to synthesizing new materials. Potential advantages of rubber blends are: improved solvent resistance and processability; better product uniformity; quick formulation changes and manufacture flexibility.

A polymer blend is defined as a mixture of two or more polymers which generate a novel material with different physical properties[1-3]. In some cases these blends are immiscible or heterogeneous and therefore, the mixture results in a multiphasic structure with a varied range of properties normally improved with regards to the single materials[4].

In the case of tire treads, blends are frequently composed of Butadiene Rubber (BR) or Natural Rubber (NR) with Styrene Butadiene Rubber (SBR)[5]. SBR improves the wet skid resistance whereas NR or BR are used to provide good elastic properties. Mixing of SBR and NR results in immiscible blend in which the continuous phase is normally NR whereas SBR appears as droplets dispersed in the NR matrix[6]. This is in part due to the different viscosities of the components: the low viscosity component (NR) encapsulates the high viscosity component (SBR)[7, 8].

The miscibility of two polymers depends, among other factors, on the specific interactions between the monomeric units and on the corresponding molecular weights. Both can lead to a phase separation; in particular, high

molecular weight polymer blends have a tendency to phase separation due to entropy gain upon mixing[6]. As a result, the immiscible blend splits into domains whose size, distribution and characteristic interfaces determine the physical properties of the mixture[9].

As previously discussed in Chapter 1, composites made of rubber blends are complex systems whose interactions determine the final features of the resulting materials. The large amount of ingredients included in the formulation of the compounds, shows the need for a good understanding of the interactions between rubbers and compounding additives. These interactions will allow or restrict the movement of the additives throughout the rubber matrix, depending on their nature, reactivity, and solubility [10]. It is well known that curatives and other compounding additives (antidegradants) migrate across the rubber compound, in both the uncured and cured states[11]. Diffusion through a rubber-to-rubber interphase can be detrimental to performance. However, in some cases it can be an advantageous process, as in the cases of oils and antidegradants, enhancing its activity by diffusion through the rubber matrix. Thus, a good understanding of the migration of the additives opens the possibility to improve the final properties of a material by controlling the distribution of additives within the rubber matrix [10, 12].

In this chapter, we analyse the macroscopic thermal and dynamical behaviour of fSBR/NR blends by means of DSC and BDS whereas the structure at the nano-scale is analysed by AFM, TEM and EDX.

6.1 Results

6.1.1 Differential scanning calorimetry (DSC)

Calorimetric measurements were performed to determine the glass transition temperature (T_g) of the materials. Figure 6.1 shows the heat flow as a function of the temperature for the fSBR/NR blends.

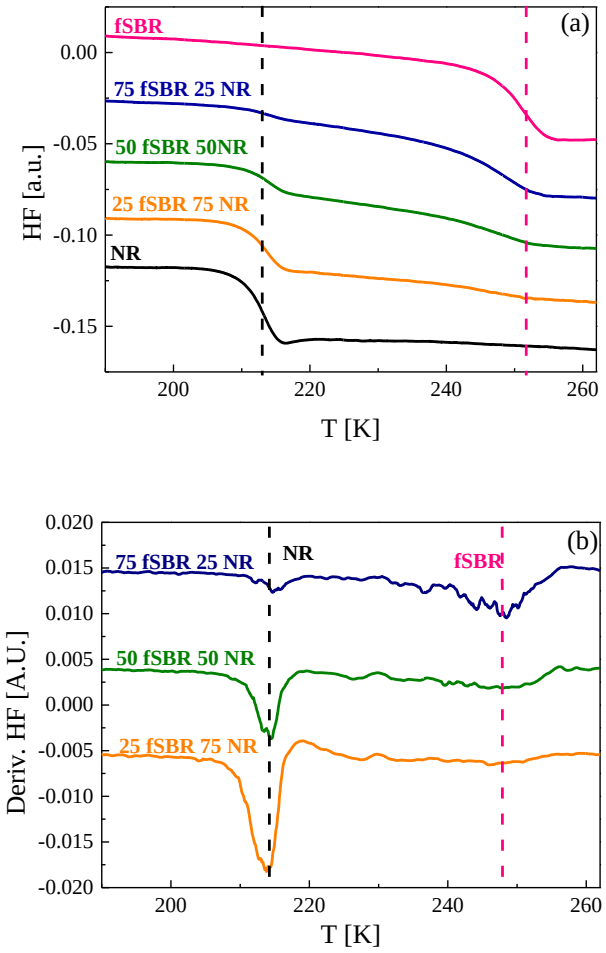

Figure 6.1 Heat flow as a function of the temperature (a), and derivative of the heat flow as a function of the temperature (b). Curves were vertically displaced to let the comparison among the different blend ratios. Dashed lines indicate the glass transition temperature of the neat compounds (fSBR and NR).

Pink and black curves correspond to neat fSBR and NR, respectively; those corresponding to the blends with different compositions are also shown in the same figure. In this case, two different T_gs are observed, in correspondence to those of the neat NR or fSBR compounds, respectively. This is a signature of immiscibility as previously analyzed for the same polymers even with a different cure recipe or mixing type[1, 2].

T_g values of pure compounds and blends are shown in Figure 6.2. As shown, whereas the value of the low T_g component is very similar to that of the neat NR compound, the value of the high T_g component systematically shifts to lower temperatures when increasing the NR content. Shifts of T_g values, could indicate partial solubility between either phases or an eventual heterogeneous distribution of additives compared to the bulk materials.

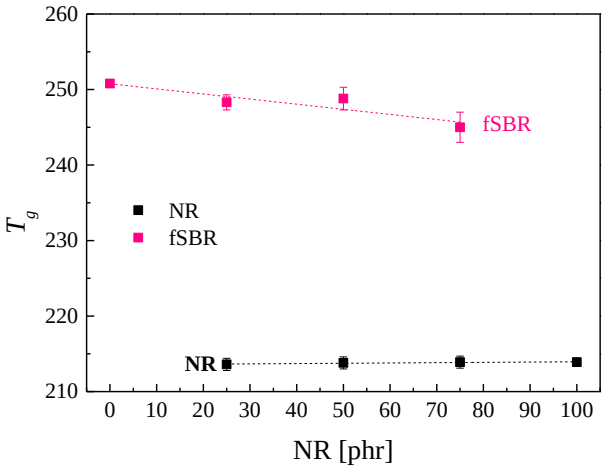

Figure 6.2 T_g values obtained from Figure 6.1 as a function of NR composition.

6.1.2 Broadband dielectric spectroscopy (BDS)

Dynamics of the neat polymers

Figure 6.3 shows the imaginary part of the dielectric permittivity as a function of the frequency at 265 K for both fSBR and NR neat polymers. To fit the data two Cole-Cole functions were used to account for the segmental relaxation and the low frequency contribution attributed (in the case of fSBR) to the presence of the secondary accelerator, as discussed in Chapter 4. In the case of NR, this slow process may be attributed to the presense of proteins and phospholipids[23]. In any case, the low frequency contribution found in NR was not investigated in this thesis. Additionally, at higher temperatures a conductivity term was added ($\sigma/j\omega\varepsilon_0$). To obtain a more accurate fit, imaginary and real parts of the dielectric permittivity have been simultaneously fitted.

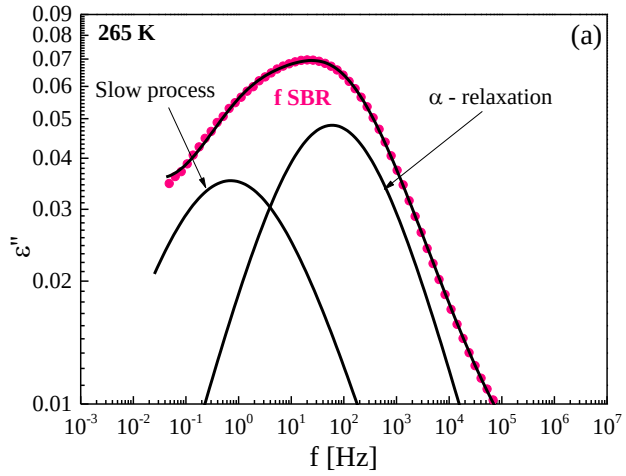

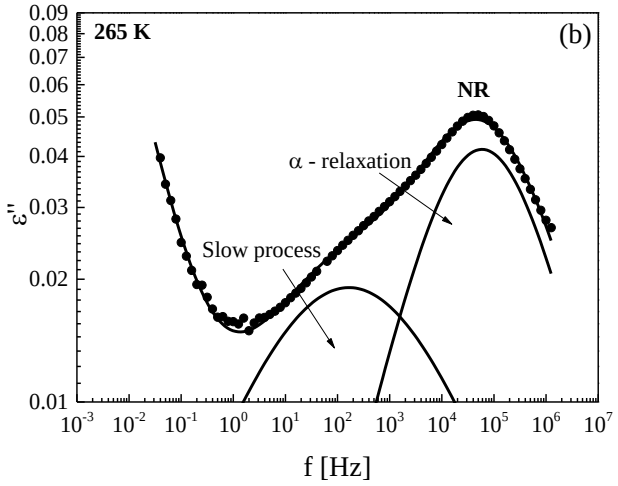

Figure 6.3 Imaginary part of the dielectric permittivity as a function of the frequency for the neat compounds fSBR(a) and NR(b) at 265 K. Solid lines correspond to the CC fitting.

The temperature dependence of the relaxation times for both fSBR and NR follows a Vogel-Fulcher- Tammann (VFT) behavior (see Figure 6.4).

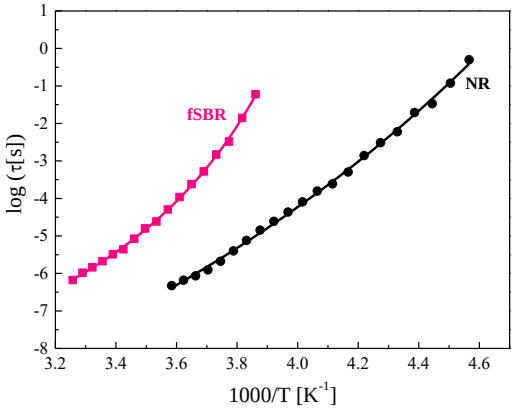

Figure 6.4 Temperature dependence of the relaxation times for the segmental relaxations of fSBR and NR. Solid lines represent the best fit by means of the VFT equation.

Dynamics of the blends

For all the blends, BDS measurements show two segmental relaxations corresponding to the two phases present in the compound, as previously discussed. Figure 6.5 shows the imaginary part of the dielectric permittivity (ε'') as a function of the frequency for the sample 25fSBR 75NR at different temperatures, where the two peaks shift to higher frequencies with increasing temperatures.

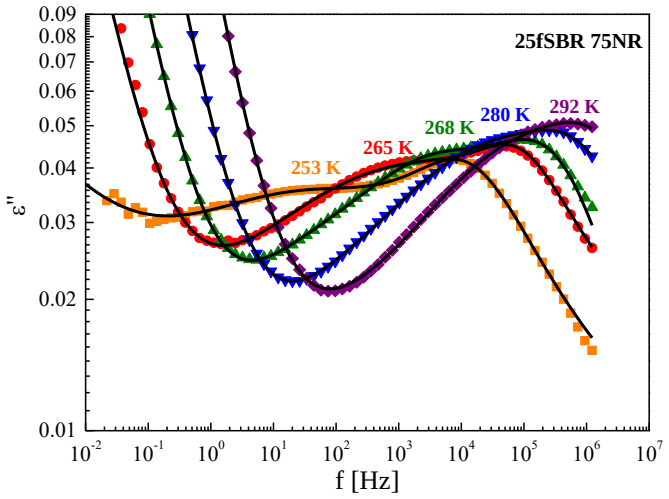

Figure 6.5 Dielectric permittivity as a function of the temperature for the 25fSBR 75NR blend at different temperatures. Solid lines correspond to the CC fitting.

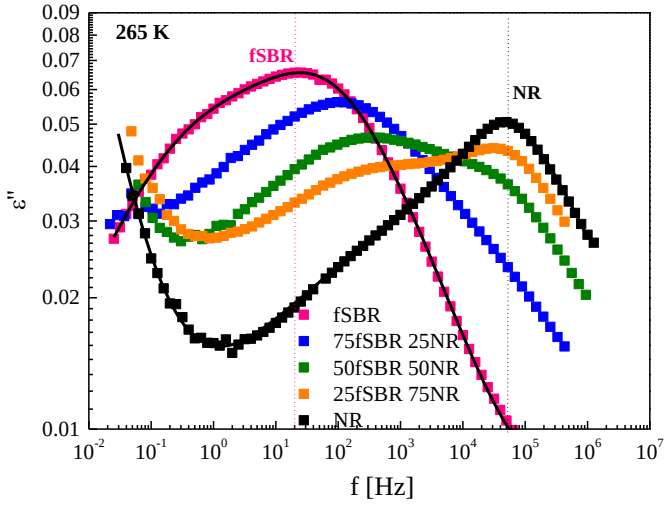

Figure 6.6 Dielectric permittivity as a function of the frequency for the neat compounds and the blends at 265 K. Solid lines correspond to the CC fitting.

Figure 6.6 shows the dielectric permittivity as a function of the frequency at 265 K for both neat compounds and blends. The temperature dependence of the relaxation times is shown in Figure 6.7 where two different time scales can be observed. The fastest dynamics correspond to the NR phase which is almost independent on the composition of the blend. The slow dynamics correspond to the fSBR phase which becomes faster with increasing NR content.

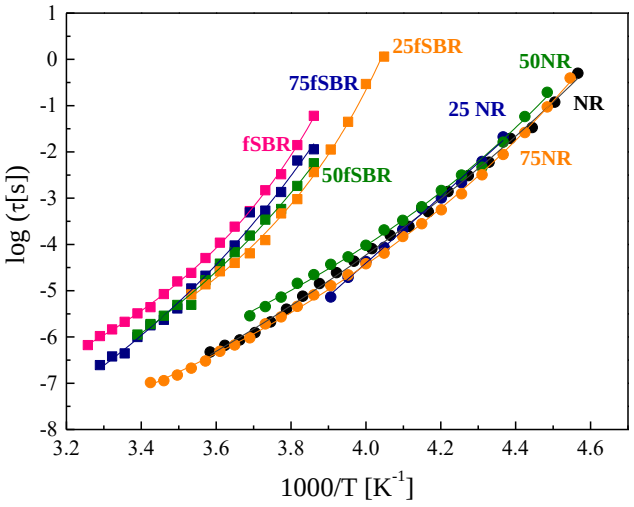

Figure 6.7 Temperature dependence of the relaxation times for the segmental relaxations of fSBR/NR blends and neat polymers. Solid lines represent the best fitting by means of the VFT equation.

As shown, the dynamics of the NR phase remain almost unaffected in the blend compared to the bulk, whereas the dynamics of the fSBR phase become faster with increasing NR content. In particular, the relaxation time of fSBR is becoming shorter by increasing NR content. Shifts of the segmental dynamics of the components could indicate either partial miscibility, confinement effects or an eventual heterogeneous distribution of the curing additives compared to the bulk materials. Concerning to this last point, previous works[13, 14] have shown how the migration of curing additives, such as the accelerator N-Cyclohexylbenzothiazole-2-sulphenamide (CBS) in SBR/NR blends, is produced from SBR to NR[14]. This would be in agreement with the speedup observed in the dynamics of the fSBR phase, when the NR content increases in the blend (Figure 6.7). However, since BDS and DSC only provide macroscopic average information, it is not possible to determine the different

properties with spatial resolution, which is necessary to understand the reason for the increased SBR dynamics. Therefore, it is necessary to use other experimental techniques which provide local information about the mechanical and structural properties. In this chapter, we propose a structural analysis at the nano-scale by means of AFM, TEM and EDX.

6.1.3 Atomic Force Microscopy (AFM)

Mechanical properties like hardness, tensile strength, and modulus of cured rubbers are strongly dependent on the network structure, such as the crosslink density[15]. In particular, mechanical modulus is sensitive to the network structure of rubbers and crosslinked polymers and can be used to qualitatively estimate the characteristics of the network[15].

Local mechanical measurements by means of atomic force microscopy (AFM) were performed in order to obtain qualitative information of the mechanical modulus of the different phases[16]. Figure 6.8 shows the surface height, DMT modulus and dissipation channels of the 50fSBR 50NR blend, where it is possible to see a continuous phase of one component with nearly spherical regions of the other one. Since the modulus of the continuous matrix is systematically lower than that of the islands, it is possible to identify the continuous matrix as NR whereas the islands correspond to fSBR[17]. This is in agreement with previous studies of SEM/TEM in the same type of blends[18].

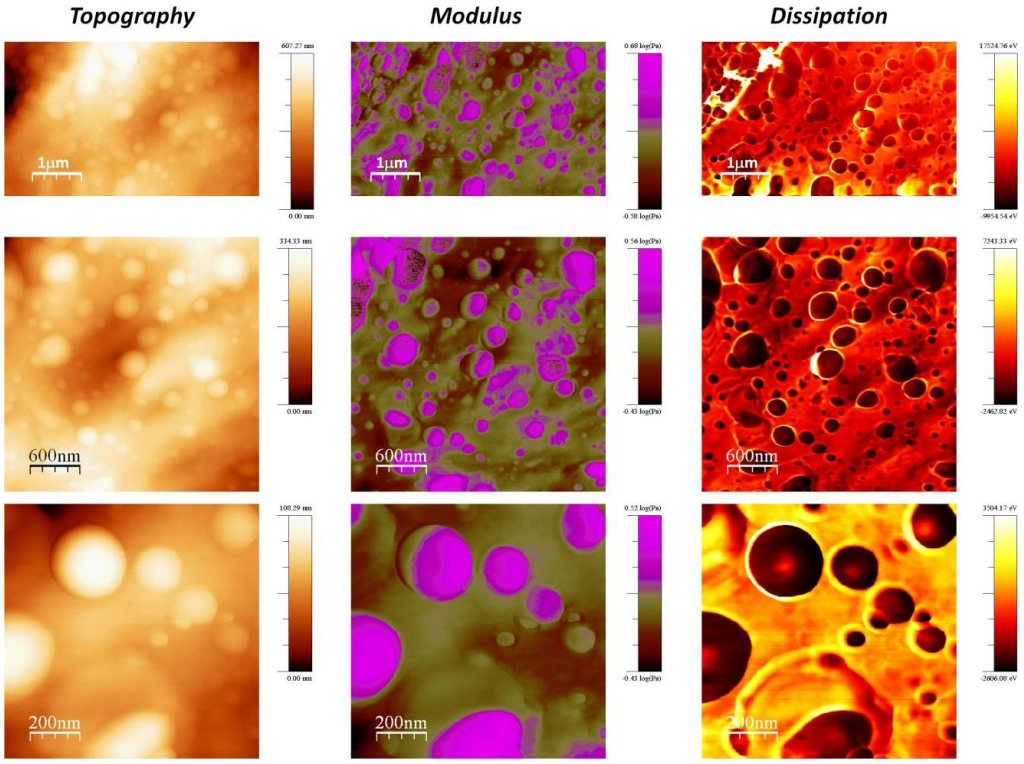

Figure 6.8 Topography, DMT modulus and dissipation images for the 50fSBR 50NR blend.

Figure 6.9 shows dissipation images of fSBR/NR blends with different compositions. As shown, as the fSBR concentration increases the amount of low-dissipation regions also increases. It is noteworthy that the observed typical size for fSBR islands presents a maximum at intermediate fSBR concentrations. Assuming the same mixing conditions, this fact could be either related to a lower miscibility or to a lower mixing efficiency of 50fSBR 50NR formulation. In any case, fSBR islands are observed for all compositions, even when fSBR is the main component.

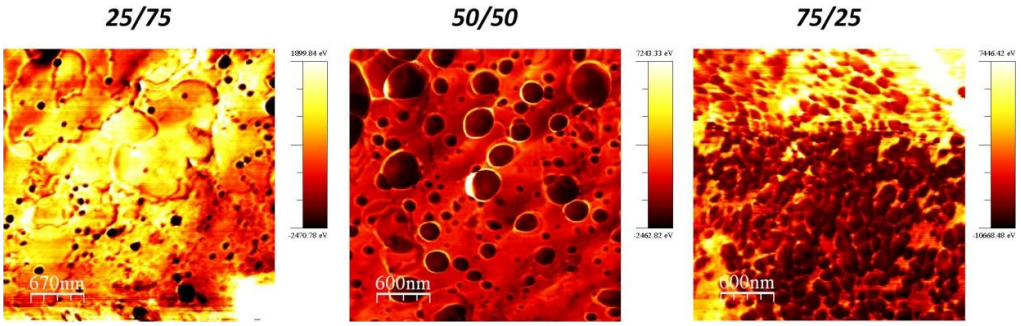

Figure 6.9 Dissipation images of fSBR/NR blends. The scan size was 3 μm.

Figure 6.10 shows the topography and DMT modulus images of the 50fSBR 50NR blend. The DMT modulus profile (Figure 6.10c) reveals two different regions: one (in orange) with a constant value independent of the position (on the continuous phase and away from the spheres) and another in which the modulus shows a distribution with a maximum towards the centre of the sphere (green line). Although the quantitative determination of the DMT modulus present some systematic errors for soft materials[19], the qualitative differences observed in Figure 6.10c are clear enough to assume a radial variation of the mechanical properties within the fSBR island. This radial dependence of the mechanical modulus in the fSBR phase has been also systematically observed for many islands of different sizes. It is worth noticing here that the interphase between both polymers is very sharp (as seen in Figure 6.11b) and this variation of the mechanical properties is not due to the interpenetration of the two polymers. This means that even being the islands made only of fSBR, we observe a radial variation of the mechanical modulus which could be related with changes on its structural network most likely due to an heterogeneous distribution of some of the vulcanization additives.

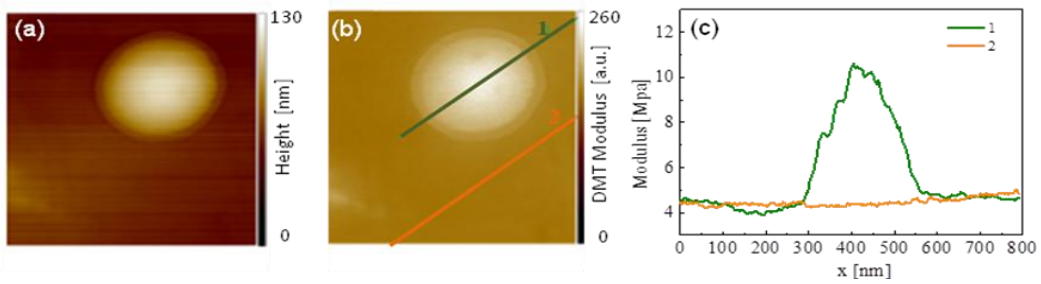

Figure 6.10 Topography (a) and modulus (b) images of the 50fSBR 50NR blend. The brighter part of image corresponds to fSBR whereas the dark continuous matrix to NR. The scan size was 1 μm. Variation of the DMT modulus along profile 1 and 2 indicated in b (c).

Different magnifications of the same region were analyzed (see Figure 6.11) showing that in all the cases the modulus increases with the position, reaching a maximum value close to the center of the sphere. Figure 6.11c shows a sharp step in the mechanical modulus when moving from one phase into the other. This narrow region (about 5 nm) corresponds to the interphase between both polymers and gives a clear evidence about the phase separation. This is also compatible with what is observed by BDS and DSC where two distinct dynamics (close to those of the neat components) are detected. In addition, no intermediate dynamics was observed by DSC nor by BDS.

The radial distribution observed in the mechanical modulus is also compatible with the big broadening of the glass transition measured by DSC as shown in Figure 6.1b. There, we can observe that the broadening of the fSBR is much bigger than for NR and this is in agreement with the distribution of the dynamics (mechanical behavior) observed in the fSBR regions as shown in Figure 6.10c.

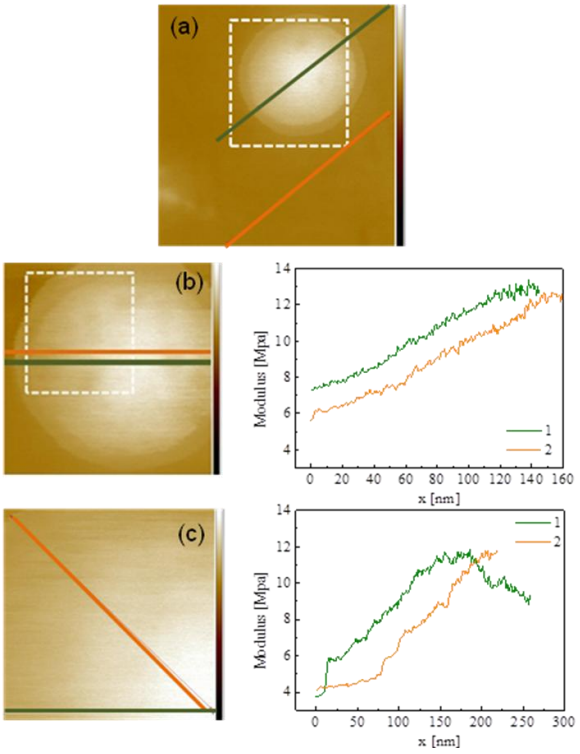

Figure 6.11 Image of the DMT modulus of the 50fSBR 50NR blend. Scans were (from bottom to top) 1 (a), 0.5 (b) and 0.3 (c) μm. Variation of the DMT modulus along the profiles 1 and 2 as indicated (b) and (c).

According to a possible migration of the curing additives from the SBR to the NR phase, one would also expect an increase in the mechanical modulus of the NR phase close to the interphase with SBR, due to the excess of additives coming from the SBR phase. However, AFM measurements do not show any changes in the modulus along the NR phase (Figure 6.10). This can be explained if we look at the diffusion coefficients of the curing additives in both polymers (Table 6.1)

Table 6.1. Diffusion coefficients for Cyclohexylbenzothiazole-2-sulphenamide (CBS)[14] at 100 ºC. (Diffusion is given in units of 10^{-7} cm^2/sec).

Accelerator	**SBR**	**NR**
CBS	0.5	0.8

As shown, the diffusivity of CBS in NR is significantly higher than in SBR. High diffusion of curing additives in NR explains the constant mechanical modulus observed along the NR phase, since curing additives are uniformly dispersed, and therefore, crosslink density is expected to be more uniform.

Although AFM can measure several mechanical properties with spatial resolution down to a few nano meters, we do not get any information about the local chemical composition of the sample. In order to get such information, we have performed elemental analysis by means of energy dispersive X-ray spectroscopy (EDX).

6.1.4 Energy-dispersive X-ray spectroscopy (EDX)

Energy Dispersive X-Ray Analysis (EDX) is an X-ray technique used to identify the elemental composition of materials. EDX systems are attachments to Electron Microscopy instruments (Scanning Electron Microscopy (SEM) or Transmission Electron Microscopy (TEM)) instruments where the imaging capability of the microscope identifies the specimen of interest. The data generated by EDX analysis consist of spectra showing peaks corresponding to the elements making up the true composition of the sample being analysed. EDX-TEM was used to monitor elemental compositions in the domains of the 50fSBR 50NR blend. The sample was cryogenically microtomed to obtain slides thin enough (~ 100 nm) to be observed by TEM. The EDX-TEM measurements were done in the "*Laboratorio de microscopías avanzadas*", Zaragoza, Spain using a Tecnai F30 (FEI company), which is a versatile high resolution Transmission Electron Microscope. It can work in TEM or STEM (Scanning-Transmission) modes and it is equipped with all the analytical techniques to obtain morphology, structure and composition information with atomic resolution. Elemental analysis (EDX) to determine the chemical composition was also done. In this mode, when the electron beam strikes the specimen surface, not only secondary electrons and backscattered electrons but also characteristics X-ray are generated at or near the specimen surface. These characteristics X-rays are used to identify the composition and to measure the abundance of elements in the sample.

Figures 6.12 to 6.14 show some representative results of the EDX-TEM measurements. Figure 6.12 shows two different areas of the EDX analysis for the 50fSBR 50NR blend. As can be seen from the chart, different sulfur, silicon, oxygen and carbon concentrations were detected.

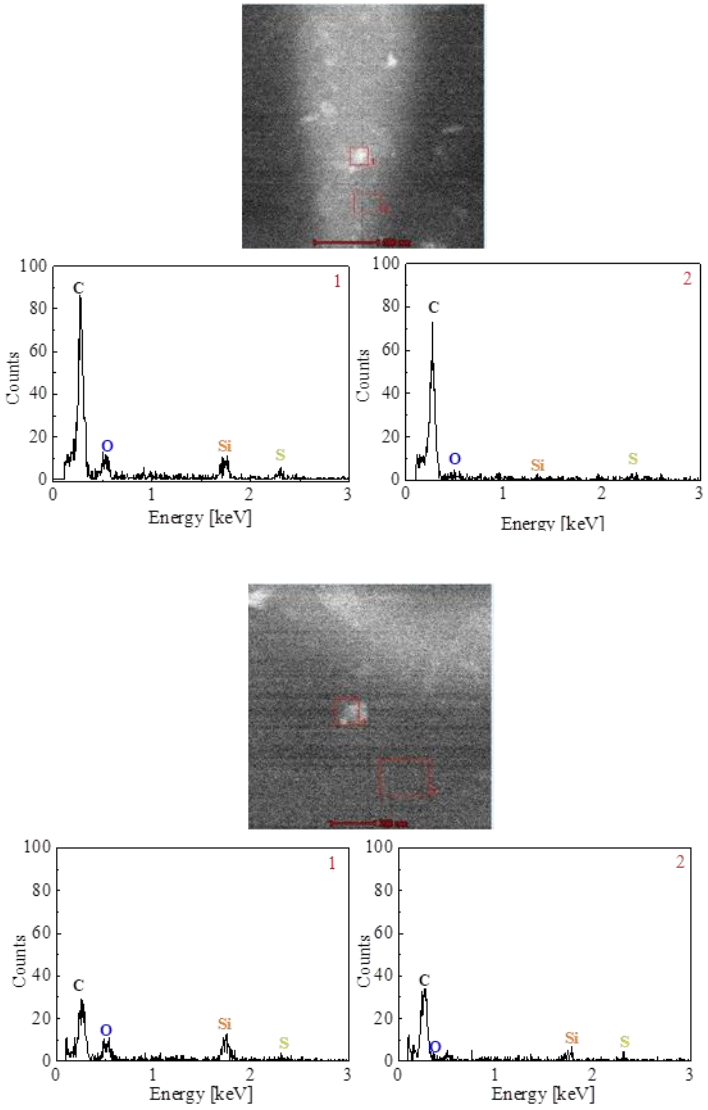

Figure 6.12 Two different areas of the surface of 50fSBR 50NR blend were scanned. EDX spectra are also shown for two different areas (inside and outside of the fSBR phase (see red squares in both photographs). Carbon, oxygen, silicon and sulphur were detected.

Figures 6.13 and 6.14 show the scans of two different areas of the blend where an island of fSBR is surrounded by NR. In both cases we also included the EDX analysis along the profile marked in the figures (see orange lines). The presence of carbon along each profile is almost constant and independent on the position since both fSBR and NR contains approximately the same amount of carbon atoms per volume unit and no specific distribution is expected. However, sulfur does show a different profile. The quantity of sulfur is higher in the inner part of the sphere (fSBR) compared to the NR phase, reaching a maximum at the center of the fSBR island.

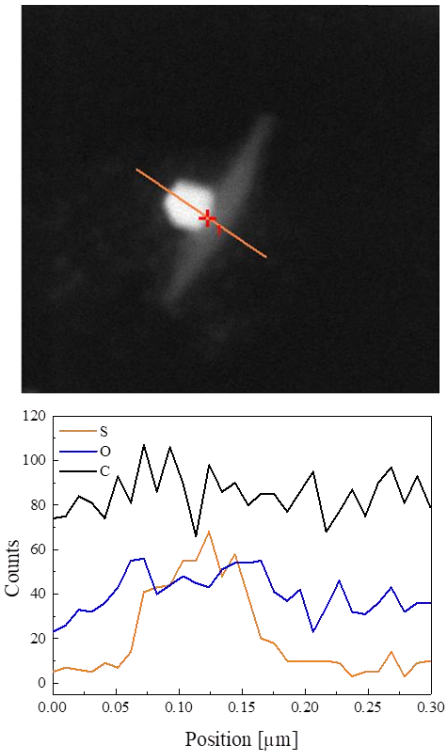

Figure 6.13 TEM image of the surface for 50fSBR 50NR blend. EDX spectrum is shown and the quantity of sulphur, oxygen and carbon is displayed in a function of the position (orange line on the image).

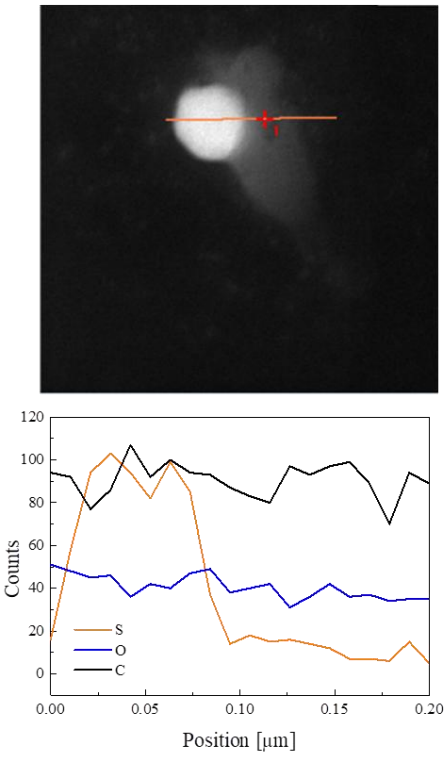

Figure 6.14 TEM image of the surface for 50-50 blend. EDX spectrum is shown and the quantity of sulphur, oxygen and carbon is displayed as a function of the position (orange line on the image).

These results show that sulphur (and possibly CBS, since it contents sulphur in its structure) is not homogeneously distributed[20] and this could lead to a non-homogeneous distribution of crosslinks along the fSBR which would be compatible with the variation of the local modulus observed by AFM (see Figure 6.10). In previous works[11, 21], the migration of curatives (sulphur and accelerators) was studied by testing some common curatives in carbon black-filled natural rubber compounds. It was found a rubber-to-rubber interface migration even at room temperature, causing significant changes in the cure system near, and at the interface. More recently, studies of the thermal

properties[13] of cured NR and SBR blends have shown a decrease in T_g associated to the SBR phase, compared with the bulk SBR. This was attributed to the migration of curatives from SBR to NR, producing a decrease in the crosslink density and therefore decreasing T_g[22]. However, as shown here both by AFM and EDX, the distribution of the mechanical modulus and the sulphur is not homogeneous within the SBR island but radially distributed.

Although these findings just constitute a preliminary exploratory work, they open the door to selectively tune the mechanical properties of the different phases in immiscible rubber blends by controlling the migration of the vulcanization additives[11, 21]. This could add a new variable in the compounding providing a fine tuning of the final properties of the rubber compounds.

6.2 Conclusions

In this chapter we have characterized the calorimetric, dielectric and mechanical behavior of fSBR/NR immiscible rubber blends. Using a combination of macroscopic (BDS and DSC) and microscopic (AFM and EDX) techniques we were able to understand different aspects of these particular blends. On the one hand, we have seen that fSBR and NR are highly immiscible polymers. The two different glass transition temperatures observed by DSC as well as the two separated dynamics detected by BDS are clear evidence in this sense. In addition, the AFM measurements show that the interphase between both polymers is also very narrow. On the other hand, a radial variation of the mechanical modulus has been observed inside the fSBR islands. In addition to this, EDX measurements show a radial distribution of sulphur for the same regions which is most likely related to a heterogeneous distribution of the crosslink density which would explains the variations in the mechanical properties.

Controlling the crosslink distribution between rubber phases can lead to improve the mechanical properties of the final compounds. However, further studies are necessary to fully understand these phenomena but a promising field opens where the selective migration of the different additives allows controlling the macroscopic properties of the blend.

6.3 References

1. Mansilla, M. A.; Silva, L.; Salgueiro, W.; Marzocca, A. J.; Somoza, A. A study about the structure of vulcanized natural rubber/styrene butadiene rubber blends and the glass transition behavior. *J. Appl. Polym. Sci.* **2012,** 125 (2), 992-999.

2. Ghilarducci, A.; Cerveny, S.; Salva, H.; Matteo, C. L.; Marzocca, A. J. Influence of the blend composition in the internal friction of NR/SBR compounds. *Kautschuk Gummi Kunststoffe* **2001,** 54 (7-8), 382-386.

3. Gardiner, J. B. Curative diffusion between dissimilar elastomers and its influence on adhesion. *Rubber Chem. Technol.* **1968,** 41 (5), 1312-1328.

4. Roland, C. M., Immiscible rubber blends. In *Advanced Structured Materials*, Springer, Ed. 2013; Vol. 11, pp 167-181.

5. Heisler, H., *Advanced Vehicle Technology*. Elsevier Science: 2002; Vol. 10.

6. Avgeropoulos, G. N.; Weissert, F. C.; Biddison, P. H.; Böhm, G. G. A. Heterogeneous blends of polymers. Rheology and morphology. *Rubber Chem. Technol.* **1976,** 49 (1), 93-104.

7. P. M. Visakh, S. T., Arup K. Chandra, Aji. P. Mathew, *Advances in Elastomers I: Blends and Interpenetrating Networks*. Springer Science: 2013.

8. M. A. Mansilla; A..J. Marzocca; C. Macchi; A. Somoza. Natural rubber/styrene-butadiene rubber blends prepared by solution mixing: Influence of vulcanization temperature using a Semi-EV sulfur curing system on the microstructural properties. *Polymer Testing* **2017,** 63, 150-157.

9. Mansilla, M. A.; Valentin, J. L.; Lopez-Manchado, M. A.; Gonzalez-Jimenez, A.; Marzocca, A. J. Effect of entanglements in the microstructure of cured NR/SBR blends prepared by solution and mixing in a two-roll mill. *Eur. Polym. J.* **2016,** 81, 365-375.

10. Tinker A. J. Distribution of crosslinks in vulcanized blends. *Rubber Chem. Technol.* **1995,** 68 (3), 461-480.

11. Frederick Ignatz-Hoover; H. Byron; R. N. Datta; Arie J. De Hoog; N. M. Huntink; Talma, A. G. Chemical additives migration in rubber. *Rubber Chem. Technol.* **2003,** 76 (3), 747-768.

12. Matthias Wunde; Manfred Klüppel. Impact of mixing procedure on phase morphology and fracture mechanical properties of carbon black-filled NR/SBR blends. *Continuum Mechanics and Thermodynamics* **2017,** 29 (5), 1135-1148.

13. S. Goyanes; C. C. Lopez; G. H. Rubiolo; F. Quasso; A..J. Marzocca. Thermal properties in cured natural rubber/styrene
butadiene rubber blends. *Eur. Polym. J.* **2008,** 44, 1525-1534.

14. James E. Lewis; Marvin L. Deviney Jr.; Whittington, L. E. Migration of antioxidants and accelerators in natural and synthetic rubber II. sulfenamide system studies and comparison of age resister migration under inert and practical conditions. *Rubber Chem. Technol.* **1969,** 42 (3), 892-902.

15. Fei Zhao; Weina Bi; Shugao Zhao. Influence of Crosslink Density on Mechanical Properties of Natural Rubber Vulcanizates. *Journal of Macromolecular Science. Part B: Physics.* **2011,** 50, 1460-1469.

16. Bijarimi, M.; Zulkafli, H.; Beg, M. D. H. Mechanical properties of industrial tyre rubber compounds. *Journal of Applied Sciences* **2010,** 10, 1345-1348.

17. I.H. Jeon; H. Kim; Kim, S. G. Characterization of rubber micro-morphology by atomic force microscopy (AFM) *Rubber Chem. Technol.* **2003,** 76 (1), 1-11.

18. Suhe Zhao; Hua Zou; Xingying Zhang. Structural Morphology and Properties of Star Styrene–Isoprene–Butadiene Rubber and Natural

Rubber/Star Styrene–Butadiene Rubber Blends. *J. Appl. Polym. Sci.* **2004,** 93 (1), 336–341.

19. Nakajima, K.; Ito, M.; Wang, D.; Liu, H.; Nguyen, H. K.; Liang, X. B.; Kumagai, A.; Fujinami, S. Nano-palpation AFM and its quantitative mechanical property mapping. *Microscopy* **2014,** 63 (3), 193-207.

20. Leila L. Y. Visconte; Agnes F. Martins; Joao C.M. Suarez; Regina C. R. Nunes. Different preparative modes for the incorporation of additives in NR/SBR blends. *J. Appl. Polym. Sci.* **2004,** 93, 483-489.

21. Anthoine, F. I.-H.; To, B. H. Migration of additives in rubber. *Gummi Fasern Kunststof* **2004,** 10, 653-662.

22. Adi Shefer; Moshe Gottlieb. Effect of crosslinks on the glass transition temperature of end-linked elastomers. *Macromolecules* **1992,** 25 (15), 4036-4042.

23. P. Ortiz-Serna, R. Díaz-Calleja, M.J. Sanchis, G. Floudas, R. C. Nunes, A. F. Martins, and L.L. Visconte. Dynamics of natural rubber as a function of frequency, temperature, and pressure. A dielectric spectroscopy investigation. *Macromolecules.* **2010,** 43, 5094-5102.

7

Concluding remarks

In this thesis, we presented a detailed study of the structure and dynamics of unfilled and silica-filled compounds of NR, BR, different types of SBR, and blends of these rubbers by means of BDS, DSC, and complementary techniques as AFM and EDX.

Vulcanized unfilled fSBR has been studied by means of BDS, and its dielectric response revealed, besides the segmental relaxation, an additional process at low frequencies. In literature, this process has been sometimes associated with immobilized polymer layers around silica particles[1] (in the case of filled compounds) or with slower polymer dynamics around zinc oxide or other additives (for unfilled samples). In this thesis we have studied compounds prepared with both a full formulation and by removing one additive type at a time. This method allows us to attribute the origin of the low frequency contribution to the presence of DPG, one of the accelerators used for vulcanization.

Secondly, we have presented an extension of the Adam-Gibbs model to account for the dynamics of crosslinked miscible polymer blends at different temperatures and compositions, by adding a single term to the excess entropy expression that accounts for the strong interactions existing between the polymers. The proposed model has been tested on several unfilled and silica filled blends with different compositions. For all these compounds, the model

provided an excellent description of the temperature dependence of the experimental relaxation times, accurately describing the dynamics of the blends based on the dynamics of the neat compounds and by means of only two fitting parameters.

Finally, we have also analyzed immiscible polymer blends of fSBR/NR by means of different techniques. On the one hand, DSC and BDS measurements showed two T_gs and two separated dynamics, respectively, which is a clear sign of immiscibility. Moreover, calorimetric and dielectric results also showed changes in the T_g as well as in the dynamics of the fSBR phase as a function of the blend composition. On the other hand, we have studied, by means of AFM, the phase morphology of the blends and observed a matrix composed of NR and islands of SBR, with a very narrow interphase. Further measurements of the mechanical properties by AFM showed a radial variation of the mechanical modulus inside the SBR islands, whereas EDX measurements have shown a radial distribution of sulfur in the same areas. These results are compatible with a likely heterogeneous distribution of the curing additives inside the SBR regions due to their migration from fSBR to NR, which could lead to an inhomogeneous crosslink density.

The results obtained in this PhD thesis allow to gain a better understanding of the dynamics of crosslinked miscible and immiscible rubber blends, as well as to study the influence of vulcanization additives and their mobility through the polymer matrix. The knowledge acquired here does not only shed some light on the understanding of some fundamental scientific problems related to rubber compounds but also establishes a solid basis for future investigations.

7.1 References

1. Hernandez, M.; Carretero-Gonzalez, J.; Verdejo, R.; Ezquerra T.A.; Lopez-Manchado, M. A., Molecular dynamics of natural rubber/layered silicate nanocomposites as studied by dielectric ralaxation spectroscopy. *Macromolecules* **2010**, 43 (2), 643-651.

Appendix

1. Influence of vulcanization additives on the dielectric response of chain-end functionalized styrene butadiene rubber (Chapter 4)

1.1 Full formulation of the compounds

Table A.1 Formulation [phr] of the samples studied in Chapter 4, where for each sample one ingredient was systematically removed leaving the rest of the formulation used for vulcanization unchanged.

Sample	Full	No oil/wax	No Antiox	No sulfur donor	No accelerators	No stearic acid
f-SBR	100					
Wax	2		2	2	2	2
Antioxidant	4	3.25		4	4	4
Processing Oil	3		3	3	3	3
Stearic Acid	3	3	3	3	3	
ZnO	2.5	2.5	2.5	2.5	2.5	2.5
Accelerator (DPG)	1.6	1.6	1.6	1.6		1.6
Accelerator (CBS)	1.2	1.2	1.2	1.2		1.2
Sulfur	1.4	1.4	1.4	1.4	1.4	1.4
Sulfur-Donor	2	2	2		2	2

Table A.2 Full formulation [phr] of the samples studied in Chapter 4, where the amount of one accelerator has kept constant and the other one has been varied.

Sample	1.2 DPG	0.9 DPG	0.6 DPG	0.3 DPG	0 DPG	1 CBS	0.4 CBS
f-SBR	100						
Wax	2						
Antioxidant	4						
Processing Oil	3						
Stearic Acid	3						
ZnO	2.5						
DPG	1.2	0.9	0.6	0.3	0	1.2	1.2
CBS	1.6	1.6	1.6	1.6	1.6	1	0.4
Sulfur	1.4						
Sulfur-Donor	2						

1.2 Dielectric strength (Δε) and shape parameter (α) of the segmental relaxation of fSBR

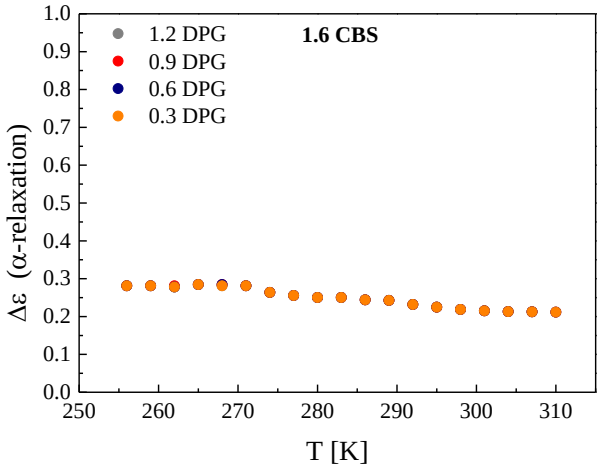

Figure A.1 Dielectric strength as a function of the temperature for samples with variations in the DPG content (from 0.3 to 1.2 phr)

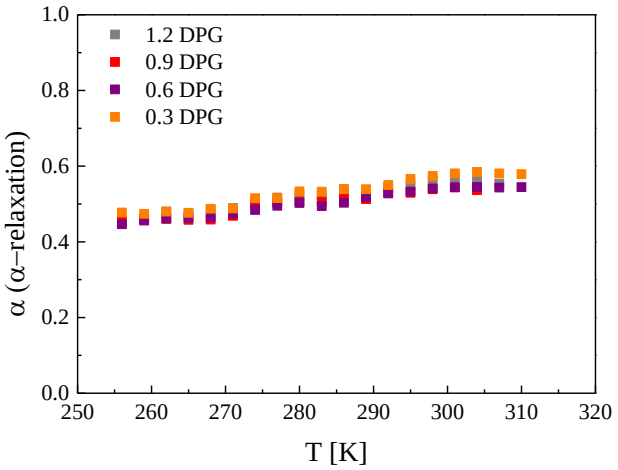

Figure A.2 Shape parameter (α) as a function of the temperature for the segmental relaxations of the samples with variations in DPG content (from 0.3 to 1.2 phr).

1.3 Determination of the crosslink density

Samples were immersed in toluene at 25 ºC for a period of 72 h, renewing the solvent every 24 h. Later, the samples were dried using tissue paper to remove the excess of toluene and weighed immediately. Finally, the samples were dried in a vacuum oven for 24 h at 60º C until constant weight[1-2].

The density of the samples was determined with the aid of a liquid whose density (ρ_l) is known (ethanol). The solid was weighed in air and then in ethanol. The density (ρ) was calculated from the two weights by using Equation (A.1):

$$\rho = \frac{P_a \rho_a - P_l \rho_a}{P_a - \rho_l} \quad \text{(A.1)}$$

where P_a and P_l are the weights of the sample in air and ethanol respectively, ρ_l is the density of ethanol (0.806 cm^3/g), and ρ_a is the density of the air (0.002 cm^3/g for relative air humidity of 75% and 25 ºC).

The density of the compounds was calculated after and before swelling in toluene in order to establish the contribution of all the soluble compounds present in the sample.

One way to obtain information about the structure of a vulcanized polymer is by means of swelling experiments. Polymer volume fraction (ν_{2m}) is directly related to crosslink density and to the free volume of the network. It can be obtained by using the Cunnen and Russell method[3] (Equation A.2):

$$\nu_{2m} = \frac{W_d/\rho}{W_d/\rho+(W_s-W_d)/\rho_s} \tag{A.2}$$

where W_d and W_s are the weights of dried and swollen samples respectively, and ρ_s is the density of the solvent (0.8669 g/cm^3 for toluene). Once ν_{2m} is known, the molecular weight between the crosslinks[1] (M_c) is given by:

$$M_C = -\frac{\rho V_s\left(1-\frac{2}{\phi}\right)\nu_{2m}^{1/3}}{ln(1-\nu_{2m})+\chi\nu_{2m}^2+\nu_{2m}} \tag{A.3}$$

Depending on the degree of swelling in the compound, M_c can be calculated by using different models. Here we have performed the calculations by means of the modified Flory-Rehner equation[4] (Equation A.3), where V_s is the molar volume of the solvent, ϕ the functionality of the crosslink, ρ the density of the crosslink network, and χ is the interaction polymer-solvent parameter given by:

$$\chi = \chi_0 + a v_{2m} \quad \text{(A.4)}$$

where χ_0 and a, are values dependent on the polymer configuration. Once M_c is known, crosslink density can be calculated by[5]:

$$\mu = \frac{\rho}{2 \cdot M_c} \quad \text{(A.5)}$$

2. Adam-Gibbs approach to study the dynamics of miscible rubber blends (Chapter 5)

2.1 Full formulation of the compounds

Table A.3 Full formulation [phr] of the unfilled SBR/BR samples studied in chapter 5.

Unfilled samples	100SBR	75SBR 25BR	60SBR 40BR	50SBR 50BR	40SBR 60BR	25SBR 75BR	100BR
SBR	100	75	60	50	40	25	-
cis-BR	-	25	40	50	60	75	100
Wax	2						
Antioxidant	4						
Processing Oil	3						
Stearic Acid	3						
ZnO	2.5						
Sulfur	1.4						
CBS	1.6						
DPG	1.6						
Sulfur-Donor	2						

Table A.4 Full formulation [phr] of the filled SBR/BR samples studied in chapter 5.

Filled samples	100 SBR	75SBR 25BR	60SBR 40BR	50SBR 50BR	40SBR 60BR	25SBR 75BR	100 BR
SBR	100	75	60	50	40	25	-
cis-BR	-	25	40	50	60	75	100
Wax	2						
Antioxidant	4						
Processing Oil	40						
Stearic Acid	3						
Coupling Agent	7.5						
Silica	120						
ZnO	2.5						
Sulfur	1.4						
CBS	1.6						
DPG	3.5						
Sulfur-Donor	2						

Table A.5 Full formulation [phr] of the unfilled fSBR/BR samples studied in chapter 5.

Unfilled samples	100 fSBR	75fSBR 25BR	60SBR 40BR	50fSBR 50BR	40fSBR 60BR	25fSBR 75BR	100 BR
f-SBR	100	75	60	50	40	25	-
cis-BR	-	25	40	50	60	75	100
Wax	2						
Antioxidant	4						
Processing Oil	3						
Stearic Acid	3						
ZnO	2.5						
Sulfur	1.4						
CBS	1.6						
DPG	1.2						
Sulfur-Donor	2						

Table A.6 Full formulation [phr] of the filled fSBR/BR samples studied in chapter 5.

Filled samples	100 fSBR	75fSBR 25BR	60fSBR 40BR	50fSBR 50BR	40fSBR 60BR	25fSBR 75BR	100 BR
f SBR	-	75	60	50	40	25	100
cis-BR	100	25	40	50	60	75	-
Wax	2						
Antioxidant	4						
Processing Oil	40						
Stearic Acid	3						
Coupling Agent	7.5						
Silica	120						
ZnO	2.5						
Sulfur	1.4						
CBS	1.6						
DPG	3.5						
Sulfur-Donor	2						

Table A.7 Full formulation [phr] of the filled and unfilled SBR2/BR samples studied in chapter 5.

Samples	Filled					Unfilled				
	100 SBR2	**75SBR2 25BR**	**50SBR2 50BR**	**25SBR2 75BR**	**100 BR**	**100 SBR2**	**75SBR2 25BR**	**50SBR2 50BR**	**25SBR2 75BR**	**100 BR**
SBR2	100	75	50	25	-	100	75	50	25	-
BR	-	25	50	75	100	-	25	50	75	100
Wax	2					2				
Antioxidant	4					4				
Processing Oil	40					3				
Stearic Acid	3					3				
Coupling agent	7.5					-				
Filler	120					-				
ZnO	2.5					2.5				
Sulfur	1.4					1.4				
CBS	1.6					1.6				
DPG	3.5					-				
Sulfur-Donor	2					2				

3. Immiscible blends (Chapter 6)

3.1 Full formulation of the compounds

Table A.8 Full formulation [phr] of the unfilled fSBR/BR samples studied in chapter 5.

Unfilled samples	100 fSBR	75fSBR 25NR	50fSBR 50NR	25fSBR 75NR	100 NR
fSBR	100	75	50	25	-
NR	-	25	50	75	100
Wax	2				
Antioxidant	4				
Processing Oil	3				
Stearic Acid	3				
ZnO	2.5				
Sulfur	1.4				
CBS	1.6				
DPG	1.2				
Sulfur-Donor	2				

4. References

1. Valentin, J. L.; Carretero-Gonzalez, J.; Mora-Barrantes, I.; Chasse, W.; Saalwachter, K., Uncertainties in the determination of cross-link density by equilibrium swelling experiments in natural rubber. *Macromolecules* **2008,** *41* (13), 4717-4729.

2. Rodríguez Garraza, A. L. Estudio de la microestructura y su influencia en propiedades físicas del caucho polibutadieno y caucho poliisopreno reticulado con peróxido. Universidad de Buenos Aires, 2015.

3. Cunneen, J. I.; Russell, R. M., Occurrence and prevention of changes in the chemical structure of natural rubber tire tread vulcanizates during service. *Rubber Chem. Technol.* **1970,** *43*, 1215.

4. Flory, P.; Rehner, J., Statistical mechanics of cross-linked polymer networks. *J. Chem. Phys.* **1943,** *11*, 521-527.

5. Gronski, W.; Hoffmann, U.; Simon, G.; Wutzler, A.; Straube, E., Structure and density of crosslinks in natural-rubber vulcanizates. A combined analysis by NMR spectroscopy, mechanical measurements, and rubber-elastic theory. *Rubber Chem. Technol.* **1992,** *65* (1), 63-77.

Acknowledgements

The successful conclusion of this PhD thesis would not have been possible without the support and encouragement of many people.
Firstly, I would like to express my sincere gratitude to my supervisors Dr. Silvina Cerveny and Dr. Gustavo A. Schwartz for all their encouragement, good advice and for sharing their immense knowledge with me during these three years. Your guidance was essential to accomplish this PhD thesis. A very special gratitude goes to the rest of the team from Goodyear GIC*L: Dr. Mathias Meyer, Dr. Clemens Sil, Dr. Nihat Isitman and Dr. Stephan Westermann for their continuous support, and for giving me the opportunity to spend two months at GIC*L. I would also like to thank François Kayser for being my supervisor and teacher during my internship at Goodyear.
I need to thank Professor Juan Colmenero for giving me the opportunity to join his group "Polymers and Soft Matter", as well as rest of the members.
Thanks to the University of the Basque Country (UPV/EHU), to DIPC for the financial support and to CFM for allowing me to perform my thesis in their facilities.

Mis compañeros del CFM han sido un apoyo muy importante en ésta etapa. Tengo que dar las gracias a Amaia por todo su cariño, su ayuda incondicional y todos los buenos momentos que pasamos juntas. Mi "cuadrilla de despacho" también ha sido muy importante, gracias Izaskun y Natalia por todo, ha sido genial poder compartir con vosotras tantos momentos, y además sé que me llevo dos amigas. Sin vosotras esto no habría sido lo mismo. Gracias también a Thomas, y por supuesto a Jorge por hacerlo todo más divertido.
No me puedo olvidar del resto de mis compañeros: Dani por toda su ayuda y sus visitas, Edurne sus contínuos ánimos, Marina, Bea, Isa, Paula, Jon, Guido,

Xavier, Julen, Jordan y Maud. Por supuesto, siempre me acordaré de los que se fueron: Manuel, Ana Lucía, Gerardo, Rubén, Guillermina, Lisa, Zita y Valerio. ¡Y tu también Alex! Gracias por todos los momentos que pasamos siendo compañeros de piso.
I also need to mention my "best coffee friends" from Goodyear: Beatriz, Robin, João, Thibaut and Chenyi; and of course Ruth, my Spanish-Luxembourgish friend. Thank you all for the good time we spent together.

Debo agradecer también a Juan Valentín toda su confianza en mí y al grupo de Elastómeros del ICTP en Madrid. Muchas gracias también a Toño y a Luis Serrano de Dynasol por haber apostado por mí.

No puedo dejar de agradecer su apoyo a todas las personas que han estado "cerca" de mí: En Madrid todos mis amigos de la universidad, a Marta, Carol y el resto de mis amigos de circo, mi gente de Tres Cantos, y en especial mis inseparables Paz y Pilar, que estemos donde estemos siempre estaremos juntas. Por supuesto en San Sebastián a mi primo Juan Diego, quien ha sido y será siempre un gran apoyo para mi, a Rafa y a Inma por ser los mejores caseros del mundo, a toda la gente de telas y acro, a Gimena y a mis ex compañeros de piso Alex, Daniel y Sheyla. ¡Sheyla ha sido genial coincidir aquí también contigo! Mi familia de Ecuador también es muy importante aunque no nos veamos mucho, gracias a todos y en especial a mi abuela, a mi tía Lucía y a mi tío Patricio por haberme apoyado en mis inicios profesionales. Isra gracias por todo tu apoyo incondicional, las locuras y buenos momentos vividos, y todos los que vendrán (yo contigo).

Y por último, muchas gracias a mi madre, mi padre, Lala, Isa y Nara. Sois lo más importante para mí y os quiero más que a nada.